GIRAFFA CAMELOPARDALIS: LIMB BONE HISTOLOGY THROUGH ONTOGENY

by

CAITLIN CARYL DANIELLE SMITH

(BSc. Hons. University of the Western Cape)

Department of Biological Sciences, University of Cape Town, Cape Town, South Africa

DISSERTATION

Presented for the degree of Master of Sciences in the Department of Biological Sciences, University of Cape Town

March 2020

SUPERVISOR: Prof. Anusuya Chinsamy-Turan

Department of Biological Sciences, University of Cape Town, Cape Town

CO-SUPERVISOR: Dr. Sybrand van Sittert

Centre for Veterinary Wildlife Studies, Faculty of Veterinary Science, University of Pretoria, Pretoria

PLAGIARISM DECLARATION

I know the meaning of plagiarism and declare that all of the work in the dissertation, save for that which is properly acknowledged, is my own.

Signed by candidate

Caitlin C D Smith

March 2020

Table of Contents

List of Figures

List of Tables

Acknowledgements

I would like to thank the following people for their help in making this thesis possible:

- The DST-NRF Center of Excellence in Palaeosciences for funding this project.
- My supervisor Prof. Anusuya Chinsamy-Turan for her boundless enthusiasm and knowledge, and for guiding me throughout this project and encouraging me to do my best.
- My co-supervisor Dr. Sybrand van Sittert for providing the giraffe material and for providing his advice about giraffes.
- To Jofred Opperman, Collections Manager of Terrestrial Vertebrates from Iziko South African Museums for allowing me to measure baby giraffe limb bones for comparison with my data, and for allowing me to house my samples after my masters.
- To the students and postdocs from the UCT Palaeobiology Research Group for their constant support, encouragement, help, patience, and friendship.
- To Erin Adams, Iyra Maharaj, and Sanjo Rose for doing final checks of my entire thesis and your unwavering support.
- And most importantly, to my family (Charles, Jacqui and Byron Smith, Etholle and Charlene Williams, and Keenan Meissenheimer) for always believing in me!

Abstract

Although there are many studies on mammalian bone histology, there are only a few that have examined the bone histology of artiodactyls or have focused specifically on osteohistological changes during ontogeny. This study investigates the microanatomy and histology of giraffe limb bones through ontogeny. Mid-diaphyseal sections were made of humeri, radii, metacarpals, femora, and tibiae of 14 individuals representing individuals of known sex, as well as at different ontogenetic stages (foetal, juveniles, subadults, and adults). Thin sections were prepared for all the bones, and microanatomical (using Bone Profiler) and histological analyses were conducted on each of the sections. The study examined three main aspects (1) cross-sectional shape changes in limb bones through ontogeny, (2) histological changes through ontogeny in each of the limb bones, and (3) histovariability among skeletons. The results of the study show that the foetus and juvenile bones have round cross-sections, with small vacant medullary cavities, while cross sections of older giraffe bones tend to be oval with variable amounts of cancellous bone surrounding the medullary cavity. The highest bone compactness values were obtained for the humerus and femur of the foetus, whereas the radius, metacarpal, and tibia bone compactness values are similar across the age classes. In terms of histology, this study found that the earlier ontogenetic stages had highly vascularised fibrolamellar bone in their cortices, which contrasts with that of the subadults and adults where more slowly deposited bone tissue is present. These observations indicate that after rapid initial growth during early ontogeny, osteogenesis (and overall growth) slows down. This research also documents the fusion of the metacarpal III and IV, and the associated changes that occur in the histology. The study also highlights that the tibia is the only bone that has long radial vascular canals in the cortex. Overall, the results of this study have provided a much better understanding of the bone histology of giraffes during ontogeny and has therefore filled an important gap in our knowledge of mammalian bone tissues. Furthermore, this study has direct implications for any future palaeohistological studies of fossil giraffids from Langebaanweg in South Africa, fossil giraffids from sites in Kenya and Ethiopia, and fossil giraffids from Eurasia.

Abbreviations

Cr	Cranial
Cd	Caudal
M	Medial
L	Lateral
MC	Medullary Cavity
OCL	Outer Circumferential Layer
EFS	External Fundamental System
ICL	Inner Circumferential Layer
FLB	Fibrolamellar Bone Tissue
ELB	Endosteal Lamellar Bone
LAGs	Lines of Arrested Growth
Mya	Million years Ago
BH	Humerus
BR	Radius
BMC	Metacarpal
BF	Femur
BT	Tibia

Chapter 1 Introduction

1.1.Giraffidae: Evolutionary History and Relationships

The origin of the giraffid lineage is linked to the origins of artiodactyl ruminants of which the oldest known fossil, a rabbit-sized animal called *Diacodexis,* dates to 60-55 Mya (Mitchell & Skinner, 2003). *Diacodexis* were forest dwelling and lived in the area that is now North America. This ancestor to pecorans has a specialized astragulus, which limits movement to the vertical plane (Theodor, 2001), an adaptation shared by all their descendants. After the climatic changes about 35-25 Mya, the surviving artiodactyls mostly occurred in modern day Eurasia. One particular group, the Gelocidae, inhabited the southern regions of Eurasia. The genus *Gelocus* had elongated metapodials which highlighted the role of speed and agility in artiodactyls (Mitchell & Skinner, 2003). It was this group of Gelocidae that gave rise to radiations that would eventually result in pecorans. The pecorans radiated and diverged between 28-23 Mya. The modern families of pecorans are Cervidae, Giraffidae, Antilocapridae, Moschidae, and Bovidae which all came from the gelocid genetic pool (Carroll, 1988; Hassanin & Douzery, 2003; Janis & Theodor, 2014).

1.1.1. African Lineage of *Giraffa*

There are two theories concerning the arrival of *Giraffa* in Africa. The first theory is based on a *Giraffa* fossil that was found in the Kenyan Rift Valley deposits that are dated to about 7-5.4 Mya (Pickford, 1975). This specimen is considered to be a derivative of the Asian *Giraffa* (*Giraffa punjabiensis*) that entered Africa by migration. However, Mitchell & Skinner (2003) suggests that this scenario is unlikely because firstly, there is an absence of a migratory route and secondly, *G. punjabiensis* is more advanced than the African *Giraffa* and differs in morphology. The alternate theory proposed by Mitchell & Skinner (2003) is that the first *Giraffa* species in Africa is ***Giraffa gracilis*** (Fig. 1.1)—a late Miocene to early Pleistocene species restricted to East Africa (Shorrocks, 2016). *Giraffa gracilis* fossils are abundant at the Laetoli deposits (5-2 Mya) in Kenya, but they are also known from the Serengeti in northern Tanzania and southwestern Kenya, and Olduvai Gorge in Tanzania—which are Plio-Pleistocene deposits (Shorrocks, 2016). *Giraffa gracilis* has an elongated neck and limbs similar to the modern giraffe, *Giraffa camelopardalis*. ***Giraffa stillei*** is a Plio-Pleistocene species also found in East Africa (particularly Ethiopia) and on occasion, it is

synonymized with *G. gracilis,* even though *G. stillei* is slightly smaller than *G. gracilis.* ***Giraffa pygmaea*** is a rare form (and the smallest in Africa) found in Northern Kenya. It is possible that *G. pygmaea* was a subspecies of *G. gracilis* (Mitchell & Skinner, 2003). ***Giraffa jumae***, a Plio-Pleistocene species (dated to between 6.5-4.5 Mya) from East Africa and Langebaanweg (Harris, 1976; Hendey, 1982; Shorrocks, 2016). While most of the previous giraffe species were found in East Africa, *G. jumae* is the first giraffe known from the west coast of South Africa. Both *G. jumae* and *G. gracilis* go extinct about 1 Mya i.e. approximately when *Giraffa camelopardalis* appears. The first ***G. camelopardalis*** fossil is known from West Turkana, East Africa (Harris, 1991). There is much debate about whether *G. jumae* evolved into *G. camelopardalis* through a reduction in size, or if *G. gracilis* evolved into *G. camelopardalis* by increasing its size. The latter appears to be a more acceptable hypothesis since *G. gracilis* is more morphologically similar to *G. camelopardalis*, and it is therefore the more likely ancestor of *G. camelopardalis* (Mitchell & Skinner, 2003; Shorrocks, 2016).

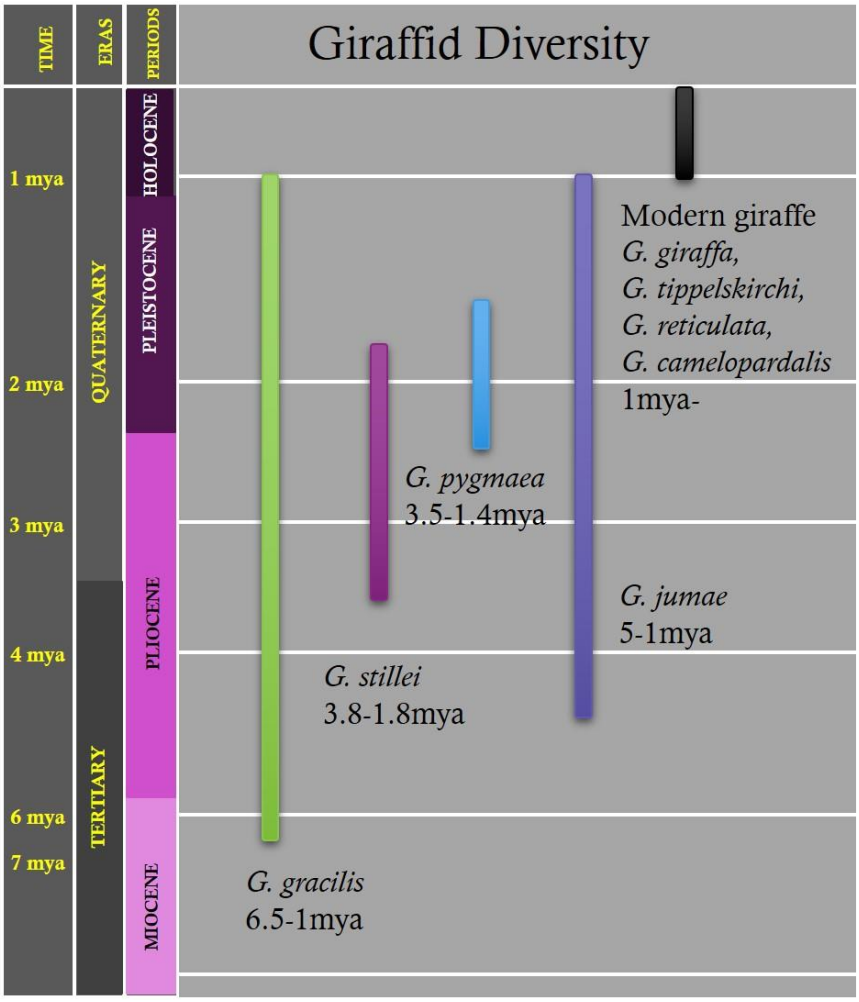

Figure 1.1 Giraffid evolutionary history in Africa drawn up by CSmith 2019

1.1.2. *Giraffa camelopardalis*: Life History

The fossil record of *Giraffa* in Africa includes *G. gracilis, G. stillei, G. pygmaea, G. jumae,* and the modern giraffe *G. camelopardalis*. The evolution of *Giraffa* has been influenced by the change in climate and resulting habitat/vegetation change (Mitchell & Skinner, 2003), i.e., with the upliftment of the Himalayas approximately 50 Mya (Zhisheng *et al.*, 2001), the vegetation became more arid and a migration route between Africa, and

Europe and Asia opened up (Ramstein *et al.*, 1997). Thus, *Giraffa* were able to migrate from Asia to Africa, during the Miocene.

One of the key features that occurs in giraffe evolution is an elongation of the distal elements of their limbs, which increases the mechanical advantages for locomotion. In order to have stability and strength in their elongated limbs, their limb skeletons underwent substantial fusion, e.g., fusion of metapodials (a reduction of five to two metapodials which underwent further fusion resulting the two remaining metapodials to fuse into one metapodial), and modification of the astragulus (Mitchell & Skinner, 2003).

Traditionally modern giraffes were categorized into species and subspecies based on their coat pattern and geographical distribution (Kingdon *et al.*, 2013; Fennessy *et al.*, 2016). However, recent genetic studies involving multi-locus analyses on all giraffe populations identified four monophyletic giraffe species as opposed to a single species with nine to eleven subspecies (Fennessy *et al.,* 2016).

Giraffa camelopardalis is the tallest terrestrial mammal with males reaching heights of 4.9-5.2 meters and females 4.3-4.6 meters (Muller *et al.*, 2018). They are distributed across southern and eastern Africa, and have smaller populations in west and central Africa (Shorrocks, 2016). Giraffe population estimates have been recorded by using photographic capture/re-capture, ground and aerial surveys, best estimates, and interviews (Muller *et al.*, 2018). In terms of reproduction, the gestation period for giraffes is 15 months, and they only have one calf at a time, however twins have occasionally been recorded (Shorrocks, 2016). Females give birth to their first calf at around 5-7 years old. The interval between births is generally two years, and the average height of a newly born calf is 1.67 cm (Shorrocks, 2016).

Giraffa camelopardalis habitat ranges from desert to woodland/savanna environments (Muller *et al.*, 2018). They browse on leaves, stems, flowers, fruits, and are also known to eat bone (osteophagia) (Kingdon *et al*., 2013). The top five trees/shrubs species that giraffes forage on are: *Vachellia* (previously *Acacia,* Kyalangalilwa *et al.* (2013). *Rhus longispina, Euclea undulata, Pappea capensis, and Schotia afra* (Shorrocks, 2016). However, in drier months, the species that they browse on varies regionally.

Giraffes have various specialized physiological attributes that allow them to be successful. For example, their cardiovascular system has adaptations that allow the regulation of blood in the head i.e., blood vessels in their neck have one-way valves (Kingdon *et al.*, 2013). Giraffes also have a rete mirabilis, which is a network of small vessels from the carotids which expands when the giraffe lowers its head—thus preventing blood rushing

down into the head. The rete mirabilis also helps when the head is raised by retaining blood, so that the head is not completely drained (Shorrocks, 2016). Giraffes have abundant air sinuses in their skull that extends from the frontal bone, over the brain case, to the occipital bone. These expansive air sinuses are possibly used to control the temperature around the brain, used as a way to reduce the mass of the skull, they may act as a resonance chamber for their low-frequency sounds, or the air sinuses could have all these functions (Badlangana *et al.*, 2011). Giraffes are ruminants (mammals with four stomachs), which enables them to extract more nutrients from their food. However, the downfall of this is that they process their food very slowly (Shorrocks, 2016). Giraffes efficiently digest cellulose and extract protein from plant material. Once the plant material has passed through the fourth stomach and the small intestine, only water is absorbed by the large intestine. Therefore, by eating succulent plant material they are able to forgo the need of drinking surface water for a couple of days.

1.1.3. *Giraffa camelopardalis*: Skeleton and Growth

The giraffe skeleton is typical of an even toed ungulate (artiodactyl) (Van Sittert, 2016). It has 50 vertebrae: seven cervicals (C1-C7), 14 thoracics (T1-T14), five lumbar (L1-L5), four sacrals that are fused, and 20 caudals (Van Sittert, 2016). The seven cervical vertebrae are 129% longer than the thoracic and lumber vertebrae (Van Sittert, 2016). Since their vertebrae are long enough for muscle attachment, they have rather shallow dorsal spines (van Sittert *et al.*, 2010). They also have unique ball and socket joints between consecutive cervical vertebrae which allows for a large amount of flexibility in their neck (van Sittert *et al.*, 2010).

Giraffe limb bones are quite elongated (as compared to other ungulates) and they show some unique characteristics such as a thicker bone walls and straighter limb bones (Van Sittert, 2016). The forelimb is composed of the humerus, radius, a poorly developed ulna, and elongated fused metacarpals. The scapula is as long as the humerus in length, making the forelimb appear longer (Van Sittert, 2016). The radius is longer than the humerus and articulates with the carpals. The two metacarpals are elongated to a similar length as the radius (Van Sittert, 2016). The hindlimb is made up of the femur, tibia, and elongated fused metatarsals. The tibia and metatarsals are longer than the femur (Van Sittert, 2016).

1.2.Bone Microstructure

Studying the microstructure of the skeleton, i.e. the bone tissue or histology, provides much information about various aspects of the life history of an individual such as its growth

dynamics, bone remodeling processes, age at maturity, etc. e.g., (Chinsamy-Turan, 2005; Kolb *et al.*, 2015a). It is also well recognized that studies of the bone microstructure of extant animals can provide much insight into the life history of extinct animals (Chinsamy-Turan, 2005; Erickson, 2005), and such studies have been useful in enabling a distinction between wild and domesticated animals, and their respective lifestyles (Zedda *et al.*, 2018). Here I will discuss the various kinds of bone tissues found in mammalian bone, as well as the growth marks that are recorded in their bones, the secondary remodeling that occurs through ontogeny, and present an overview of the bone histology of artiodactyls.

1.2.1. Types of Bone Tissue

At a gross morphological level, it is clear that bone is made up of compact and cancellous or spongy bone (Currey, 2002). Compact bone, also known as cortical bone, typically makes up the bone wall and in long bones, encloses the medullary cavity (Chinsamy & Dodson, 1995; Currey, 2002; Chinsamy-Turan, 2005; Chinsamy-Turan, 2012). Primary cancellous bone, also known as trabecular bone, forms as a result of endochondral ossification at the growing ends of the bone (Chinsamy & Dodson, 1995; Chinsamy-Turan, 2005). It can also be found lining the medullary cavity of long bones, pelvic bones, vertebrae or ribs. Secondary cancellous bone results from the resorption of primary bone tissue (Currey, 2002). This occurs when resorption rates exceed the redeposition of bone and the bone becomes increasingly porous with permanent resorption cavities in the bone cortex (Currey, 2002).

When osteogenesis is rapid, fibrolamellar bone tissue results (Starck & Chinsamy, 2002; de Margerie *et al.*, 2004; Chinsamy-Turan, 2012; Kolb *et al.*, 2015b). Fibrolamellar bone tissue is characterized by a woven bone matrix wherein the fibrillar organization (the arrangement of collagen fibers in the bone matrix) is disorganized (Francillon-Vieillot *et al.*, 1990; de Margerie *et al.*, 2002). It is the main primary bone tissue in large mammals (e.g. Currey, 2002). Fibrolamellar bone tissue, found in the cortex of the bone, can be classified into three types based on the arrangement of the vascular channels. (1) Laminar bone tissue has a network of channels that run parallel to the bone periphery (e.g. Francillon-Vieillot *et al.*, 1990; Chinsamy-Turan, 2005; Kolb *et al.*, 2015b). (2) Plexiform bone tissue has a network of both circumferential and radial channels (Francillon-Vieillot *et al.*, 1990; Currey, 2002). (3) Reticular bone tissue comprises a network of disorganized vascular canals (Francillon-Vieillot *et al.*, 1990; Chinsamy-Turan, 2005; Kolb *et al.*, 2015b). When osteogenesis is slow, lamellar bone tissue is produced (Francillon-Vieillot *et al.*, 1990;

Currey, 2002). Lamellar bone comprises thin, successive layers of lamellae in which collagen fibers are orientated parallel to each other (Reid, 1996; Chinsamy-Turan, 2005). Under polarized light, lamellar bone appears as alternating layers of light and dark bands (e.g. Chinsamy-Turan, 2012).

Other bone tissues found in mammalian bones includes (1) lamellated bone, (2) parallel-fibered bone, (3) coarse cancellous bone, and (4) inner and outer circumferential layers. 1) Lamellated bone tissue is also organised in layers and is formed from cyclical variations of mineral microstructure (Reid, 1996). 2) Parallel-fibered bone has collagen fibrils that are organised parallel to one another (Francillon-Vieillot *et al.*, 1990; Ziv *et al.*, 1996; Chinsamy-Turan, 2012) i.e. the fiber bundles are aligned in the same plane as the long bone axis (Francillon-Vieillot *et al.*, 1990; Ziv *et al.*, 1996). 3) Coarse cancellous bone mainly appears in the metaphyseal part of long bones (Enlow, 1963). As the bone grows, the coarse cancellous bone is infilled with lamellar bone tissue, which results in compact coarse cancellous bone tissue (Enlow, 1963). When the long bone grows and elongates, the cancellous bone tissue near the distal and proximal regions of the bone is relocated to the metaphyseal region of the bone (Enlow, 1963). 4) The inner circumferential layer (ICL) consists of layers of bone tissue that lines the medullary cavity once medullary expansion is complete. It is often composed of lamellar, parallel-fibered or lamellated bone (Enlow, 1963; Chinsamy-Turan, 2005). The outer circumferential layer (OCL) or external fundamental system (EFS) consists of layers of avascular lamellar bone tissue that is periosteally formed along the periphery of the bone surface (Enlow & Brown, 1957; Jordana *et al.,* Calderón *et al.,* 2019). The presence of an OCL or EFS either marks the attainment of skeletal or sexual maturity (Ponton *et al.*, 2004; Woodward *et al.*, 2011; Kolb *et al.*, 2015b).

1.2.2. Growths Marks

Different types of growth marks are found in the cortical bones of vertebrates, e.g. lines of arrested growth (LAGs), rest lines, neonatal line, reversal lines, cement lines (Klevezal, 1996; Castanet *et al.*, 2004; Chinsamy-Turan, 2005; Kohler *et al.*, 2012; Kolb *et al.*, 2015a; Kolb *et al.*, 2015b; Nacarino-Meneses & Kohler, 2018). Lines of arrested growth are hyper-mineralized lines that indicate an arrest in growth (Castanet *et al.*, 2004; Chinsamy-Turan, 2012). They have a smooth appearance that follows the contour of the external surface of the bone. The periodic arrest of bone deposition results in LAGs in the bone cortex which results in stratification. (Klevezal, 1996; Castanet *et al.*, 2004; Chinsamy-Turan, 2012). As a result, LAGs are often used for age determination or skeletochronological studies (e.g.

Castanet *et al.*, 2004; Nacarino-Meneses *et al.*, 2016b). Rest lines on the other hand are grouped close together near the peripheral margin of the bone wall and are formed when appositional growth (the increase of bone diameter) has almost stopped (Klevezal, 1996; Castanet, 2006; Chinsamy-Turan, 2012). They are smooth and are generally formed on unresorbed bone surfaces. Rest lines are often located in the OCL of mammal and bird bones, which could suggest the attainment of maximum body size ((Klevezal, 1996; Castanet *et al.*, 2004; Ponton *et al.*, 2004; Chinsamy-Turan, 2012). Reversal lines/tide lines are found on resorbed bone surfaces, and as the name suggests they are associated with bone remodeling or reversals in bone deposition, and as a result, the lines have a wavy appearance (Klevezal, 1996; Chinsamy-Turan, 2012). The neonatal line is considered to be a non-cyclical growth mark related to the birth of an animal (Nacarino-Meneses & Kohler, 2018). These have been described in young *Equus* limb bones and in a mandible of a juvenile southern elephant seal, *Mirounga leonina* (Nacarino-Meneses & Kohler, 2018; Woolley *et al.*, 2019).

According to Castanet *et al.* (2004), cortical bone with low vascularization or low remodeling is best for recording cyclical growth marks, and for their use in skeletochronology. Different bones, in different animals, record growth marks best. For example, in horses the femur is best for growth mark preservation (Nacarino-Meneses *et al.*, 2016b), whereas in deer the humerus, femur, and tibia all keep a good record of growth marks (Kolb *et al.*, 2015a). However, the tibia is the best skeletal element for skeletochronology in the mouse lemur (Castanet *et al.*, 2004) and the angulate tortoise (Bhat *et al.*, 2019).

1.2.3. Secondary Remodeling

Secondary bone remodeling is a process whereby osteoclasts resorbs primary bone tissue and result in erosion cavities in the bone (Chinsamy-Turan, 2005). Later, osteoblasts infill the empty space by centripetally depositing lamellar bone tissue (Lieberman *et al.* 2003; McFarlin *et al.* 2008; Chinsamy-Turan 2012), which results in the formation of secondary osteons. Secondary osteons are easily distinguishable from primary osteons in having a cement line which marks the furthest extent of bone removal (Chinsamy-Turan, 2012).

The amount of secondary reconstruction that occurs is highly variable among mammals (Enlow & Brown, 1958; Enlow, 1963; Schaffler & Burr, 1984; Currey, 2002; Lieberman *et al.*, 2003; Skedros *et al.*, 2007; McFarlin *et al.*, 2008; Chinsamy-Turan, 2012). A study by Schaffler & Burr (1984) suggest that the distribution and amount of strain on the bone increases remodeling (Schaffler & Burr, 1984), and that remodeling is a mechanism that removes and replaces fatigued cortical bone tissue (Schaffler & Burr, 1984). These

differences in distribution and abundance of secondary remodeling in the limb bones relates to how the animal uses its limbs, e.g. in primates (Schaffler & Burr, 1984; McFarlin *et al.*, 2008) there is variation in the extent of secondary remodeling in the femora of the different primates, with the smaller arboreal types generally having less secondary remodeling. Interestingly despite weighing more, chimpanzees have similar amounts of secondary remodeling as compared to spider monkeys (Schaffler & Burr, 1984). Skedros *et al.* (2007) suggests that the shape and size of secondary osteons in cortical bone can relate to the type and amount of strain experienced in bones. For example, in macaques, there is higher density of secondary osteons in higher stress regions of the mandible (Bouvier & Hylander, 1996). Since secondary remodeling often erases LAGs, annuli or other growth marks present in the primary bone, it can affect studies applying skeletochronology.

1.2.4. Bone Microstructure of Artiodactyls

There have been many studies of mammal bone histology (Table 1.1), however, for this section I am focusing on the order Artiodactyla. Artiodactyla is a mammal order which includes pigs, hippopotamus, antelope, deer, giraffe, okapi, camels, llamas, alpacas, sheep, goat, buffalo, and cattle (Theodor, 2001). These animal are known as even-toed ungulates (hoofed animals), which bears weight evenly on two, or four toes as opposed to five (Theodor, 2001). Despite the abundance of species in this order, limb bone histology has only focused on a select few, namely; pigs (*Sus,* Mori *et al.* (2005), deer; fossil and extant deer, (*Cadiacervus ropalophorus, Megaloceros giganteus, Procervulus praelucidus, Dama dama, Muntiacus muntjak, Cervus elaphus*, and *Alces alces*, Kolb *et al.* (2015a); red deer, (*Cervus elaphus hippelaphus* and *C. e. hispanicus*, Calderón *et al.* (2019); and rocky mountain mule deer, (*Odocoileus hemionus hemionus,* Skedros *et al.* (2003), sheep (*Ovis*, Skedros *et al.* (1997); Mori *et al.* (2005), elk (*Cervus elaphus*, Skedros *et al.* (1997), spiral-horned antelope (*Tragelaphus,* Jordana *et al.,* 2016), reedbuck (*Redunca,* Jordana *et al.,* 2016), and oryxes (*Oryx,* Jordana *et al.,* 2016). There are also studies on bone strains and loading on sheep (*Ovis*, Skedros *et al.* (1994), and goats (domestic, *Capra hircus*, Main & Biewener (2004); Main & Biewener (2006)).

Newborn and one-month old pigs typically exhibit laminar FLB in their bone cortices, whereas, in the six-month old pig, primary osteons are scattered in the FLB cortex, although this was more extensively developed in the inner cortex region (Mori *et al.*, 2005).The cortices of newborn and one-month old calves generally have laminar FLB, without any secondary reconstruction whereas, six-month and one-year olds do have secondary osteons

present in their cortices (Mori *et al.*, 2005). A similar trend was observed in (Mori *et al.*, 2005). In adult sheep, circumferential lamellar bone tissue is found in the compression region of the cortex, but in non-compression regions secondary osteons are extensive (Skedros *et al.*, 1997). Indeed, in adult elk, secondary osteon density is higher in the compression regions than the tension region of bone cortices (Skedros *et al.*, 1997). The Plio-Pleistocene dwarf bovid, *Myotragus*, exhibits zonal bone in the cortex of the tibia and femora with the appearance of multiple LAGs. In older individuals, the LAGs are closer together in the peripheral region of the cortex (Köhler & Moyà-Solà, 2009). In young specimens, the predominant bone tissue is zonal FLB bone or lamellar bone with annuli and primary osteons (Köhler & Moyà-Solà, 2009). The occurrence of lamellar-zonal bone indicates that at some periods of its life it grew rather slowly. In red deer (*Cervus elaphus hippelaphus* and *C. e. hispanicus*, Calderón *et al.* (2019), plexiform FLB is predominant in femora with localized patches of reticular FLB in the medial region of the inner cortex. However, in the tibia, laminar FLB is predominant in nine of the 15 specimens. Through ontogeny, secondary remodeling expands from the inner to the outer cortex in the femora (Calderón *et al.*, 2019). The long bones of eight species of fossil and extant deer (Kolb *et al.*, 2015a) all have similar bone tissue types. The limb bones of medium to large deer have predominantly plexiform FLB in the cortex, whereas laminar FLB is prominent in the limb bones of small sized deer. LAGs are found in all the deer, and Kolb *et al.* (2015a) found that the humeri, tibia, and femora record the highest number of LAGs

Table 1.1 List of some examples of vertebrates that have been studied histologically.

Taxa	**References**
Multiple taxa (extinct and extant)	(Enlow & Brown, 1957; Enlow & Brown, 1958; Enlow, 1963)
Multiple taxa	(Klevezal, 1996)
Felids and Mustelids	(Singh *et al.*, 1974)
Elk	(Skedros *et al.*, 1997)
Polar Bears	(Chinsamy & Dodson, 1995)
Cave Bear (Extinct and Extant)	(Veitschegger *et al.*, 2018)
Sheep	(Skedros *et al.*, 1997; Mori *et al.*, 2005)
Pigs	(Mori *et al.*, 2005)
Extinct Cave Goat	(Köhler & Moyà-Solà, 2009)
Deer	(Skedros *et al.*, 2003; Kolb *et al.*, 2015a; Calderón *et al.*, 2019)
Primates	(Castanet *et al.*, 2004; McFarlin *et al.*, 2008)

Monotremes	(Chinsamy & Hurum, 2006)
Antelope	(Marín-Moratalla *et al.*, 2013)
Miocene Hipparion	(Martinez-Maza *et al.*, 2014)
Equus	(Nacarino-Meneses *et al.*, 2016a; Nacarino-Meneses *et al.*, 2016b; Nacarino-Meneses *et al.*, 2017; Nacarino-Meneses & Kohler, 2018; Nacarino-Meneses & Orlandi-Oliveras, 2019)
Mole rats	(Montoya-Sanhueza & Chinsamy, 2017)
Ruminants	(Jordana *et al.*, 2016)
Dwarf Hipparions	(Orlandi-Oliveras *et al.*, 2018)
Aardvark	(Legendre & Botha-Brink, 2018)
Xenarthra	(Straehl *et al.*, 2013; Heck *et al.*, 2019)
Seals	(Woolley *et al.*, 2019)

1.3. Rationale and Philosophical Framework

Despite all the above studies on artiodactyl limb bones, except for Foote (1916) no others reported on the bone histology of giraffes. Foote (1916) examined a left femur of *Giraffa camelopardalis* wherein he noted that in the periphery to mid cortical regions of the anterior, medial and lateral parts of the compacta, bands of laminae interrupted Haversian bone tissue, whereas in the posterior and inner cortex of the medial and lateral regions Haversian bone tissue was abundant (Foote, 1916). In a study of the crystallographic organization of giant extinct and extant animals Dumont *et al.,* (2014), included a giraffe humerus. Although no histological descriptions of the bone tissue was provided, the study demonstrated that the crystallographic organization of the bone mineral in giraffes was orientated along the bone axes (i.e. 001-fibre texture), like that of bison, elephants and *Apatosaurus* in response to similar static stresses along the long bone axis (Dumont *et al.,* 2014). Thus, the focus of the current research is to fill this gap in our knowledge by examining 14 individual giraffes spanning different ontogenetic ages of known sex. It is evident that bone tissues change during ontogeny, therefore, the current study examines and compares the individual bones at different ontogenetic ages. Bone histology also varies in different bones of the skeleton, and this study compares the histological differences between three forelimb (humerus, radius, and metacarpal) and two hindlimb (femur, and tibia) elements within each skeleton.

1.3.1. Hypotheses

The overall hypothesis that will be examined in the thesis is that the bone histology of *G. camelopardalis* records various aspects of their life history, such as growth dynamics

through ontogeny, lifestyle adaptations, and the onset of skeletal maturity. If this hypothesis is true, I expect that:

1. Each ontogenetic stage (foetal, juvenile, subadult adult) of *G. camelopardalis* will exhibit distinct bone histology patterns, i.e. earlier stages of ontogeny will have more highly vascularised fibrolamellar bone tissue, while later stages will show a preponderance of more slowly deposited lamellar bone tissue and lines of arrested growth (LAGs) in the bone cortex.
2. There will be microanatomical differences between forelimb and hindlimb elements that reflect their weight bearing capabilities i.e. it is expected that the forelimb elements, humeri and radii, will have thicker bone walls to support the weight of their elongated neck.
3. The attainment of skeletal maturity will result in higher levels of secondary reconstruction in the bone cortices of females, and particularly pregnant females, as compared to males.

1.3.2. Aim and Research Objectives

The aim of this aspect of the study is to examine and describe the histological changes, through ontogeny of giraffe limb bones (humeri, radii, metacarpals, femora, and tibia).

Research objectives

1. Assess and compare the bone microanatomy of the long bones of modern *Giraffa camelopardalis.*
2. Describe the bone histology of the long bones of modern *G. camelopardalis.*
3. Compare the histovariability between the skeletal elements
    a. For each age class of *G. camelopardalis*.
    b. For both males and females of *G. camelopardalis*.

Chapter 2 Materials and Methods

2.1 Specimen and data collection

Giraffa camelopardalis limb bones used in the current study were originally collected for the PhD research (project number V043-08) of Van Sittert (2016). Forty-eight giraffes were culled by a professional hunter over two years (April 2007, November 2007, April 2008, November 2008, and April 2009) as part of a population management strategy in a conservancy in south eastern Zimbabwe (21°42 S, 29°54 E).

The sample utilized in the current study comprised of mid-shaft sections of the limb bones (humerus, radius, femur, tibia, and metacarpals) of 21 individuals (Table A.1). Thus, in total, this study examined 64 skeletal elements that were recovered from a wide ontogenetic range of giraffes i.e. from foetus through to adult. The dataset for the 21 individuals includes morphological information such as sex and body mass, and for each of the bones it includes data such as, bone length (mm), bone mass (g), cranial-caudal diameter (mm), medial-lateral diameter (mm), and bone circumference (mm). It should be noted that the age categories were based on the mass of each giraffe. Therefore, estimates among the subadults and adults are not clear cut (Van Sittert, 2016). Generally, the following categorization was considered: foetus' weigh < 100 kg, juveniles weigh between 100 kg-300 kg, and fully grown females weigh between 750 kg-1000 kg, whilst males weigh about 800 kg-1400 kg. Thus, subadults weigh between 300 kg-750 kg. The samples are housed in the Iziko Museums of South Africa.

2.2 External measurements and photographs

Eight measurements were taken of each sample (listed in Fig. 2.1). Photos of the distal, proximal, medial (M), lateral (L), caudal (Cd), and cranial (Cr) sides were taken for each sample (Fig. 2.2).

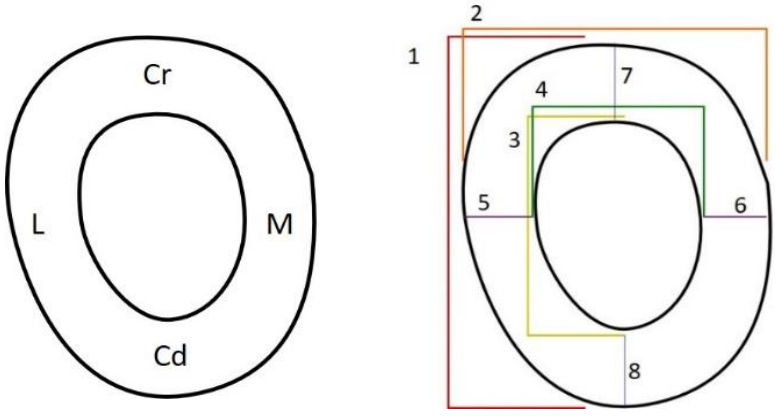

Figure 2.1 The eight measurements taken for each bone sample. 1. Bone Diameter of Cr-Cd, 2. Bone Diameter of L-M, 3. Medullary Cavity Diameter from Cr-Cd, 4. Medullary cavity Diameter from M-L, 5. L-MC, 6. M-MC, 7. Cr-MC, 8. Cd-MC (see page 9 for abbreviations)

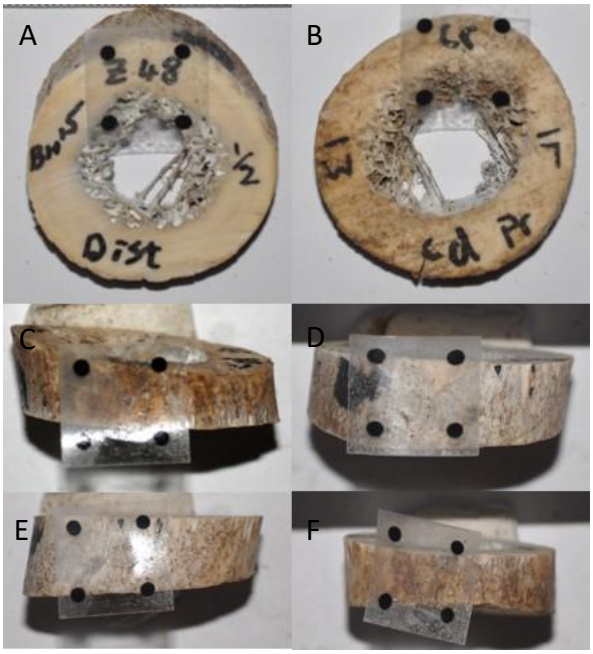

Figure 2.2 Photographs of each side of each bone. A) Distal, B) Proximal, C) Medial, D) Lateral, E) Cranial, and F) Caudal. The clear squares with black dots on each corner represent centimeter measures as a scale bar.

2.3 Osteohistological methodology

Prior to processing for thin sectioning, the midshaft sections of each of the limb bones were pretreated in 95% ethanol, for eight hours (repeated thrice), and thereafter in 95% acetone, for eight hours (repeated twice). Samples were then cleaned using a soft toothbrush and a mixture of water and dishwashing liquid solution. Standard histological procedures were used to obtain thin sections (Chinsamy & Raath, 1992) Samples (Fig. 2.3) were embedded in clear resin consisting of Epoxacast resin and Epoxacast hardener (100:30) and left to harden for two days. The block was then cut with a diamond-edged saw (Abrasive cutter Impetech C 10) to fit a petrographic slide (55 x 75mm, ~1mm thickness). The block was polished on the exposed surface using a series of abrasive carbide grinding discs (400p, 600p, 800p, and 1200p). The last polish was done using Struers OP-U suspension solution on a velvet cloth covered lap-wheel. At this point, the exposed surface was flat, polished, and without any irregularities. The polished surface was then mounted onto a frosted petrographic slide using Epoxacast resin and Epoxacast hardener (100:30). Slides were left to cure for two

days. The specimens mounted onto the slides were then sectioned using an Accutom precision cut-off machine (Struers Accutom). Thin sections of 120-300 um were obtained. It was determined that it was best to leave the cut off thin sections overnight to dry completely before they were ground down with the Accutom grinding disc or graded carbide grinding discs. Sections were checked frequently under the microscope until optimal thickness was obtained —if they were too thick, they were ground down again. Final thin sections were obtained and were polished using OP-U suspension solution again. High quality photomicrographs were taken using normal, and polarized light using a Nikon Eclipse E200 polarizing microscope and a Zeiss AX10. The complete cross-sectional images, used for Bone Profiler, was taken using a Nikon SMZ745T.

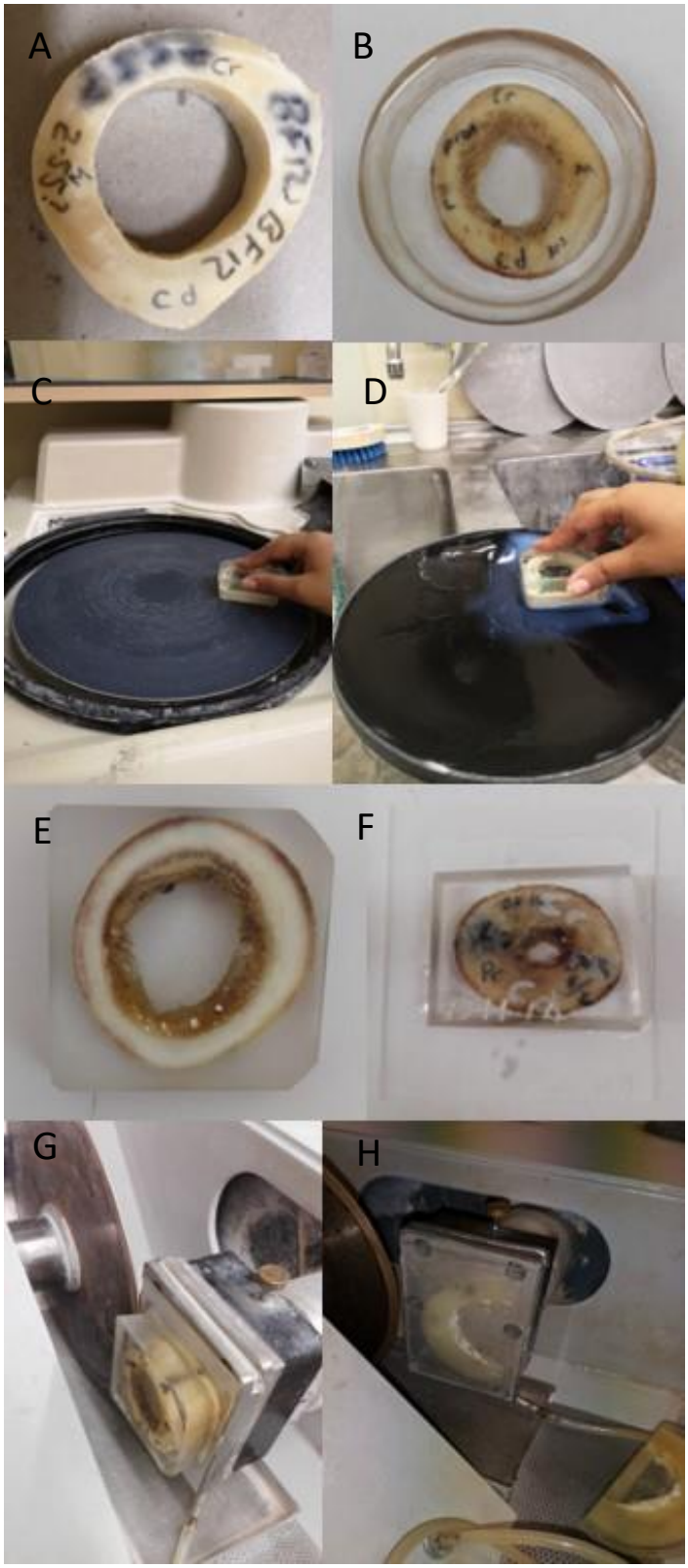

Figure 2.3 Preparing histological sections of bones. A) mid-diaphyseal section of the bone. B) The bone is embedded in resin. C & D) The surface of interest is polished using a grinder-polisher machine. E) The surface of interest is now smooth and polished ready for gluing to a slide. F) Bone block glued onto a frosted glass slide. G & H) The thin section is performed with an Accutom machine which has two different blades (one for cutting and one for grinding). Thin sections are then polished using the same cloth in D and is then ready for viewing under a petrographic microscope.

2.4 Bone Compactness

Bone Profiler was used to measure the degree of compactness of the cortex of thin sections of the long bones. This software estimates the compactness of the bone by quantifying the ratio of bone in the cross section. Bone profiler does this by finding the center of the bone then reading each pixel of the image until the whole cross section has been read (Girondot & Laurin, 2003). Bone profiler is a standardized way to analyze compactness and cortical thickness in bone cross-sections (Girondot & Laurin, 2003), thus allowing authors to compare these values. For the purpose of this study bone profiler was used to measure the compactness of the bone tissue (black) excluding the medullary cavity and resorption cavities (white) (Fig. 2.4).

Figure 2.4 An image of a femoral cross section used in Bone Profiler.

Black represents the bone tissue.

Chapter 3 Results

3.1 Microanatomy and Histology of the Humeri

3.1.1 Foetus

The midshaft cross section of the humerus of the foetus is circular in shape and has a thick bone wall (~10-12 mm) (Table A.2), which encloses a small medullary cavity (Fig. 3.1A). Active resorption of the early bone tissue is evident in the perimedullary region. The large resorption cavities cut into the primary bone compacta (Fig. 3.1B). The peripheral regions of the bone wall are highly vascularised with vascular canals arranged in a predominately laminar pattern (Fig. 3.1C, 3.1D). The midcortical bone has vascular canals in a reticular arrangement (Fig. 3.1D). A nutrient foramen is present in the cranial region of the bone wall (Fig. 3.1E). The margins of the nutrient foramen appear resorptive and it is not lined with lamellar bone.

3.1.2 Juvenile

The midshaft cross section of the humerus of the two juvenile individuals studied are more or less circular in shape (Fig. 3.1F, 3.1G), although there appears to be a widening along the cranial-caudal direction (8-10 mm) (Fig. 3.1G). Their bone walls are thinner as compared to the foetus (Table A.2) and they enclose a large medullary cavity (Fig. 3.1F, 3.1G). Some remnants of the original primary bone tissue extend into the medullary cavity as trabeculae (Fig. 3.1H, 3.1I). It is evident that the bone tissue closest to the medullary cavity (and also that of the trabeculae) was formed during an earlier stage of ontogeny and comprises of reticular fibrolamellar bone (FLB) (Fig. 3.1H). The outer parts of the cortex have circumferentially arranged vascular canals (Fig. 3.1J-3.1L), although there is a distinctive patch of reticular FLB present in a localized region (Fig. 3.1K). The perimedullary region of the bone wall has many large erosion cavities (white arrows) that overall give this region a rather cancellous appearance (white bracket) (Fig. 3.1L), although in places there are also several small resorption cavities that cut into the primary bone tissue (Fig. 3.1M). FLB with primary osteons in the caudal region of the cortical bone (Fig. 3.1N).

3.1.3 Subadult

The midshaft cross section of the humerus of the subadults are elliptical in shape and tend to be wider along the cranial-caudal plane as opposed to the medio-lateral plane (Fig. 3.2A-3.2D). As compared to the earlier growth stages, the bones have predominately thinner bone walls, particularly in the cranial region, while the caudal-lateral regions tend to be fairly thick (~9-40 mm) (Table A.2). A large, predominately vacant medullary cavity is enclosed by the bone wall. Some cancellous bone occurs in the perimedullary regions, particularly in the

cranial and lateral regions of the cross sections (Fig. 3.2E-3.2G). The cancellous bone appears to be formed as a result of resorption of pre-existing primary bone tissue. Several of the enlarged cancellous spaces are lined by narrow bands of lamellar bone tissue (Fig. 3.2G). When the endosteal margin is void of cancellous bone it tends to be lined with lamellar bone (Fig. 3.2H). A nutrient foramen is visible in a female (Fig. 3.2A) and in male subadults (Fig. 3.2C). In the female it is near the periphery of the medial part of the bone wall (Fig. 3.2A). This enlarged cavity is unlined, and has uneven margins suggesting that it was formed by resorption of the surrounding bone tissue. In both males the nutrient foramina are present in the caudal region of the bone wall and they also have uneven, resorptive margins. In two male specimens, BH7 and BH10 (Fig. 3.2I-3.2M), the periosteal margin is uneven suggesting that bone deposition is underway, and there is evidence of secondary reconstruction (Fig. 3.2J, 3.2L, 3.2M). BH10 has extensive resorption cavities scattered throughout the cortical bone (Fig. 3.2I-3.2K). BH10 is a male that shows unusual and extensive cancellous bone tissue and secondary reconstruction. The predominant bone tissue is laminar FLB bone tissue, with vascular canals in circumferential organization with some radial connections (Fig. 3.2H, 3.2K, 3.2N, 3.2O). In the cranial region, the cortex is a mixture of primary and secondary bone tissue with both primary and secondary osteons present (Fig. 3.2E, 3.2J). Annuli are evident transecting the plexiform and laminar FLB on the medial-caudal-lateral regions of the bone (Fig. 3.2N, 3.2O). Growth marks are not present in the cranial region as secondary remodeling has erased any evidence of growth marks. Annuli are predominately found in, males and females, in the caudal and cranial region (Table 3.1), the maximum number of growth marks recorded in the male subadults is 6 (Z51), and in the female subadults is 4 (Z24).

3.1.4 Adult

The midshaft cross section of the humerus of the adults are elliptical in shape and they tend to be wider along the cranial-caudal plane. Except for the caudal part of the section, the bone walls of the adult's measures between (~9-25 mm) i.e. the maximum thickness is much thinner than that of the earlier ontogenetic stages (Table A.2) The caudal region is the thickest part of the bone wall and measures ~11-20 mm. The mostly compacted humeral bone wall encloses a large, centrally open medullary cavity. In most of the specimens, a narrow band of cancellous bone occurs along the margins of the cranial and caudal regions (Fig. 3.3B-3.3D). However, in four (of seven) specimens the cancellous bone tissue extends to the medial and to a limited extent to the lateral sides of the bone wall (3.3A-3.3D). The bony struts that make up the cancellous bone tissue is lined with lamellar bone tissue (Fig. 3.3E-3.3I), and they extend into the medullary cavity. The endosteal margins that do not have cancellous bone tissue are

lined with lamellar bone tissue, which has several rest lines (indicated with white arrows) (Fig. 3.3J, 3.3K). The peripheral regions of the cortex have FLB (Fig. 3.3L-3.3R) that appears to be interrupted by growth marks consisting of annuli composed of narrow bands of lamellar bone tissue. However not all of the growth marks can be followed throughout the cortex due to the secondary intracortical bone remodeling that occurs (Fig. 3.3N, 3.3R). The cortical bone in specimen BH5 and BH8 has extensive secondary osteons in the cortical bone in the medial side (Fig. 3.3S) and lateral-caudal side (Fig. 3.3Q). Annuli are predominately found, in males and females, in the caudal and lateral regions of the bone (Table 3.1). The number of growth marks recorded in adult humeri is between 5-8, and in the females 3-4.

3.1.5 Bone Profiler Data

The observed compactness data for all specimens shows that the foetus humerus has the highest compactness value (0.914, Table 3.2) followed by the two juveniles. The subadult, and adult humerus compactness values are similar, ranging between 0.5-0.8 compactness (Table 3.2). Two of the largest adult individuals have similar compactness values, which show that they are comparatively thinner walled as compared to the humeri of the other adults and also as compared to the younger individuals (Fig. 3.4).

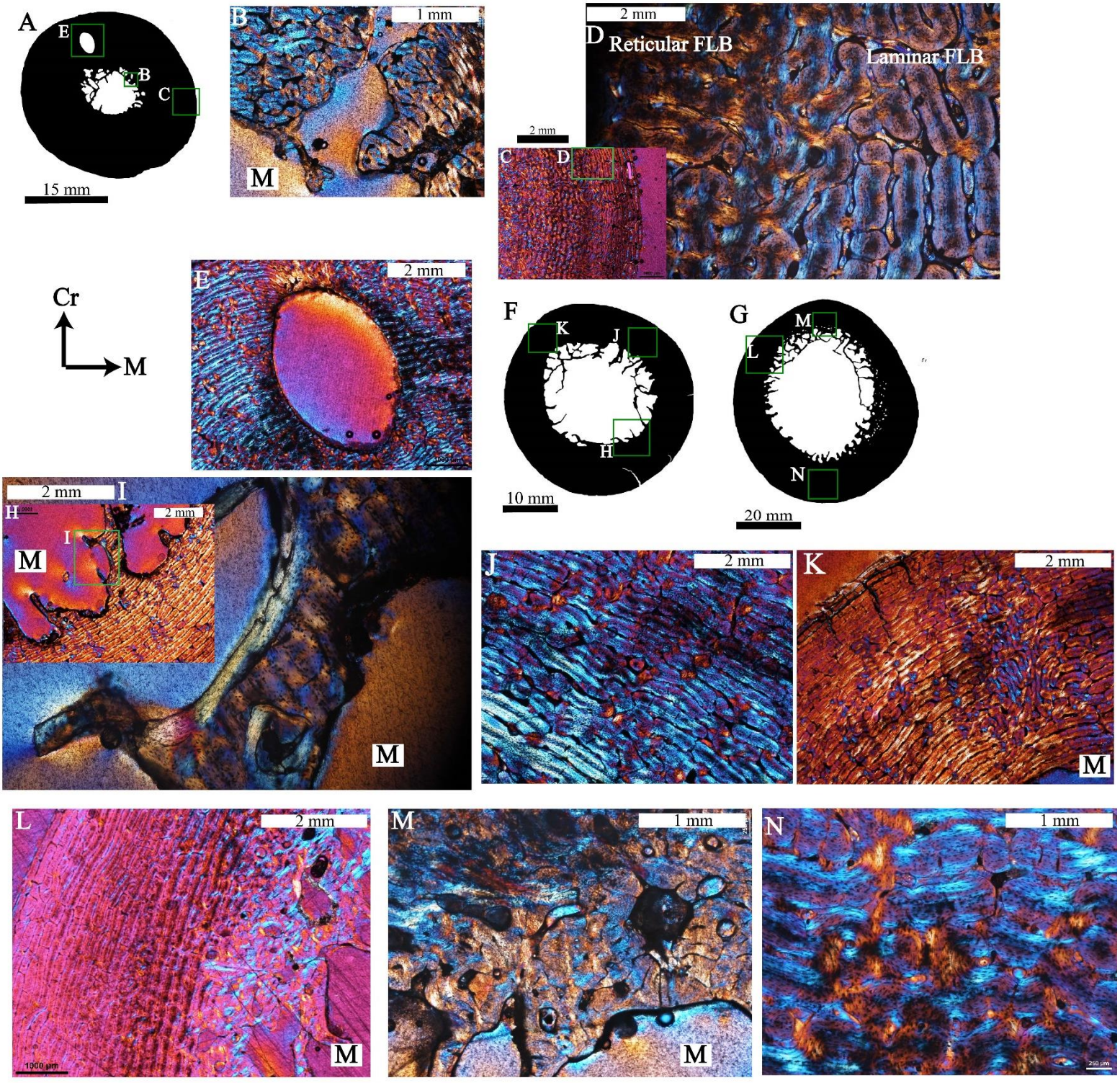
A
E
B
C
15 mm
B
1 mm
M
2 mm
D
Reticular FLB
Laminar FLB
2 mm
C
D
Cr
M
E
2 mm
F
K
J
H
10 mm
G
M
L
N
20 mm
2 mm
I
H
2 mm
I
M
M
J
2 mm
K
2 mm
M
L
2 mm
M
1000 µm
M
1 mm
M
N
1 mm
250 µm

Figure 3.1: Humeral cortical bone tissues in the foetus and juveniles of *Giraffa camelopardalis*. (A) Microanatomy for the cross-section of the foetal humerus (BH14 ♂), cortical wall enclosing a medullary cavity. Frames indicated regions for which higher magnification images are provided. (B) Higher magnification of (A) shows active resorption of the perimedullary region. (C) Highly vascularised cortical bone of fibrolamellar bone tissue (FLB). (D) Higher magnification of frame (C) showing reticular FLB. (E) Nutrient foramen in cranial region. The foramen is not lined and appears resorptive. (F & G) Microanatomy for the cross-section of the juvenile humeri (BH15 ♀ & BH2 ♀), showing cortical wall enclosing a medullary cavity with trabeculae. (I) Higher magnification of (H) shows that the trabeculae in the perimedullary region consists of reticular FLB, some trabeculae are lined with lamellar bone (white arrow). (J) Laminar FLB in the cortex. (K) Localized patches of reticular FLB (white brackets) in between laminar FLB. (L) Laminar FLB on the lateral side of cortex, with secondary bone tissue next to nearest the medullary cavity (white bracket). (M) Small resorption cavities in the perimedullary region. (N) Reticular FLB in caudal region of cortex.

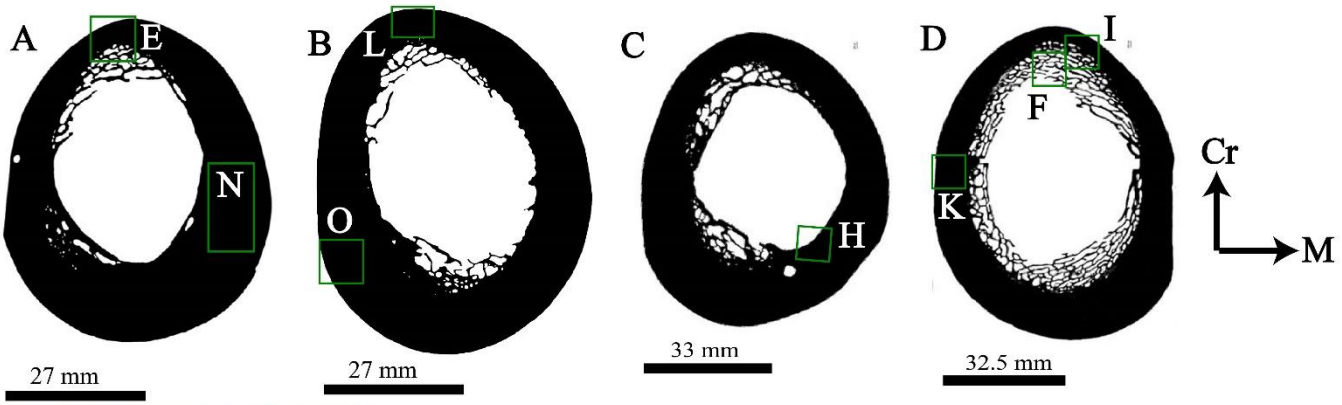
A
E
N
27 mm
B
L
O
27 mm
C
H
33 mm
D
I
F
K
32.5 mm
Cr
M

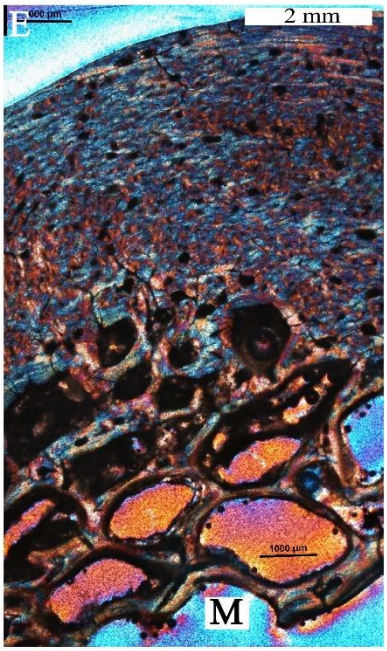
E
2 mm
M

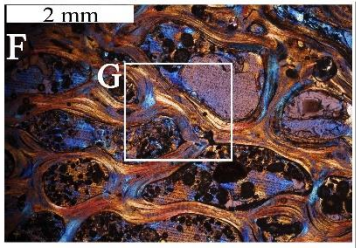
2 mm
F
G

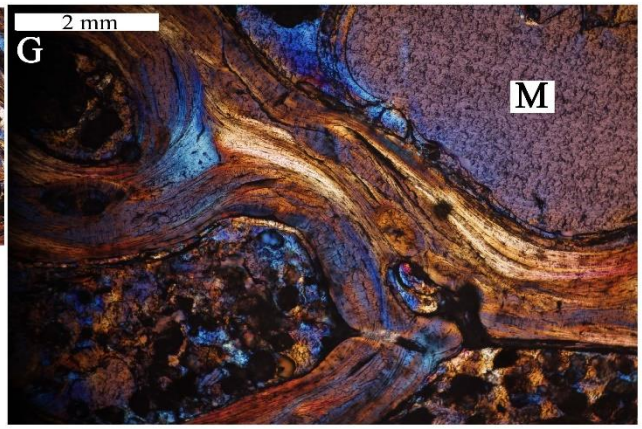
2 mm
G
M

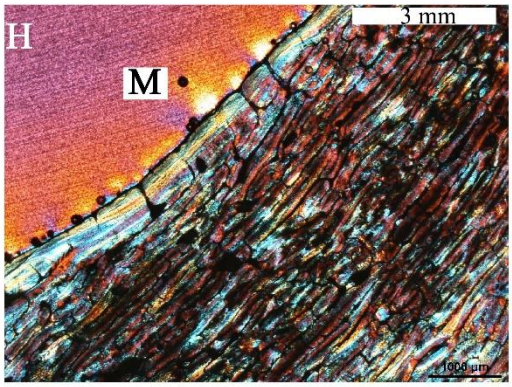
3 mm
H
M

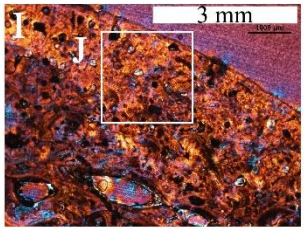
3 mm
I
J

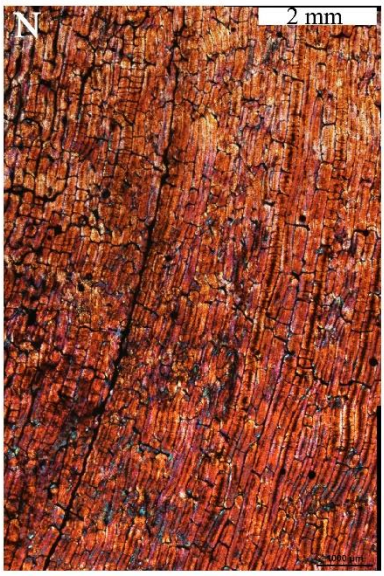
N
2 mm

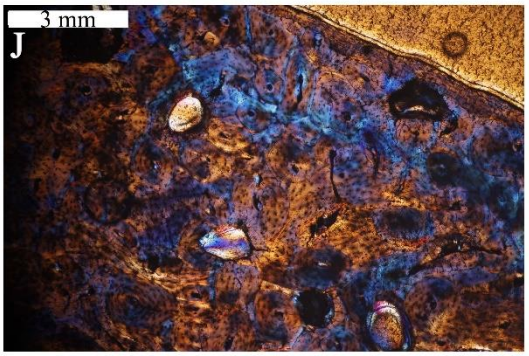
3 mm
J

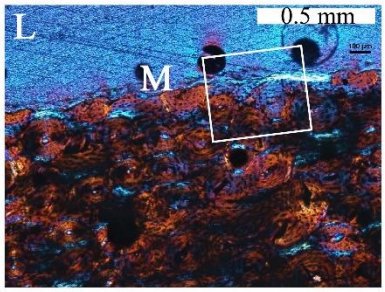
0.5 mm
L
M

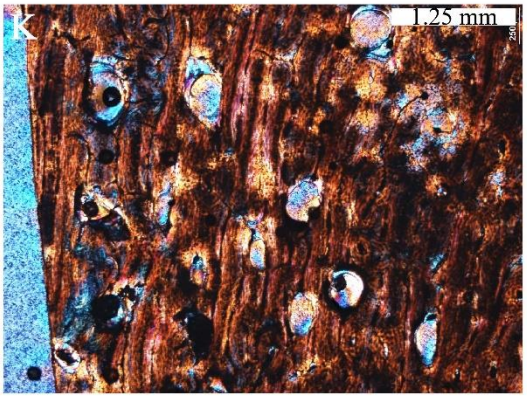
1.25 mm
K

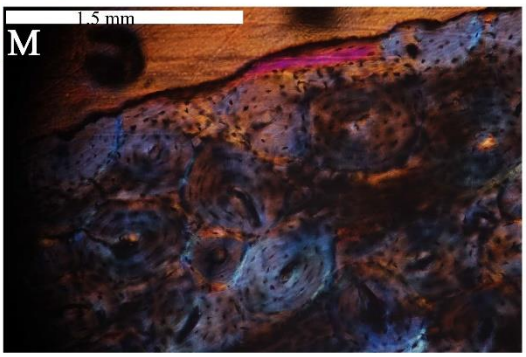
1.5 mm
M

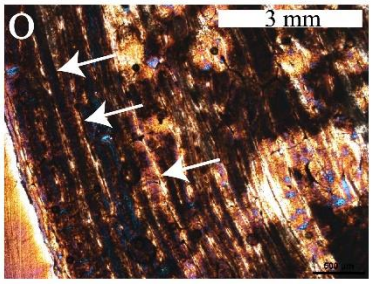
3 mm
O

Figure 3.2: Humeral cortical bone tissues of the subadults of *Giraffa camelopardalis*. (A) Microanatomy of the cross-sections of the subadult humeri, (A) BH1 ♀, showing a thin cranial cortical wall and thick medial-caudal cortical wall enclosing an open medullary cavity. (B) BH7 ♂, showing a cortical wall enclosing a medullary cavity with trabeculae. (C) BH11 ♂, showing cortical wall enclosing an open medullary cavity. (D) BH10 ♂, showing cortical wall with extensive cancellous bone surrounding the mostly open medullary cavity. Frames indicated regions for which higher magnification images are provided. (E) Higher magnification of the framed region indicated in (A) showing secondary reconstructed bone tissue in the cortical bone and cancellous bone tissue in the perimedullary region. Note that the cancellous spaces are lined with lamellar bone (arrow). (F) Higher magnification of cancellous bone in (D), (G) Higher magnification of the framed region on (F) cancellous bone is lined with lamellar bone tissue (white arrows). (H) Lamellar bone tissue (arrow) lining the medullary cavity on the medial side of framed region in (C). (I) Higher magnification of the framed region in (D), extensive secondary reconstruction and resorption cavities in the cranial region. (J) Higher magnification of (I) and (K) higher magnification of (D) shows resorption cavities in the peripheral zone of the cortex. (M) Higher magnification of (L) showing lamellar bone tissue in the periosteal margin. (N) and (O) Higher magnification of (A) and (B) showing growth marks in the cortex (white arrows).

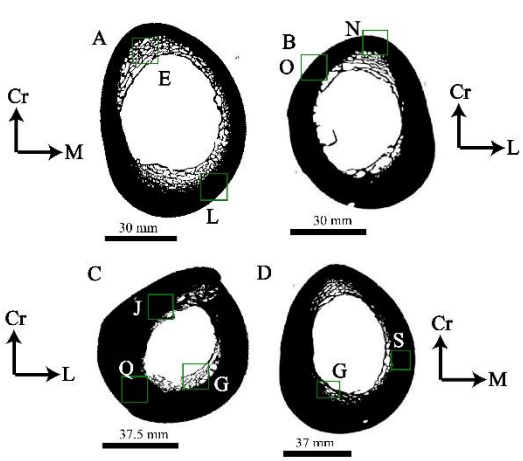
A
E
B
O
N
Cr
M
L
30 mm
30 mm
C
J
Q
G
D
S
G
37.5 mm
37 mm

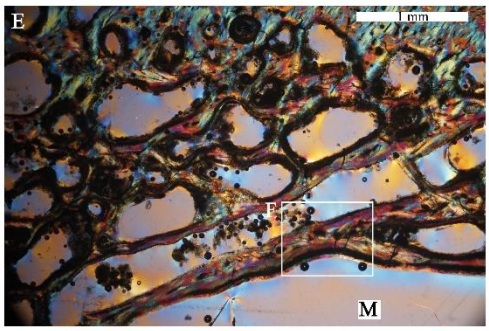
E
1 mm
P
M

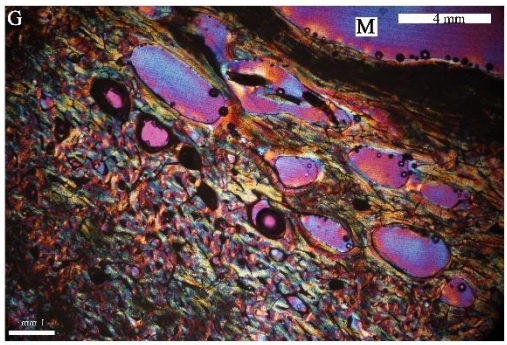
G
M
4 mm

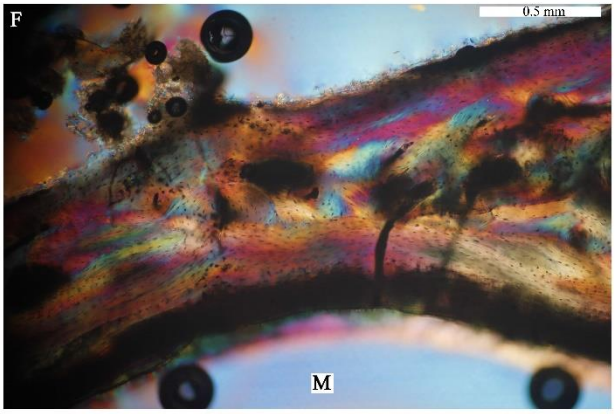
F
0.5 mm
M

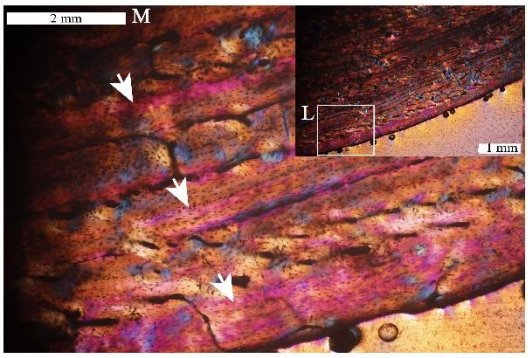
2 mm
M
L
1 mm

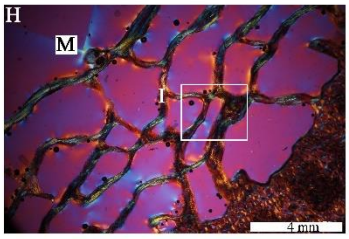
H
M
I
4 mm

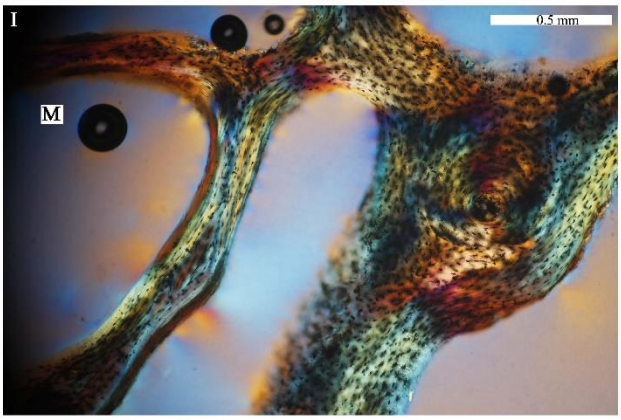
I
0.5 mm
M

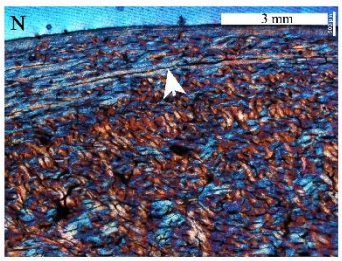
N
3 mm

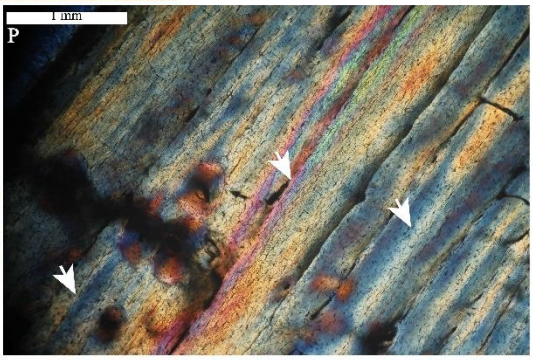
1 mm
P

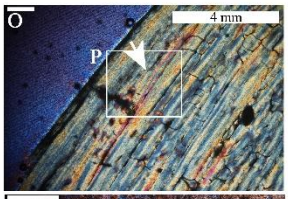
O
4 mm
P

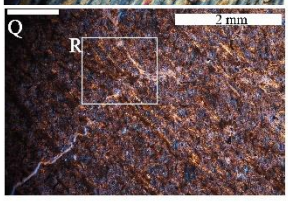
Q
2 mm
R

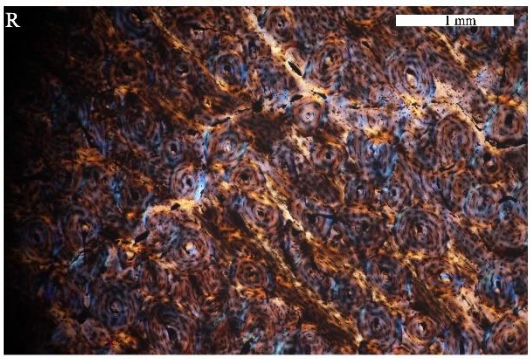
R
1 mm

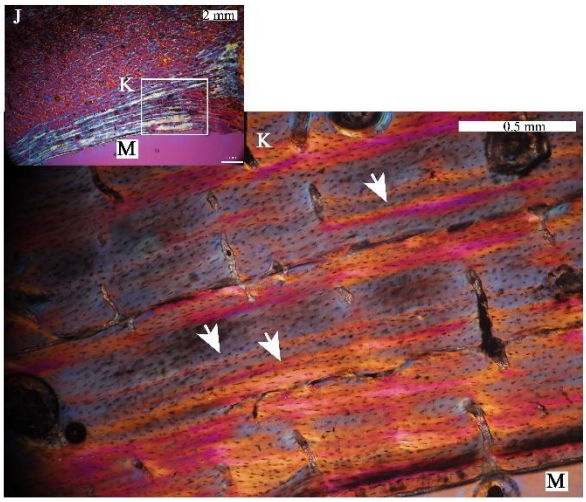
J
2 mm
K
M
K
0.5 mm
M

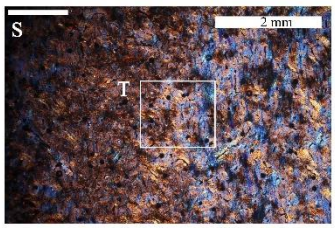
S
2 mm
T

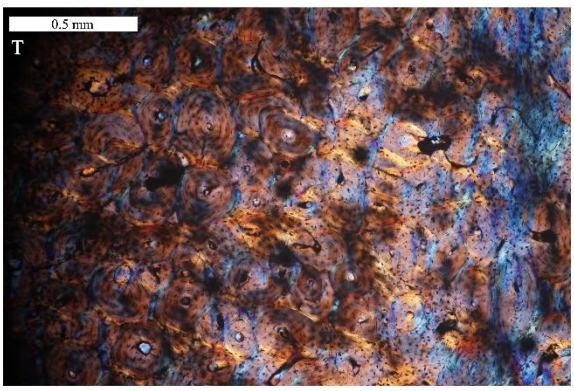
0.5 mm
T

Figure 3.3: Humeral cortical bone tissues in the adults of *Giraffa camelopardalis*. Microanatomy for the cross-section of the adult humeri, (A) BH3 ♀, showing cortical wall enclosing a medullary cavity with extensive cancellous bone tissue. (B) BH6 ♀, showing cortical wall enclosing a partially vacant medullary cavity with trabeculae. (C) BH5 ♂, cortical wall enclosing a partially vacant medullary cavity, (D) BH8 ♂, showing cortical wall enclosing an open medullary cavity. Frames indicated regions for which higher magnification images are provided. (E) Higher magnification of the framed region (A) showing extensive cancellous bone tissue in the perimedullary region. (F) Higher magnification of framed region (E) showing lamellar bone lining the cancellous bone tissue. (G) Higher magnification of framed region (D) showing cancellous bone in the caudal region of BH6. (I) Higher magnification of framed region in (H) showing lamellar bone tissue lining cancellous bone. (K) Higher magnification of the framed region in (J) showing rest lines (white arrows) in the lamellar bone lining the medullary cavity. Growth marks (white arrows) in the peripheral region of the adult humeri pictured in (L-R). (T) Higher magnification of (S) showing secondary osteons in cortical bone.

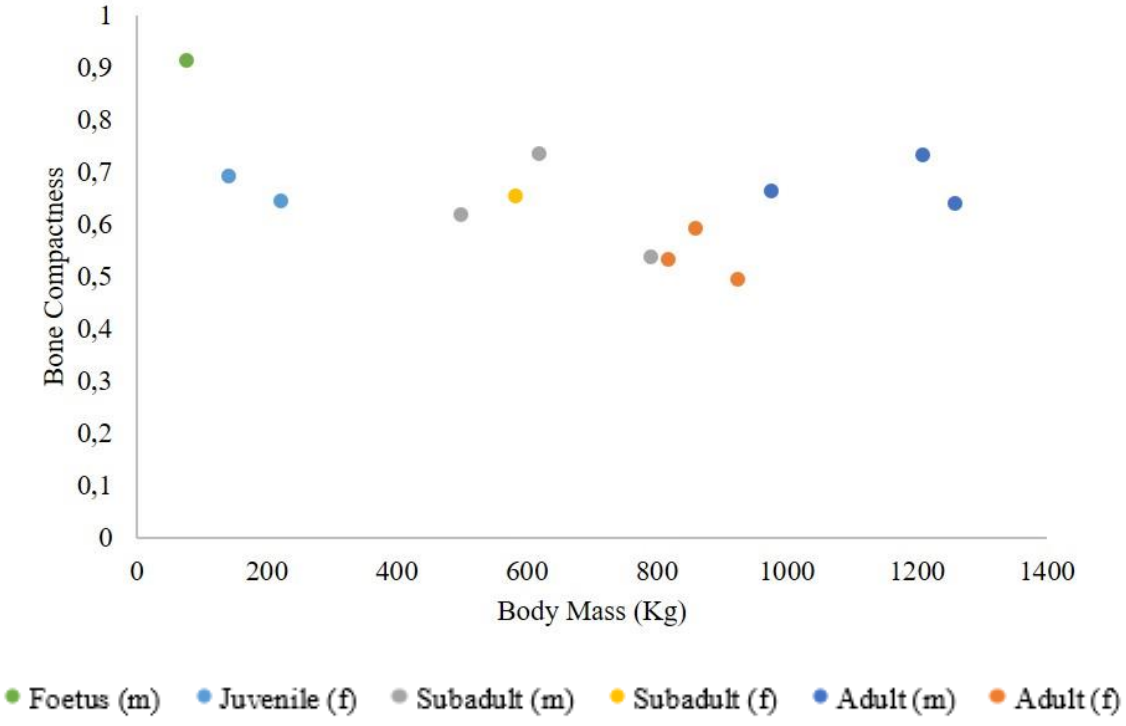

Figure 3.4: Bone profiler data (bone compactness) of the humeri plotted against the body mass (kg) of giraffe metacarpals (m is male, f is female). Table 3.2, Table A.1

3.2 Microanatomy and Histology of the Radii

3.2.1 Foetus

The midshaft cross section of the radius of the foetus is approximately circular in shape (Fig. 3.5A), with an unevenly thick bone wall in which the thickest part (measuring ~13mm) is on the medial side (Table A.2), while the narrowest region on the caudal side measures ~6.5mm. The medullary cavity is vacant except for some trabeculae organised circumferentially along the inner edge of the bone wall (Fig. 3.5B, 3.5C). Active resorption of the bone formed during earlier stages of ontogeny is evident in the perimedullary region (Fig. 3.5C). The periosteal margin of the bone wall has a rather spongy texture since it is at an early stage of FLB bone formation i.e., the woven bone matrix has formed, but the lamellar bone deposits around the lumen of the vascular canals are still in the process of being deposited (Fig. 3.5D , 3.5E). On the cranial edge of the radius, a small section of the ulna has been fortuitously sectioned. The region of fusion appears to be lamellar bone tissue (Fig. 3.5F).

3.2.2 Juvenile

The midshaft cross section of the radii of the juveniles tend to have a more or less circular shape (Fig. 3.5G, 3.5H), but they are slightly wider along the medial-lateral plane. The thickness of the bone wall measures on average about (~5-12 mm) (Table A.2) and surrounds an open medullary cavity. Remodeling of the internal cortex has been extensive, and only remnants of the earlier formed primary bone tissue extends into the medullary cavity as trabeculae (Fig. 3.5I, 3.5J). It is evident that the bone tissue closest to the medullary cavity (including that of the trabeculae) comprises of reticular FLB. On the medial side of the bone wall of the radius of one juvenile, there appears to be a stratification of the cortex (Fig. 3.5K) i.e. an inner zone consisting of circumferential vascular canals (Fig. 3.5L) and an outer zone consisting of reticular vascular canals (Fig. 3.5M). In the older juvenile (Fig. 3.5H), the cortical bone consists mainly of plexiform FLB tissue (Fig. 3.5N-3.5O). The perimedullary region of the bone wall has many large erosion cavities that give this region a cancellous appearance, indicated by white arrows (Fig. 3.5Q).

3.2.3 Subadult

The midshaft cross section of the radii of the subadults are more or less elliptical in shape, and tend to be wider along the medial-lateral plane (Fig. 3.6A-3.6C). They have comparatively thin bone walls (~7-19 mm) (Table A.2), which encloses a large medullary cavity. The endosteal margin of the bone wall is either lined with lamellar bone tissue or consists of laminar FLB tissue, or shows secondary reconstruction (Fig. 3.6D-3.6I). There is hardly any cancellous bone tissue in the perimedullary region, however numerous resorption

cavities occur in this region (Fig. 3.6D, 3.6E). The larger resorption cavities and several of the enlarged cancellous spaces are lined with lamellar bone tissue (Fig. 3.6 E). In Fig. 3.6F-3.6I, the lamellar bone tissue lining the medullary cavity appears to have rest lines. The main cortical bone, on the lateral and medial sides, appear to be secondary bone tissue, with many secondary osteons in the cortex (Fig. 3.6H, 3.6J). And in the midcortical to the peripheral zones of the cranial and caudal regions have circumferential vascular canals (Fig. 3.6K, 3.6L). The annuli found in the male (maximum 2) and female (maximum 4) subadults are mainly in the peripheral regions of the cranial, caudal, and medial sides (Table 3.1). Fig. 3.6L shows annuli in the cortex (arrows).

3.2.4 Adult

The midshaft cross section of the radii of the adults also tend to be elliptical in shape, although the caudal region of the bone wall tends to be flatter rather than curved (Fig. 3.7A-3.7D). The bone walls (~9-24 mm in thickness) (Table A.2) encloses a large mostly vacant medullary cavity. The structure of the perimedullary regions varies across the different specimens: The endosteal margin of Fig. 3.7A shows a number of resorption cavities (Fig. 3.7E), while two specimens (Fig. 3.7B , 3.7C, specimens BR5 and BR8) have no cancellous bone and their medullary cavities are lined with lamellar bone tissue (Fig. 3.7F). In BR5 (Fig. 3.7B), there is a layer of lamellar bone tissue—with rest lines— (Fig. 3.7I) and a layer of reticular FLB overlaying the lamellar bone tissue. (Fig. 3.7F-3.7I). Specimens that have cancellous bone often have lamellar bone tissue in the medial-cranial-lateral region of the perimedullary cavity (Fig. 3.7D). The cancellous spaces are lined with lamellar bone tissue (Fig. 3.7J-3.7K). The cortical bone has undergone extensive secondary bone remodeling (Fig. 3.7L-3.7O). Possible remnants of 3 or 4 growth marks in the lateral-cranial periphery are indicated between white brackets (Fig. 3.7L). The cortical bone has been extensively remodeled, as indicated by the presences of secondary osteons and resorption cavities (Fig. 3.7M-3.7O). Several resorption cavities are found distributed throughout the cortex, particularly in the peripheral zone of BR20 (Fig. 3.7O). In specimen BR20 a section of the ulna has been fortuitously sectioned with the radius. The periosteal margin of the ulna has a thin layer of lamellar bone tissue. Like the radius, the ulna is extensively reconstructed (Fig. 3.7P). Annuli were only observed in the cranial region of the female adult (Table 3.1).

3.2.5 Bone Profiler Data

The observed compactness for the radii shows that all the bones are similarly compact with values ranging between 0.6-0.9 (Table 3.2) Interestingly, an adult male, BR5, has the

highest compactness which is mainly due to the small size of the medullary cavity (Fig., 3.7B; Table 1) and the lack of cancellous bone tissue (Fig. 3.8).

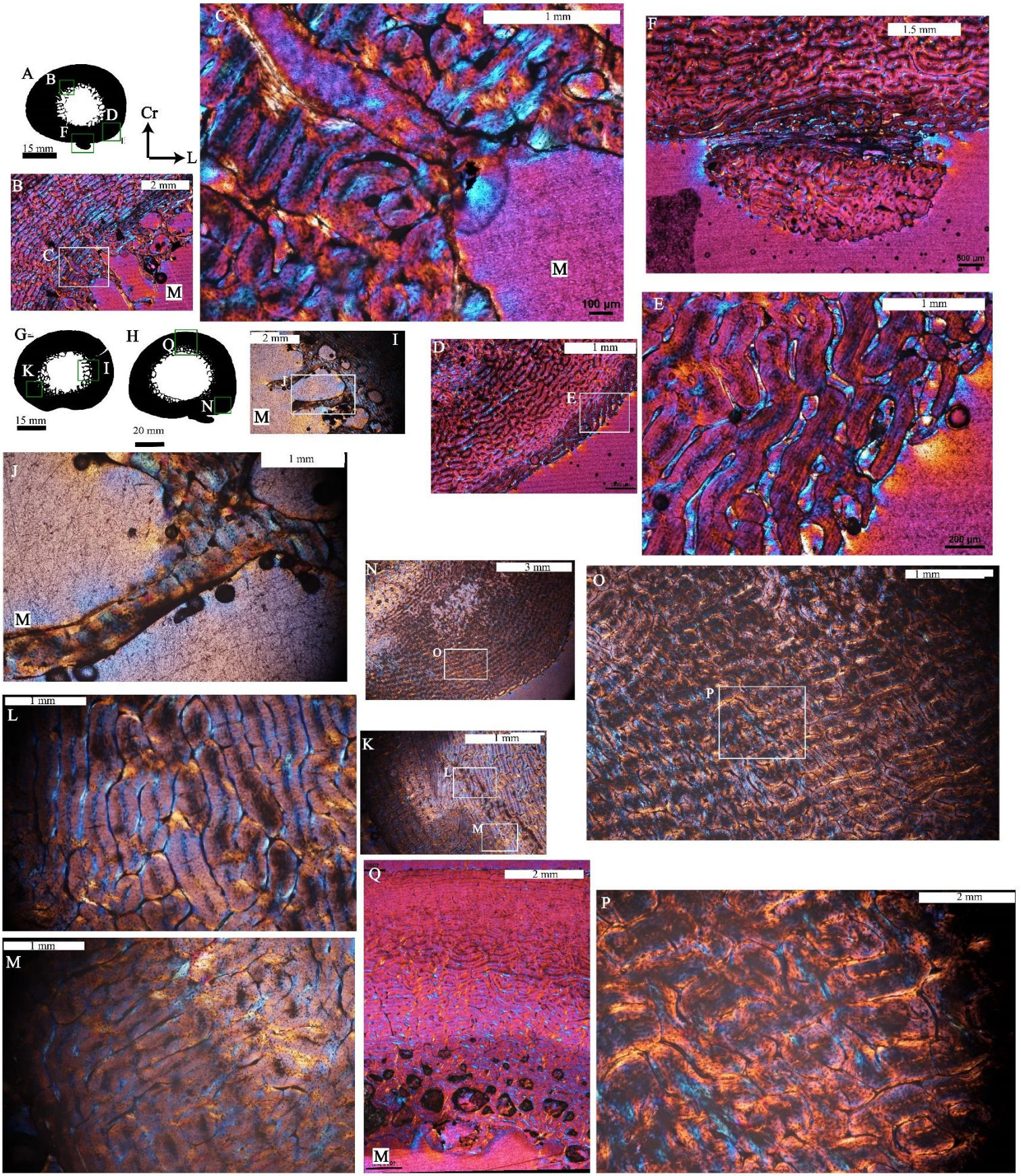

Figure 3.5: Cortical bone tissues of the radius of the foetus and juveniles of *Giraffa camelopardalis*. (A) Microanatomy for the cross-section of the foetal radius (BR14 ♂) showing the cortical bone wall enclosing a medullary cavity with trabeculae along the margins. (C) Higher magnification of the frame in (B) showing the compact bone tissue and the resorption evident in the perimedullary region. (D) Peripheral region in caudal section of cortex, (E) Higher magnification of (D) showing reticular FLB in the periosteal region. Note the large open lumen of the vascular canals (arrows) that give the overall spongy texture. (F) Shows the ulna (small arrow) that has been fortuitously sectioned. The area of fusion between the radius and the ulna consists of lamellar bone tissue (arrow), while the other parts of the bones consist of highly vascularised FLB. (G & H) Microanatomy of the cross-section of the juvenile radii (BR15 ♀ & BR2 ♀) showing the compacted cortical bone enclosing a medullary cavity with trabeculae extending into it. (I) Trabeculae in the perimedullary region comprises of FLB. (J) Higher magnification of the framed region in (I) showing lamellar bone tissue lining the trabeculae extending into the medullary cavity. (K) cortical bone in the medial region of the radius. (L & M) Higher magnification of the framed regions in (K) showing two distinct zones of FLB tissue occur in the medial region of the bone wall. (N) Low magnification of the caudal zone in (H). (O) Higher magnification of the framed region in (N) shows laminar FLB cortical bone in caudal region, and (P) Higher magnification of the framed region of laminar FLB in (O). (Q) Cranial region of (H) showing FLB cortical bone tissue and several resorption cavities (white arrows) in the perimedullary region. M, medullary cavity.

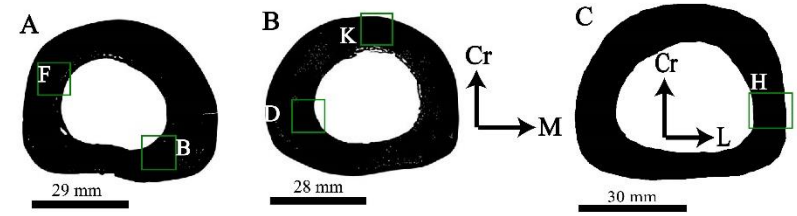
A
F
B
29 mm
B
K
D
28 mm
Cr
M
C
Cr
H
L
30 mm

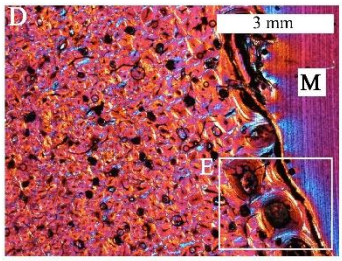
D
3 mm
M
E

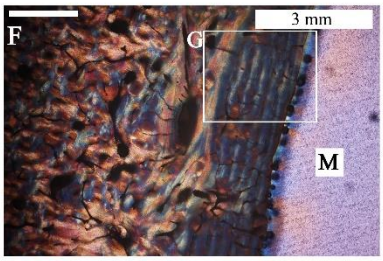
F
3 mm
G
M

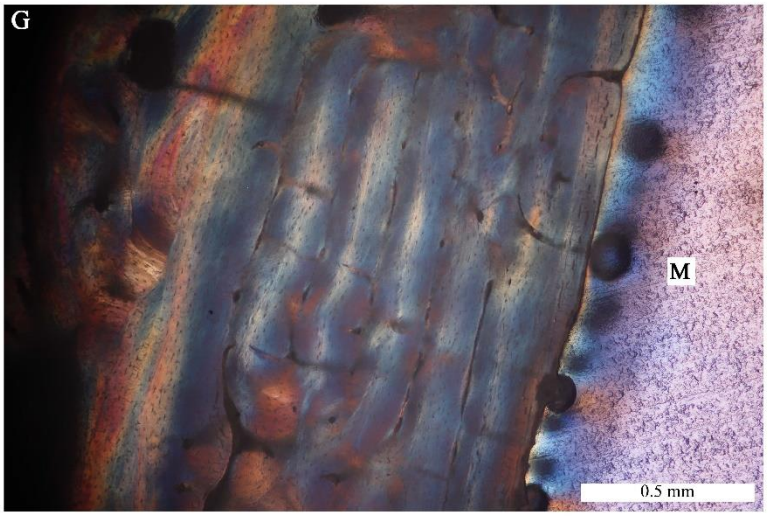
G
M
0.5 mm

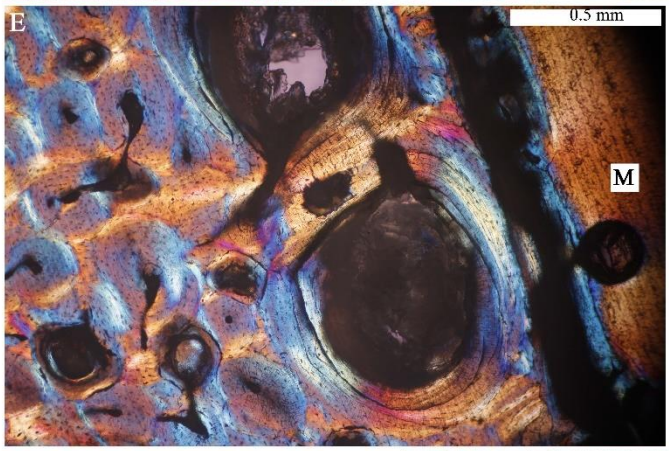
E
0.5 mm
M


I
0.5 mm
M

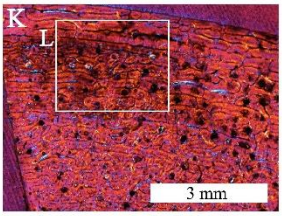
K
L
3 mm

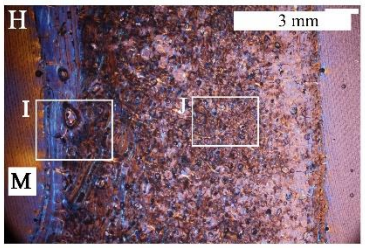
H
3 mm
I
J
M

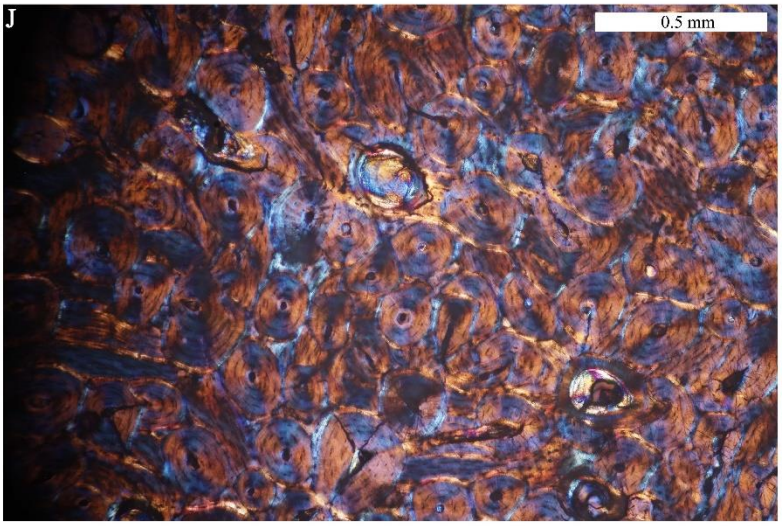
J
0.5 mm

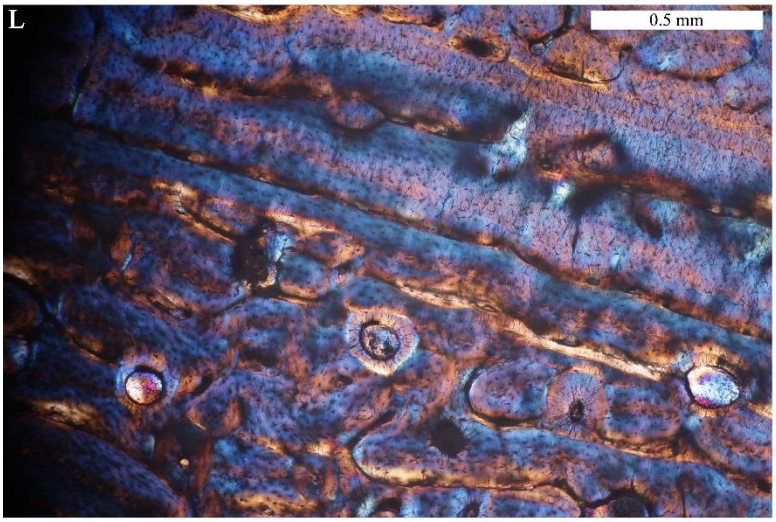
L
0.5 mm

Figure 3.6: Cortical bone tissues of the radius of the subadults of *Giraffa camelopardalis*. Microanatomy of the cross-section of the subadult radii, showing a thick band of cortical bone enclosing a large vacant medullary cavity (A) BR1 ♀, (B) BR4 ♂, (C) BR10 ♂. Frames indicate regions for which higher magnification images are provided. (D) Higher magnification of the endosteal region of (B). (E) Higher magnification of the framed region in (D) showing the lamellar bone lining the medullary cavity and resorption cavities. (F) Shows the medial endosteal margin. (G) Higher magnification of the framed region in (F) shows lamellar bone tissue lining the medullary cavity. (H) Cortical bone tissue in lateral region. (I) Higher magnification of the framed region in (H) showing lamellar bone lining the medullary cavity, with rest lines interrupting the lamellar growth. (J) Secondary osteons in the cortical bone tissue. (K) Higher magnification of cranial region. (L) Higher magnification of framed region in (K) showing lamellar bone tissue, with annuli (white bracket) interrupting the FLB deposition.

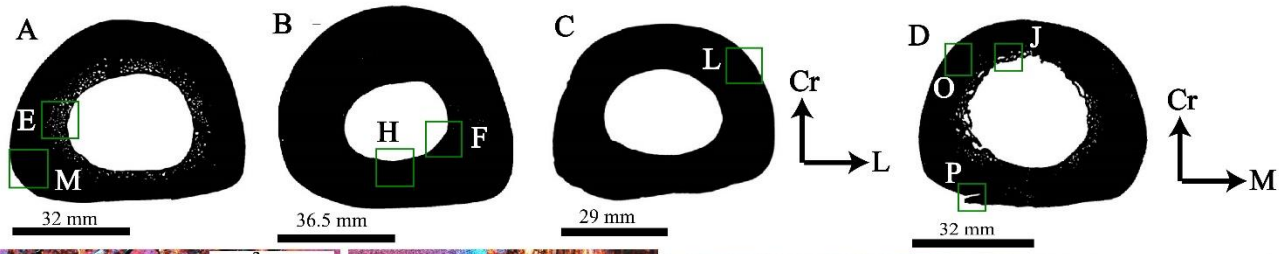
A
E
M
32 mm
B
H
F
36.5 mm
C
L
Cr
L
29 mm
D
J
O
P
Cr
M
32 mm

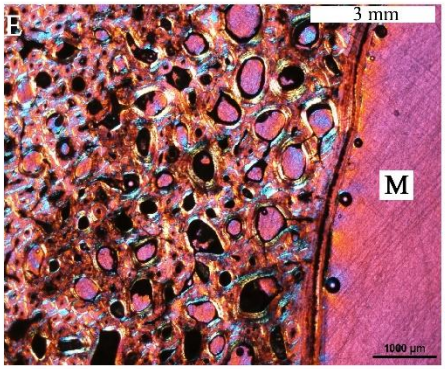
E
3 mm
M
1000 µm

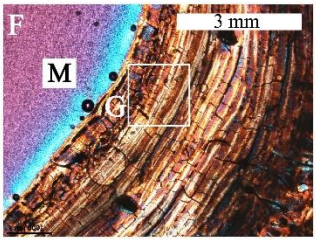
F
3 mm
M
G


0.5 mm
G

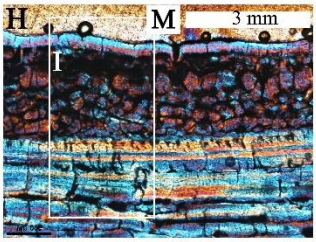
H
M
3 mm
I

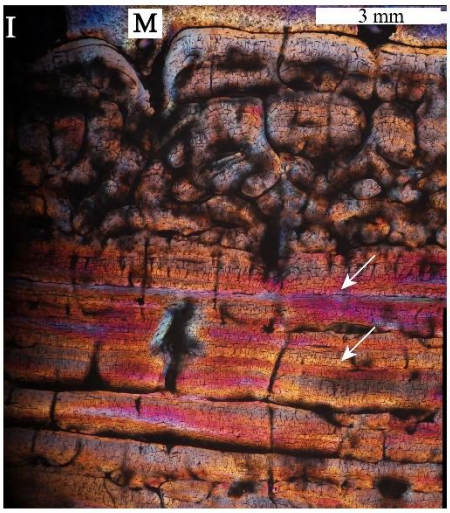
I
M
3 mm

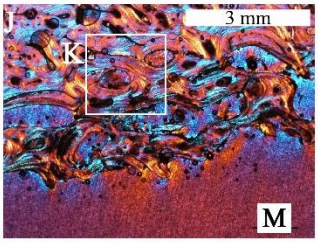
J
3 mm
K
M

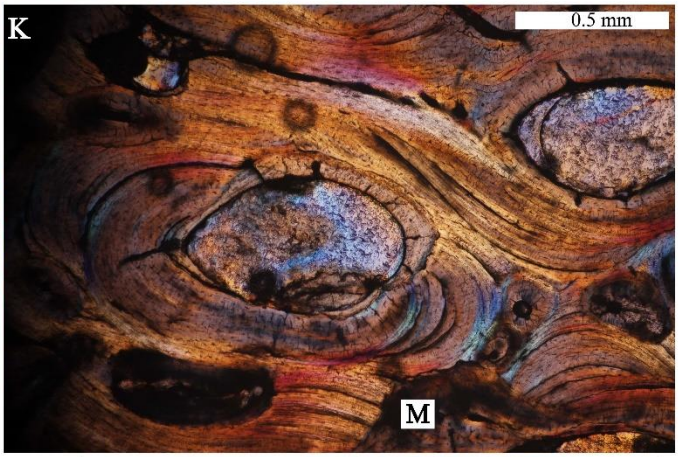
K
0.5 mm
M

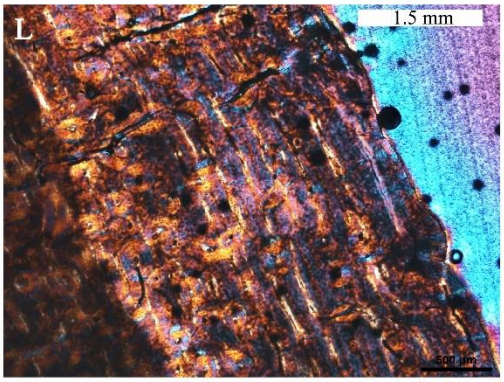
L
1.5 mm

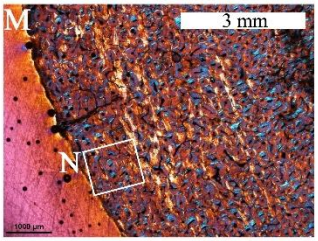
M
3 mm
N

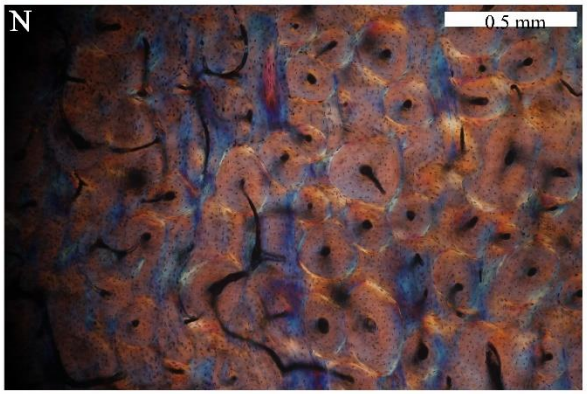
N
0.5 mm

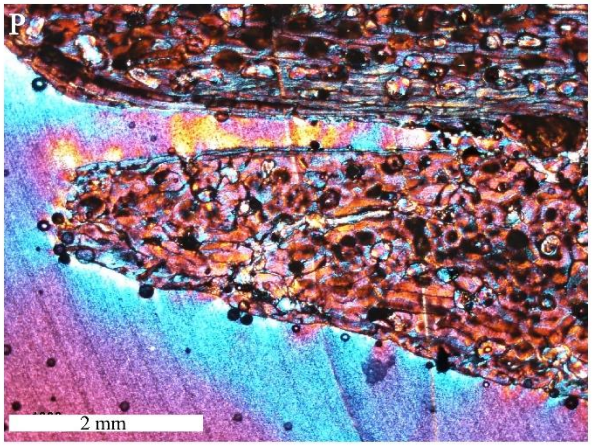
P
2 mm

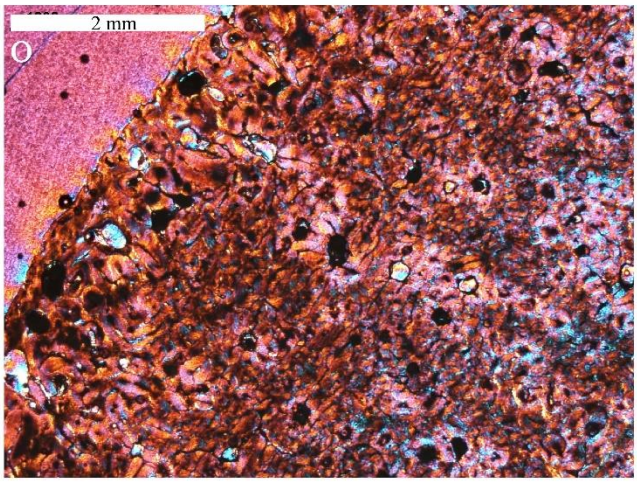
2 mm
O

Figure 3.7: Cortical bone tissues of the radius of the adults of *Giraffa camelopardalis*. Microanatomy of the cross-section of the adult radii, showing cortical bone enclosing a large vacant medullary cavity, (A) BR3 ♀, (B) BR5 ♂, (C) BR8 ♂. (D) BR20, showing a mostly compacted bone wall enclosing a central vacant medullary cavity. Frames indicated regions for which higher magnification images are provided. (E) Higher magnification of framed region in (A) showing resorption cavities lined with lamellar bone tissue. (F) Showing the lateral endosteal margin. (G) Higher magnification of the framed region in (F) showing rest lines interrupting the lamellar bone tissue lining the endosteal margin. (H) Showing caudal endosteal margin. (I) Higher magnification of framed region in (H) showing reticular FLB nearest that medullary cavity (white bracket) overlaying lamellar bone tissue (white arrows). (I) Extensive remodeling of the cortical bone in the region. (J) Showing the cranial endosteal margin of cancellous bone tissue (K) Higher magnification of the framed region in (J) showing lamellar bone tissue lining the resorption cavities. (L) Showing laminar FLB along the peripheral margin of the bone wall (white brackets). (M) Showing the medial periosteal margin. (N) Higher magnification of the framed region in (M) showing secondary osteons in the peripheral zone of the cortex. (O) Lateral periosteal region of cortex showing secondary bone tissue with resorption cavities (arrows). (P) Caudal region there is a section of the ulna that has been fortuitously sectioned. The area of fusion between the radius and the ulna shows a thin layer of lamellar bone tissue (arrow), while the ulna consists of secondary osteons and resorption cavities.

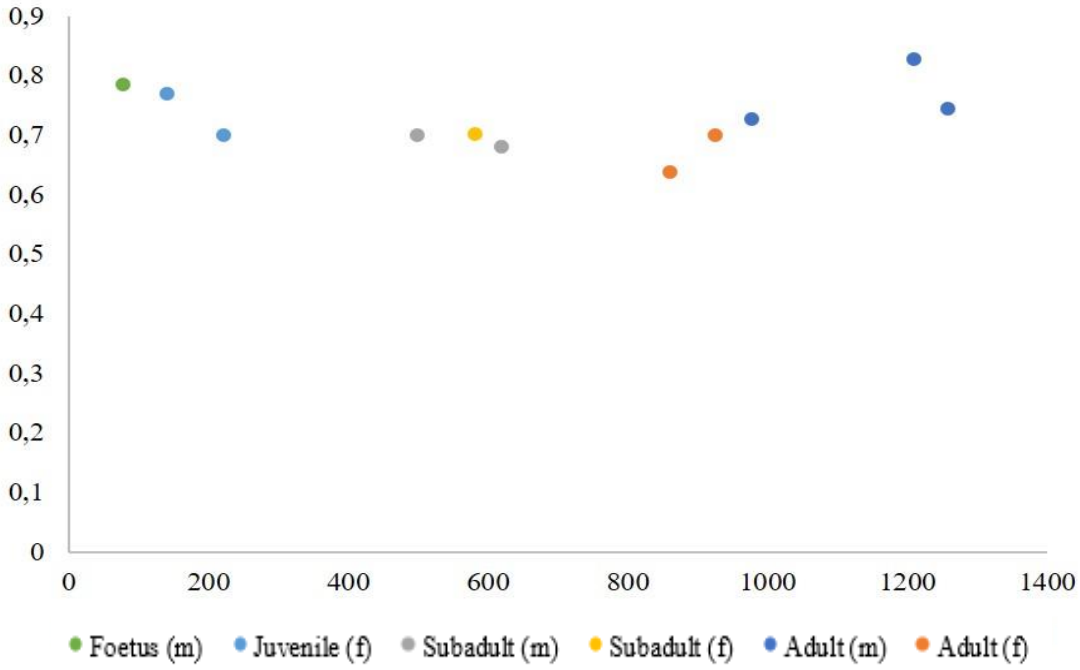

Figure 3.8: Bone profiler data (bone compactness) of the radii plotted against the body mass (kg) of giraffe metacarpals (m is male, f is female). Refer to data Table 3.2, Table A.1

3.3 Microanatomy and Histology of the Metacarpals

The cross sections of the metacarpals are distinct in that the medullary cavity appears to be bisected by a band of primary bone tissue. Closer inspection of the bone tissues revealed that the unusual microanatomy is the result of the fusion of metacarpal III and IV (Fig. 3.9A, 3.9F, 3.9G). The cross sections of the separate metacarpals are clearly visible with each having their own distinctive medullary cavities. Overall, the bone wall of the cross section of the fused metacarpal is unevenly thick with the thickest part of the compacta in the cranial region, whilst the thinnest bone wall is in the caudal region in the vicinity of the fusion (Table A.2). In the foetal and juvenile bones, it should be noted however, that the lateral bone wall of metacarpal III and the medial bone wall of metacarpal IV are the thinnest, but they have become fused and now bisect the joined medullary cavities (Fig. 3.9). The region of fusion has an unusual structure in that it forms a distinct band of FLB tissue that runs from the cranial to the caudal region (Fig. 3.9A, 3.9F, 3.9G, 3.9I)

3.3.1 Foetus

The fused midshaft cross section of the metacarpal of the foetus is circular in shape and has an uneven cortical wall thickness (~5-12mm) (Table A.2). The small medullary cavity of MC III and IV are clearly visible and separated by a band of bone tissue that represents the merged medial and lateral walls of MC III and IV respectively. (Fig. 3.9A). The periosteal margins are clearly in a state of active osteogenesis (Fig. 3.9B, 3.9C), while the perimedullary margins of both the separate medullary cavities are highly resorptive (Fig. 3.9E). Overall, the bone wall comprises of highly vascularised reticular FLB tissue (Fig. 3.9D).

3.3.2 Juvenile

The midshaft cross section of the metacarpals of the juveniles are circular in shape (Fig. 3.9F, 3.9G). Overall, the cortical wall of the fused metacarpal ranges from ~4-9 mm (Table A.2). The region of fusion of metacarpal III and IV is substantially reduced in thickness as compared to the foetus, and there appears to be a distinct compaction of the original medial and lateral bone walls of the separate MC III and IV, and the vascular canals increasingly become more laminar (Fig. 3.9H, 3.9I) in organization. The periosteal region of the bone wall comprises of plexiform FLB that is being actively formed (Fig. 3.9J). The endosteal margin is uneven and indicates active resorption of the bone tissue (Fig. 3.9K). In the older juvenile (Fig. 3.9G), the cortical bone tissue is predominately reticular FLB (Fig. 3.9L, 3.9M).

3.3.3 Subadult

At this stage all traces of the independent MC III and IV are not visible. The midshaft cross section of the metacarpals of the subadults are circular in shape (Fig. 3.10A, 3.10B,

3.10C). The cortical wall is evenly thick (~11-17 mm), except for the caudal region which has the thinnest part of the bone wall (~5-7 mm) (Table A.2). Only one of the four subadults metacarpals studied has cancellous bone present in the perimedullary region of the cranial part of the bone wall (Fig. 3.10A, 3.10D, 3.10E). The cancellous spaces are lined with lamellar bone tissue (Fig. 3.10E). The periosteal margin of the caudal region is uneven, and consists of early stages of FLB tissue (Fig. 3.10F-3.10I). Specimen BMC23, (Fig. 3.10B) shows lower magnification of reticular FLB up to the endosteal margin (Fig. 3.10J). The predominant cortical bone tissue is reticular FLB (Fig. 3.10K), with small resorption cavities distributed throughout the cortex (Fig. 3.10K). In the metacarpal of the female (Fig. 3.10C) and one male (not pictured), the medullary cavity is lined with lamellar bone tissue with rest lines (white arrows) interrupting the lamellar deposition (Fig. 3.10M). The two other males (BMC23 and BMC28) do not have lamellar bone lining the medullary cavity.

3.3.4 Adult

At this stage all traces of the independent MC III and IV are not visible. The midshaft cross section of the metacarpals of the adults are more or less circular in shape with bone wall thickness measuring ~6-11 mm, and the thinnest region measuring ~4-11 mm, in the caudal region where the original two MC fused (Table A.2). (Fig. 3.11A, 3.11B, 3.11C). The cancellous bone tissue in the adults vary in quantity and distribution (Fig. 3.11D, 3.11E): this tissue tends to be present in the cranial region, and to a lesser extent on the medial and lateral sides. The cancellous bone appears to be formed as a result of resorption of pre-existing primary bone tissue (Fig. 3.11D, 3.11E). Several of the enlarged cancellous spaces, and resorption cavities, are lined by narrow bands of lamellar bone tissue. Specimen BMC6, (Fig. 3.11C) has no cancellous bone tissue, but many resorption cavities are present in the cranial region. The cortical bone tissue in all the adults are highly remodeled, with many secondary osteons present and resorption cavities (Fig. 3.11F, 3.11G, 3.11K). The periosteal margin is uneven and it appears to still be actively growing (Fig. 3.11H, 3.11I). The endosteal margin of the caudal region of specimen BMC4 (Fig. 3.11J) is lined with lamellar bone tissue.

3.3.5 Bone Profiler Data

The observed compactness for the metacarpals shows that all the bones observe a similar compactness, ranging between 0.7-0.9 compactness (Fig. 3.12, Table 3.2).

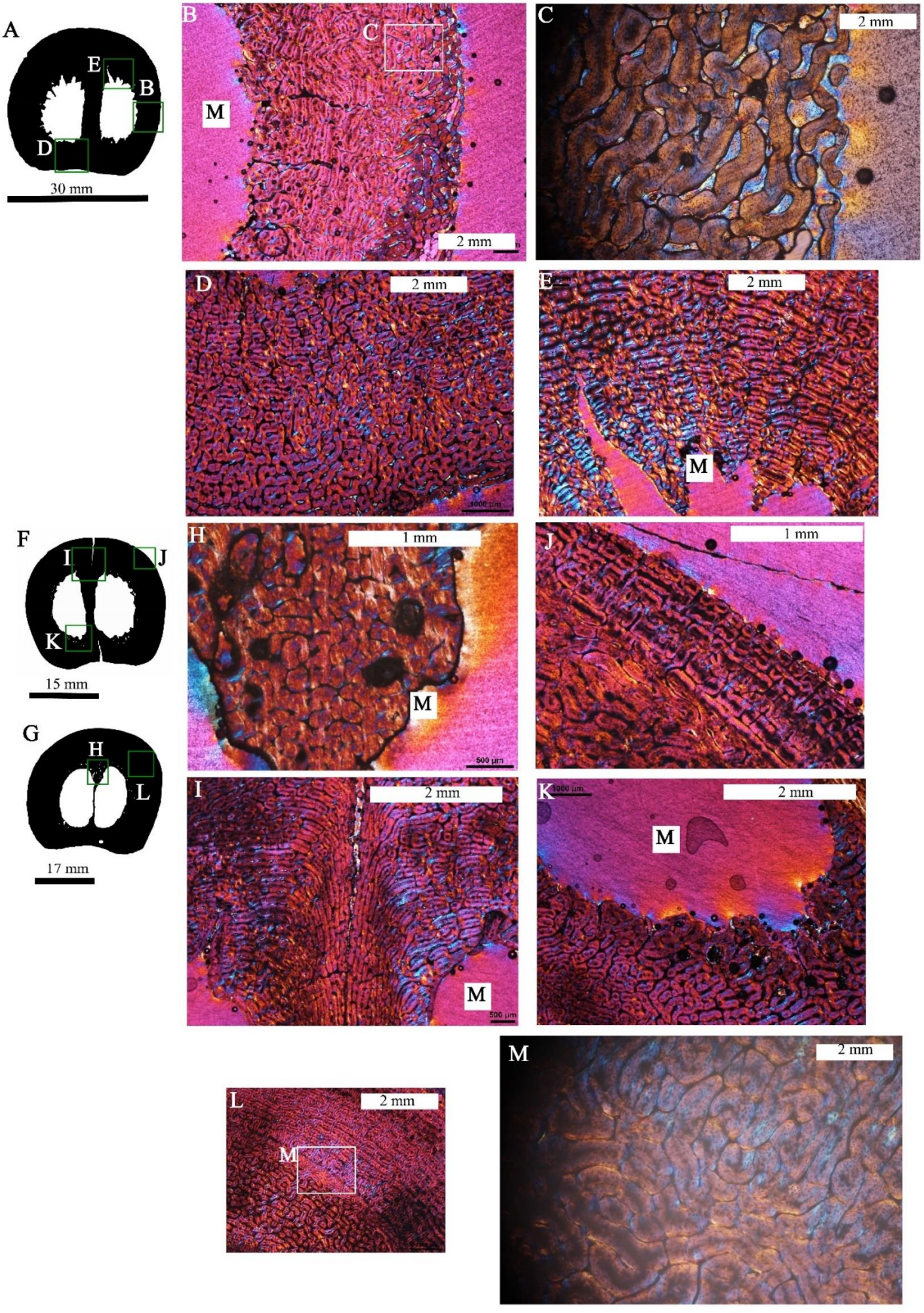
A
E
B
D
30 mm
B
C
M
2 mm
C
2 mm
D
2 mm
E
2 mm
M
F
I
J
K
15 mm
H
1 mm
M
500 µm
J
1 mm
G
H
L
17 mm
I
2 mm
M
500 µm
K
1000 µm
2 mm
M
L
2 mm
M
M
2 mm

Figure 3.9: Metacarpal cortical bone tissues in the foetus and juveniles of *Giraffa camelopardalis*. Microanatomy for the cross-section of the foetal metacarpal, (A) BMC46 ♂, fused metacarpals III and IV showing the cortical wall enclosing two vacant medullary cavities. Frames indicated regions for which higher magnification images are provided. (B) Cortical wall of metacarpal IV. (C) Higher magnification of the framed region in (B) showing highly vascularised reticular FLB and uneven endosteal and periosteal margins. (D) Highly vascularised cortical bone caudal and (E) cranial regions. Microanatomy for the cross-section of the juvenile metacarpals. (F) BMC47 ♀ and (G) BMC2 ♀, showing a band of compacted cortical bone enclosing two vacant medullary cavities that are separated by a 'column" of primary bone tissue. (H & I) Region of fusion of MCIII and MCIV. (J) Plexiform FLB in the periosteal region (white bracket). (K) Highly vascularised FLB in the endosteal region of the cortex. (L) Showing cranial cortical bone tissue. (M) Higher magnification of framed region in (L) showing reticular FLB.

Figure 3.10: Metacarpal cortical bone tissues in the subadults of *Giraffa camelopardalis*. Microanatomy for the cross-section of the subadult metacarpals, (A) BMC1 ♀, (B) BMC23 ♂, and (C) BMC 33 variably thick cortical wall enclosing a vacant medullary cavity. Frames indicated regions for which higher magnification images are provided. (D) Showing the cranial endosteal region. (E) Higher magnification of the cancellous bone framed in (D) showing lamellar bone tissue lining the cancellous spaces. (F) Showing periosteal region of (A). (G) Higher magnification of framed region in (F) showing spongy-texture of the early stages of FLB formation (white bracket). (H) Showing cranial periosteal zone. (I) Higher magnification of framed region in (H) showing plexiform FLB tissue. (J) Showing cranial endosteal region. (K) Higher magnification of framed region in (J) shows highly vascularised FLB and scattered resorption cavities (white arrows). (L) Showing cranial endosteal region. (M) Higher magnification of framed region in (L) showing lamellar bone tissue interrupted by rest lines (white arrows).

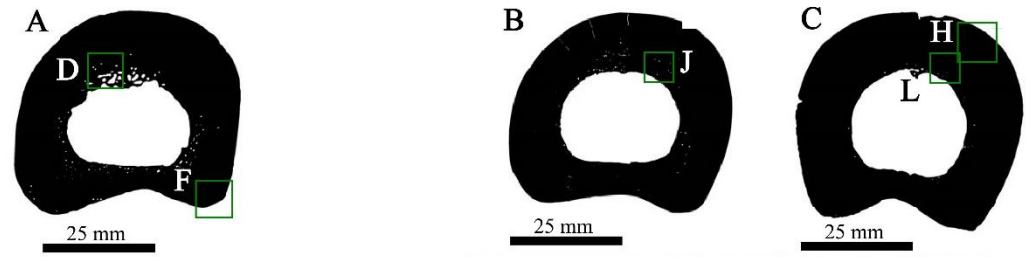
A
D
F
25 mm
B
J
25 mm
C
H
L
25 mm

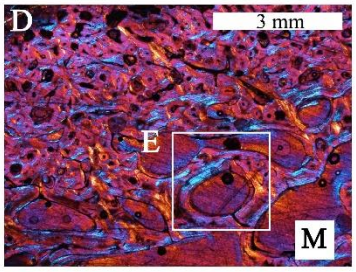
D
3 mm
E
M

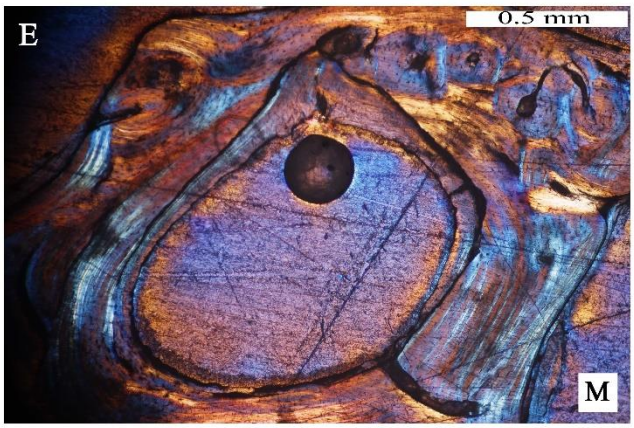
E
0.5 mm
M

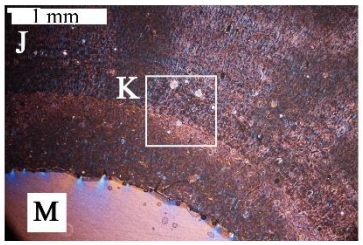
1 mm
J
K
M

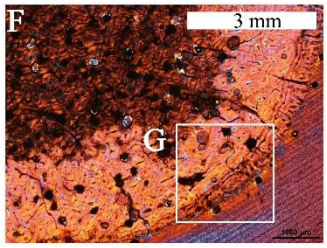
F
3 mm
G

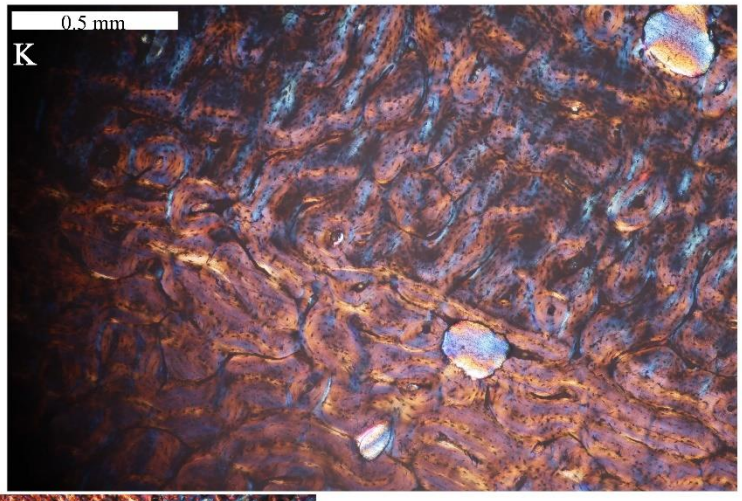
0.5 mm
K

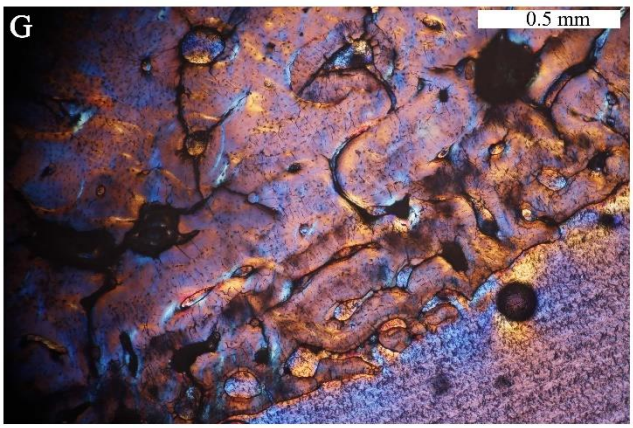
G
0.5 mm

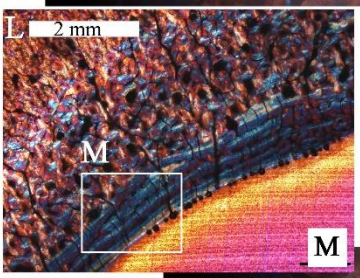
L
2 mm
M
M

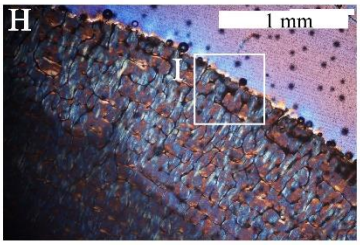
H
1 mm
I

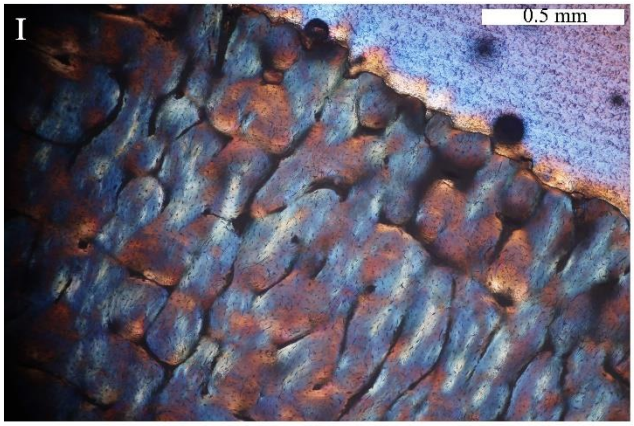
I
0.5 mm


M
3 mm
M

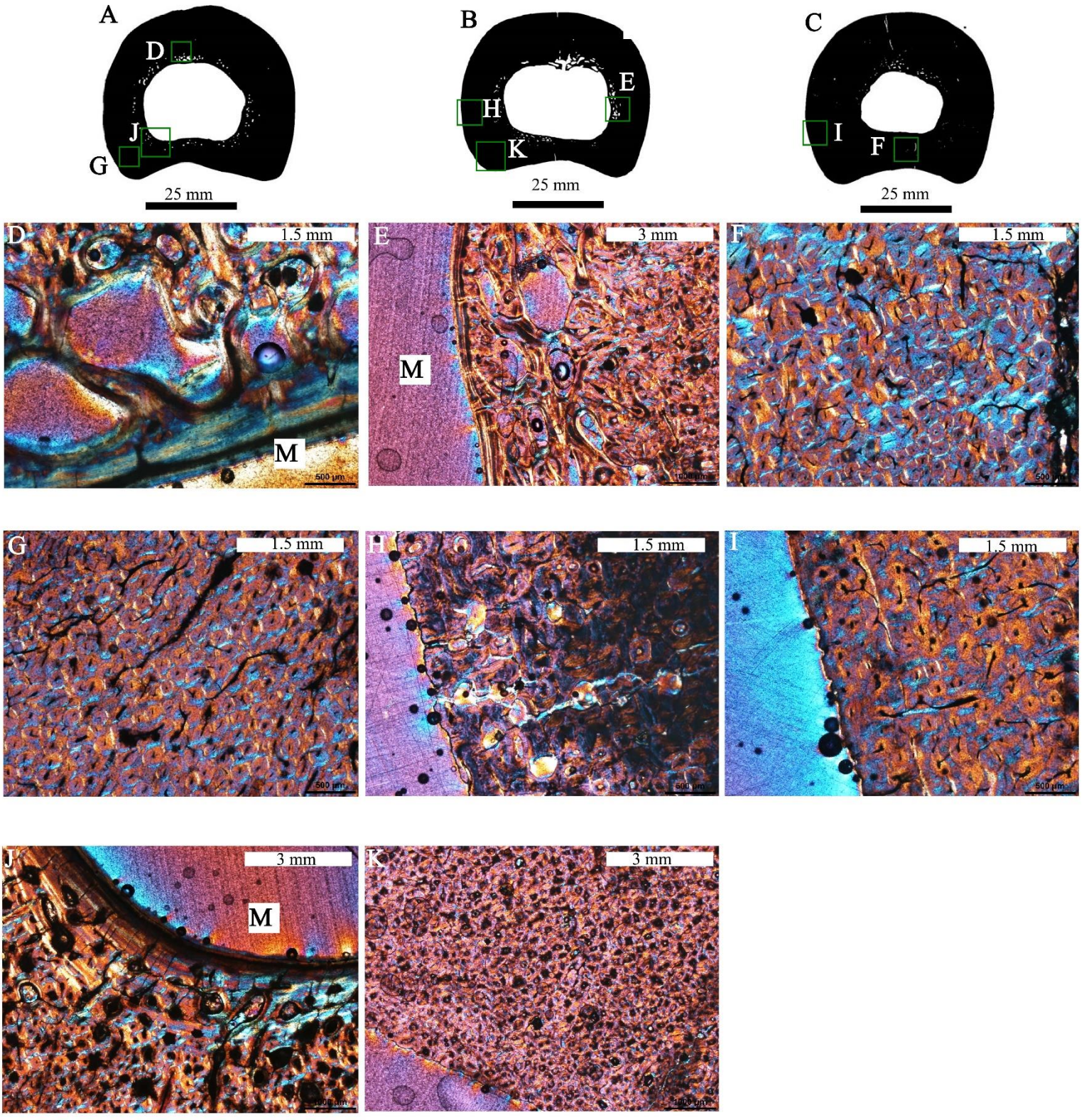
A
D
J
G
25 mm
B
E
H
K
25 mm
C
I
F
25 mm
D
1.5 mm
M
500 µm
E
3 mm
M
F
1.5 mm
G
1.5 mm
H
1.5 mm
I
1.5 mm
J
3 mm
M
K
3 mm

Figure 3.11: Metacarpal cortical bone tissues in the adults of *Giraffa camelopardalis*. Microanatomy for the cross-section of the adult metacarpals, (A) BMC 4 ♀, (B) BMC 6 ♂, and (C) BMC 16 ♂, showing cortical wall enclosing a vacant medullary cavity. Frames indicate regions for which higher magnification images are provided. (D) Higher magnification of framed region in (A) shows lamellar bone lining the medullary cavity and resorption cavities just preceding this region. (E) Higher magnification of framed region in (B) showing lamellar bone lining the resorption cavities in the perimedullary cavity. (F) Secondary remodeling of the cortical bone tissue nearest the original fusion part of the metacarpals III and IV. (G) Secondary osteons in the caudal region of (A). (H & I) Higher magnification of the framed regions in (B & C) showing a partially uneven periosteal margin due to secondary remodeling of the bone tissue. (J) Higher magnification of caudal endosteal region framed in (A) showing lamellar bone tissue lining the medullary cavity. (K) Heavily remodeled cortical bone in the caudal part of the bone wall.

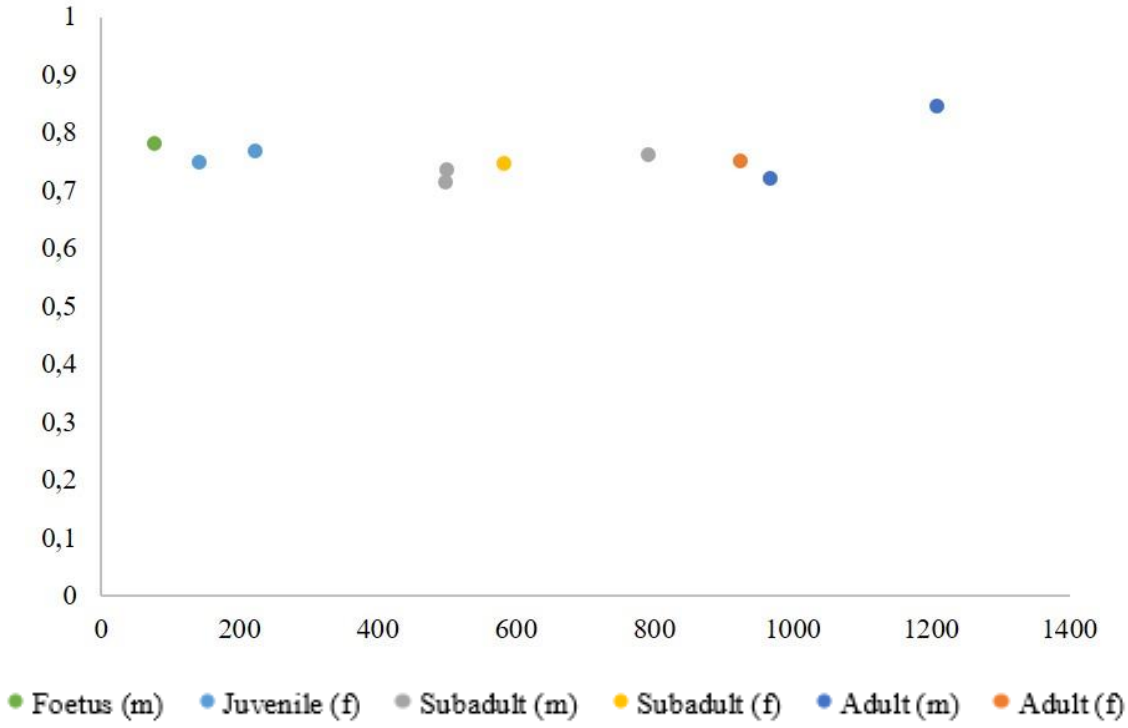

Figure 3.12: Bone profiler data (bone compactness) of the metacarpals plotted against the body mass (kg) of giraffe metacarpals (m is male, f is female). Refer to data Table 3.2, Table A.1

3.4 Microanatomy and Histology of the Femora

3.4.1 Foetus

The midshaft cross section of the femur of the foetus is oval in shape (with the longer axis being along the caudal-cranial plane) and encloses a vacant medullary cavity (Fig. 3.13A). The cortical wall on the lateral side is thinner (~6 mm) than the medial side (~13 mm) (Table A.2). Active resorption of the early bone tissue is evident in the perimedullary region (Fig. 3.13B). The peripheral region of the bone wall is highly vascularised, and the newer bone tissue here appears to be plexiform fibrolamellar bone tissue (Fig. 3.13C). The periosteal margin is spongy-textured and shows the early stages of fibrolamellar bone formation in this region (Fig. 3.13C).

3.4.2 Juvenile

The midshaft cross section of the femora of the juveniles are elliptical in shape (Fig. 3.13D, 3.13E) being elongated in the cranial-caudal plane. The average cortical wall thickness is between ~6-10 mm (Table A.2). The perimedullary region of the bone wall shows extensive erosion, and it is evident that this region of the bone wall has been resorbed to form large cancellous spaces (Fig. 3.13D, 3.13E). Some remnants of the original primary bone tissue extend into the medullary cavity as trabeculae (Fig. 3.13F, 3.13H). However, not all the trabeculae consist of primary bone tissue; some are lined with lamellar bone tissue (Fig. 3.13G, 3.13I). In juvenile BF15, there are two distinct zones in medial-caudal side of the bone wall (Fig. 3.13J). Higher magnification of Fig. 3.13J shows that the bone tissue in the peripheral region consists of more radial FLB (Fig. 3.13K), while the bone tissue underlying this tissue is a mixture of laminar and reticular FLB (Fig. 3.13L). In the older juvenile, specimen BF2, the peripheral bone tissue is laminar FLB. The cortical bone tissue in both juveniles is predominately a mixture of laminar and reticular FLB, in both the lateral and medial sides (Fig. 3.13N-3.13P).

3.4.3 Subadult

The midshaft cross section of the femora of the subadults are generally more elliptical in shape (with the larger diameter in the cranial-caudal plane) (Fig. 3.14A, 3.14B) with a large medullary cavity. The average cortical wall thickness is between ~10-22 mm (Table A.2). Cancellous bone tissue is only found in the cranial and caudal endosteal regions (Fig. 3.14A). Nearest the medullary cavity, cancellous spaces are lined with lamellar bone tissue (Fig. 3.14C, 3.14D). The endosteal regions of the medial-lateral parts of the bone wall are either unlined (Fig. 3.14E, 3.14F) or have lamellar bone tissue (Fig. 3.14G). BF1 has vascularised lamellar bone, and the cancellous bone tissue, in all four specimens, is lined with lamellar bone is

vascularised. The periosteal margin in the caudal regions are uneven, and there appears to be extensive secondary reconstruction in the cortex as indicated by the presence of secondary osteons right up to the periosteal surface (Fig. 3.14H, 3.14I). The peripheral regions on the medial and lateral sides have laminar FLB tissue (Fig. 3.14J). Three to four annuli found in male subadults (BF10 and BF4) tend to be located in the peripheral parts of the cranial and medial region of the cortex (Table 3.1). The female subadult BF1, did not exhibit growth marks. BF11 (Z51) shows a possible (thin) OCL in the cranial-lateral region.

3.4.4 Adult

The midshaft cross section of the femora of the adults are elliptical in shape, with the caudal region tapering to a point/apex (Fig. 3.15A, 3.15B, 3.15C). The average cortical wall thickness is between ~7-19 mm (Table A.2). Endosteal regions void of cancellous bone tissue are lined with lamellar bone tissue (Fig. 3.15D, 3.15E, 3.15F, 3.15I, 3.15H). Cancellous bone tissue is distributed mainly in the cranial and caudal regions (Fig. 3.15G). The cancellous bone appears to be formed as a result of resorption of pre-existing primary bone tissue. Several of the enlarged cancellous spaces are lined by narrow bands of lamellar bone tissue. The periosteal margin in the caudal region (Fig. 3.15J) has an uneven matrix of woven bone indicated between the white brackets. However, further in, the cortex is extensively remodeled with primary and secondary osteons present (Fig. 3.15K). BF3 (Fig. 3.15N), has a layer of lamellar bone tissue in the peripheral part of the compacta, which is an outer circumferential layer (OCL). The cortical bone tissue has extensive primary osteons with a couple of erosion cavities (Fig. 3.15P, 3.15Q). Annuli are present (~4 in the female and ~5-8 in males) in the peripheral regions of the cranial and medial parts of the of the bone wall (Fig. 3.15L, 3.15M, 3.15O; Table 3.1).

3.4.5 Bone Profiler Data

The observed compactness for the femora shows that the foetal bone has the compactnss index is relatively smilar among all of the bones, ranging between 0.5-0.8 compactness. It is perhaps curious that the female subadult (yellow) and adults (orange) have the lowest observed compactness 0.5-0.6 (Fig. 3.16, Table 3.20).

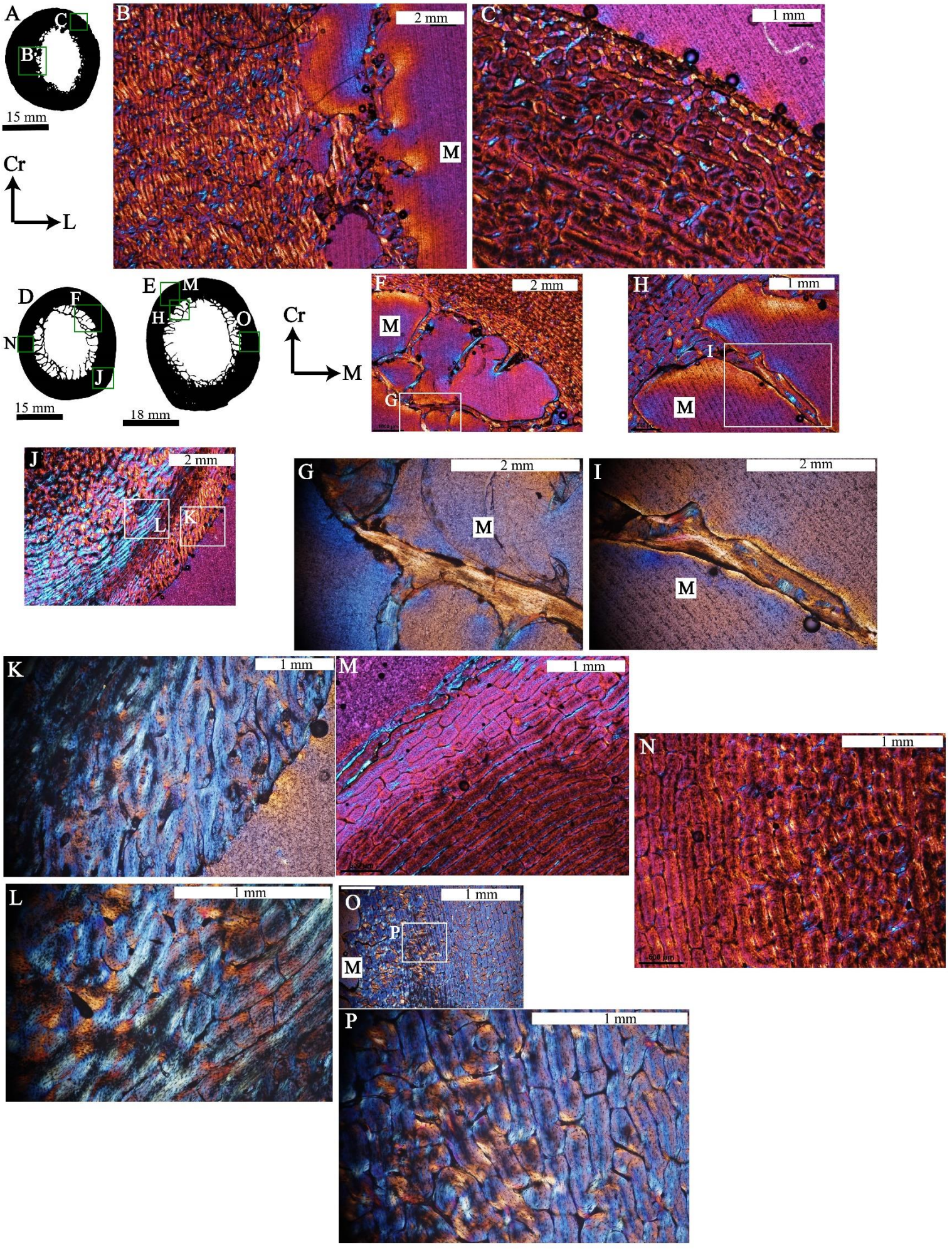
A
C
B
15 mm
Cr
L
B
2 mm
M
C
1 mm
D
F
N
J
15 mm
E
M
H
O
18 mm
Cr
M
F
2 mm
M
G
H
1 mm
I
M
J
2 mm
L
K
G
2 mm
M
I
2 mm
M
K
1 mm
M
1 mm
N
1 mm
L
1 mm
O
1 mm
P
M
P
1 mm

Figure 3.13: Femoral cortical bone tissues in the foetus and juveniles of *Giraffa camelopardalis* Microanatomy of the cross-section of the foetal femur, (A) BF14 ♂, showing a thick medial cortical wall and thin lateral cortical wall enclosing an open medullary cavity. Frames indicated regions for which higher magnification images are provided. (B) Higher magnification of the frame in (A) shows resorption cavities in the perimedullary region. (C) Higher magnification of the frame in (A) showing the osteogenic periosteal margin. Microanatomy for the cross-section of the juvenile femora. (D) BF15 ♀, and (E) BF2 ♀, showing cortical bone wall enclosing a medullary cavity surrounded by extensive cancellous bone and trabeculae. Frames indicated regions for which higher magnification images are provided. Note the perimedullary margin of the cross section has a cancellous texture. (F & H) Higher magnification of the frame in (D & E) showing cancellous bone in the perimedullary region. (G & I) The trabeculae comprise predominately FLB, however some trabeculae are showing lamellar bone. (J) Higher magnification of the caudal-lateral region shows two zones. (K) Outer more peripheral zone with a number of radial canals, and (L) an inner zone consisting of reticular vascular canals. (M) Laminar FLB in the peripheral region of the cortex. (N) Laminar FLB in the medial side of the bone wall. (O) Showing medial endosteal region. (P) Higher magnification of (O) showing FLB in the cortex.

Figure 3.14: Femoral cortical bone tissues in the subadult of *Giraffa camelopardalis* Microanatomy for the cross-section of the subadult femora, (A) BF1 ♂, showing cortical wall enclosing a partially vacant medullary cavity. (B) BF10 ♂, showing cortical wall enclosing a partially vacant medullary cavity. Frames indicated regions for which higher magnification images are provided. (C) Showing cancellous bone tissue in caudal region. (D) Higher magnification of framed region in (C) showing the caudal endosteal margin of the bone wall. Note the cancellous bone lined with lamellar bone (white arrow). (E) Showing caudal endosteal margin. (F) Higher magnification of framed region in (E) showing secondary osteons in the FLB. (G) Higher mag of the framed region in (A) showing lamellar bone tissue lining the medullary cavity on the medial side. Note the surprisingly well vascularized nature of this tissue. (H) Showing caudal periosteal region. (I) Secondary osteons right up to the periosteal margin. (J) Higher magnification of framed region in (B) showing laminar FLB in peripheral region of cortex. (K) Primary and secondary osteons in the caudal region of the bone cortex. (L) Showing cortical bone in cranial region. (M) Higher magnification of framed region in (L) showing a mixture of primary and secondary bone tissue in the cortex (white brackets).

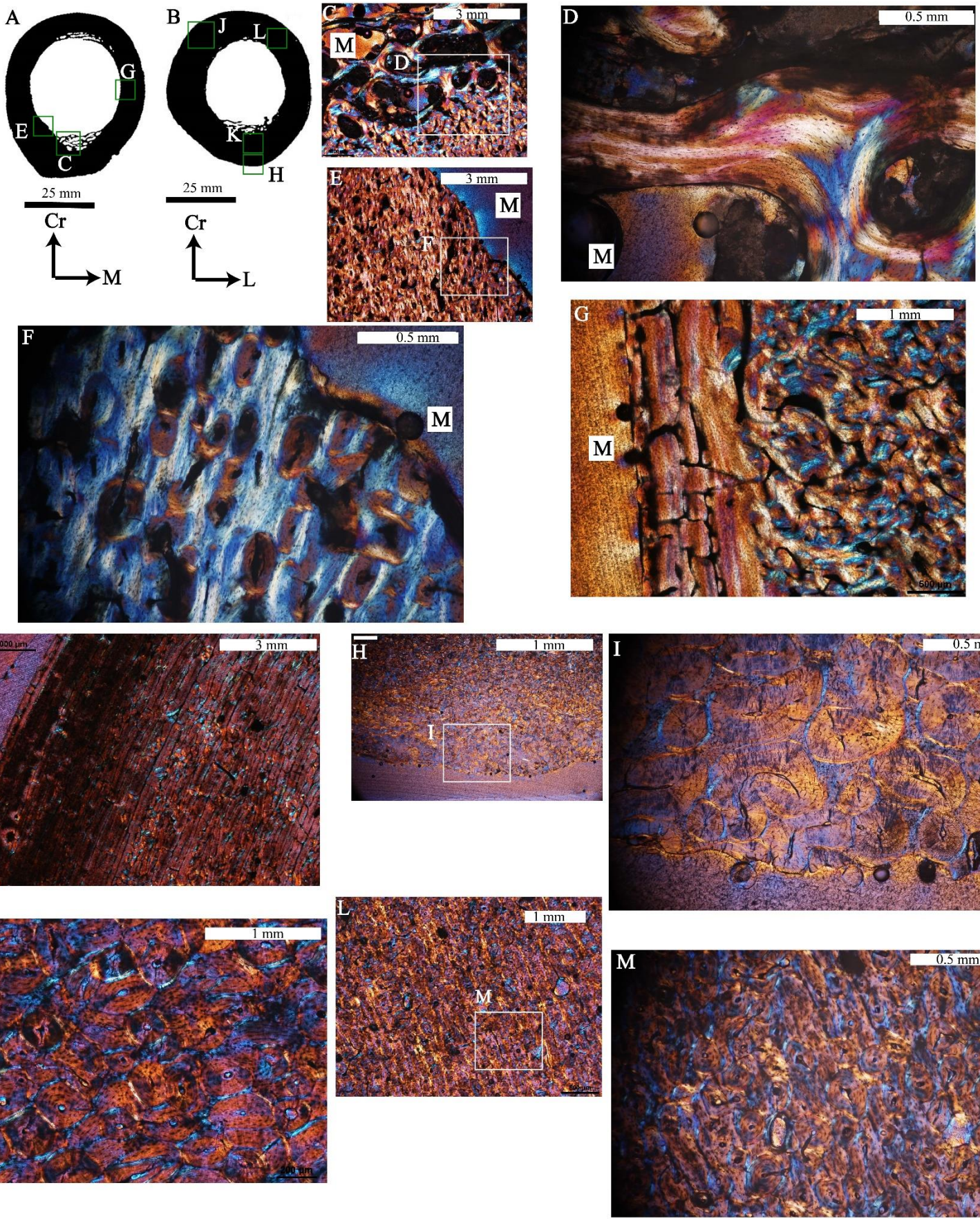
A
G
E
C
25 mm
Cr
M
B
J
L
K
H
25 mm
Cr
L
C
3 mm
M
D
D
0.5 mm
M
E
3 mm
M
F
F
0.5 mm
M
G
1 mm
M
500 µm
J
1000 µm
3 mm
H
1 mm
I
I
0.5 mm
K
1 mm
200 µm
L
1 mm
M
M
0.5 mm

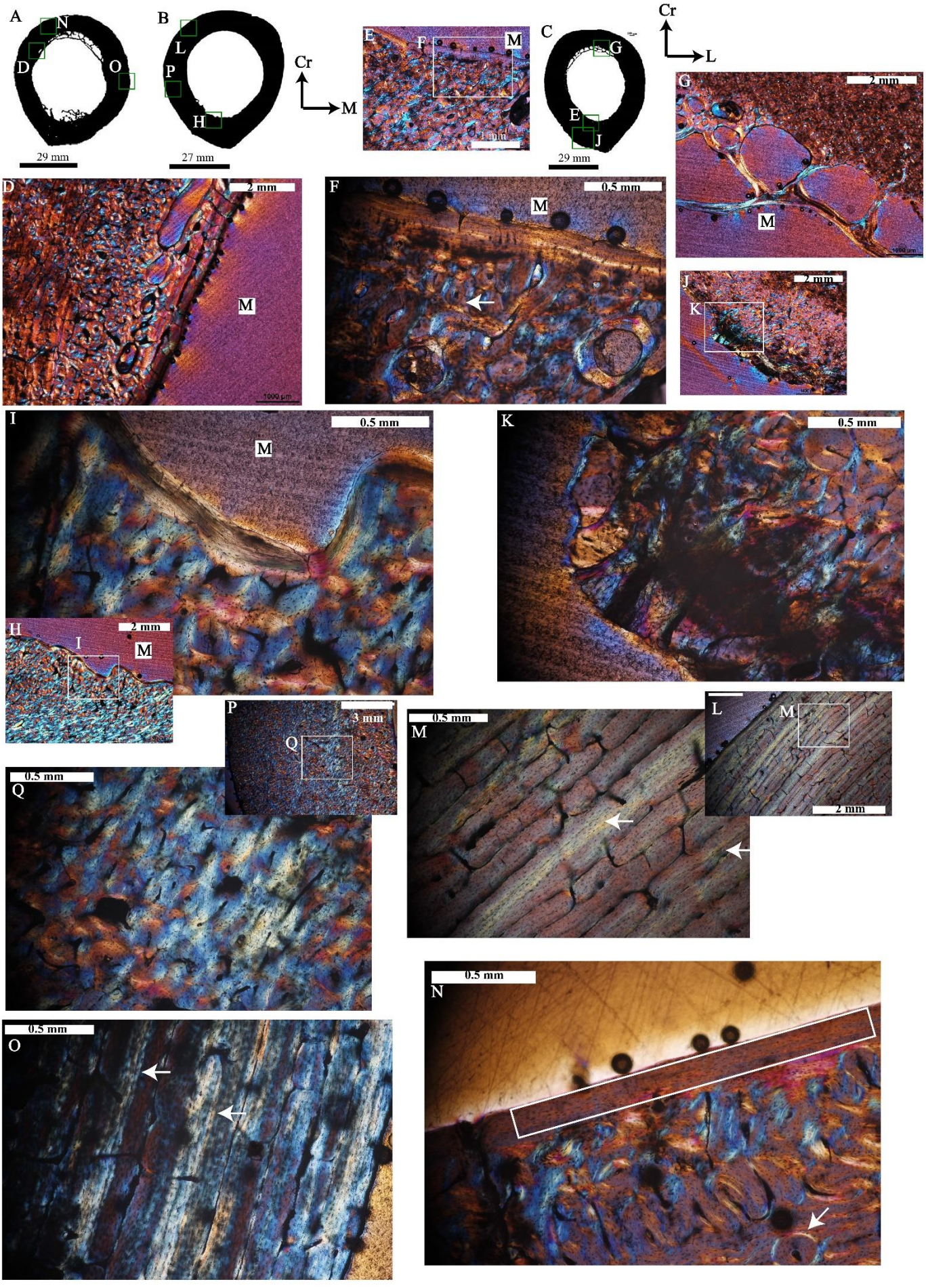
A
N
D
O
29 mm
B
L
P
H
27 mm
Cr
M
E
F
M
1 mm
C
G
E
J
29 mm
Cr
L
G
2 mm
M
D
2 mm
M
1000 µm
F
0.5 mm
M
J
2 mm
K
I
0.5 mm
M
K
0.5 mm
H
2 mm
I
M
P
3 mm
Q
M
0.5 mm
L
M
2 mm
Q
0.5 mm
O
0.5 mm
N
0.5 mm

Figure 3.15: Femoral cortical bone tissues in the adult of *Giraffa camelopardalis* Microanatomy for the cross-section of the adult femora, (A) BF 3 ♀, showing cortical wall enclosing a partially vacant medullary cavity. (B) BF 8 ♂, and (C) BF12, showing cortical wall enclosing an open medullary cavity. Frames indicated regions for which higher magnification images are provided. (D) Higher magnification of (A) shows many of the resorption cavities as well as the medullary cavity are lined with lamellar bone tissue (white arrow). (E) Showing caudal endosteal margin. (F) Higher magnification of framed region in (E) shows lamellar bone tissue lining medullary cavity. (G) Extensive secondary remodeling in bone tissue surrounding the medullary cavity, the cancellous bone tissue is thinly lined with lamellar bone tissue. (H) Showing caudal endosteal region. (I) Higher magnification of region framed in (H) showing lamellar bone tissue lining the medullary cavity (white arrow). (J) Showing caudal periosteal region. (K) Higher magnification of the uneven periosteal margin in the framed region of (J) (white bracket). (L) Annuli in periphery of femoral cortex. (M) Higher magnification of annuli in periphery (white arrow). (N) Outer circumferential layer (lamellar bone tissue) in the cranial region. (O) Growth marks in the peripheral region of (A) (white arrow).

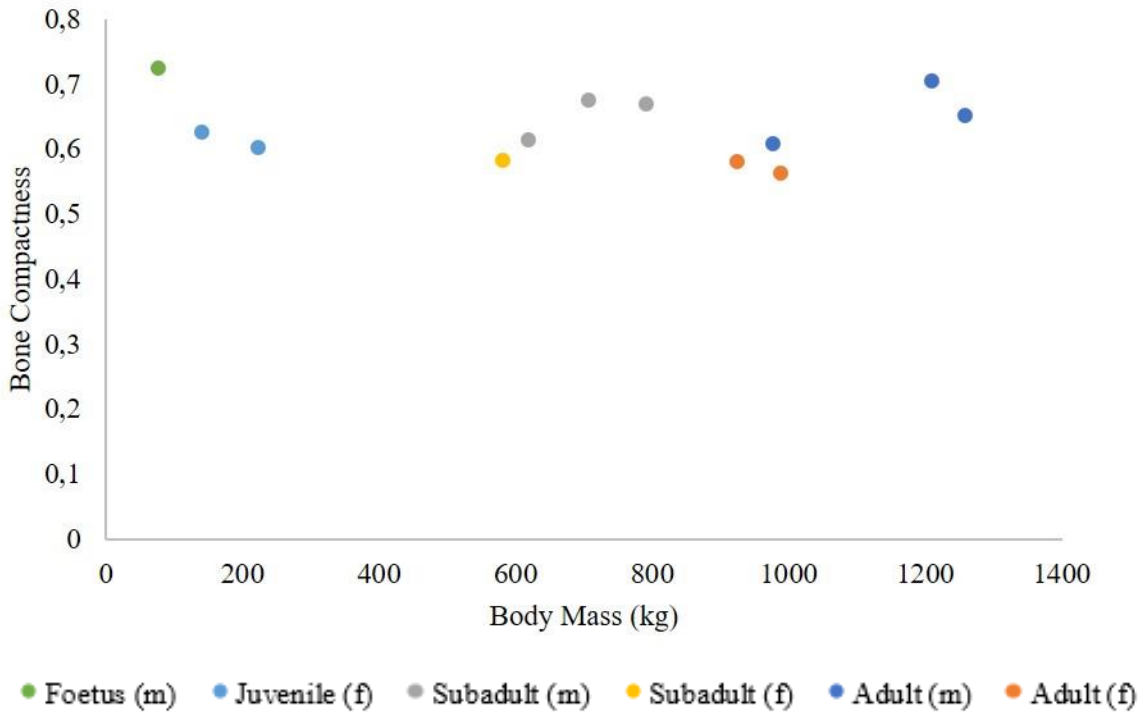

Figure 3.16: Bone profiler data (bone compactness) of the femora plotted against the body mass (kg) of giraffe femora (m is male, f is female). Refer to data Table 3.2, Table A.1

3.5 Microanatomy and Histology of the Tibia

3.5.1 Foetus

The midshaft cross section of the tibia of the foetus is oval in shape with the larger diameter in the medial-lateral plane (Fig. 3.17A). The average bone wall thickness is between ~9-13 mm (Table A.2), and it encloses a small medullary cavity. All around the perimedullary region, it is apparent that active resorption is underway (Fig. 3.17B). There are also a number of large erosion cavities in medial region that overall give this perimedullary region a cancellous appearance Fig. 3.17B). The peripheral and cortical bone comprises predominately laminar FLB (Fig. 3.17C), however there are long radial vascular canals in the cortex that appear to connect across several laminae (Fig. 3.17D).

3.5.2 Juvenile

The midshaft cross section of the tibia of the juveniles are elongated in the medial-lateral plane (Fig. 3.17E, 3.17F), and their bone walls have uneven thicknesses (Table A.2). The average bone wall thickness is between ~7-12 mm, and it encloses a small medullary cavity. The cancellous bone in the perimedullary region is variably distributed. In specimen BT15, the cancellous bone is predominately in the lateral-cranial-medial regions (Fig. 3.17E), but in the older specimen it is distributed in the lateral-caudal regions (Fig. 3.17F). It is evident that the bone tissue closest to the medullary cavity (and also that of the trabeculae) consists of bone formed during an earlier stage of ontogeny and comprises of reticular FLB (Fig. 3.17G-3.17J). The vascular arrangement in the periosteal margin is predominately circumferential (Fig. 3.17K, 3.17M), however there is a localized patch of reticular FLB shown in (Fig. 3.17L) which could be a site of muscle attachment (white brackets). The cortical bone is predominately laminar FLB, with long radial vascular canals and resorption cavities cutting through the bone tissue (Fig 3.17N-3.17P).

3.5.3 Subadult

The midshaft cross section of the tibia of the subadults are elongated into an oval shape, and are wider along the medial-lateral plane (Fig. 3.18A, 3.18B, 3.18C). The average bone wall thickness is between ~7-26.5 mm (Table A.2), which encloses a vacant medullary cavity. Three of the six specimens have cancellous bone in the perimedullary region, which has a limited distribution in the perimedullary region of the medial part of the cross section, and is overlain by a narrow band of lamellar bone tissue (Fig. 3.18D). Some parts of the perimedullary region has secondary reconstruction right up to the endosteal edge (Fig. 3.18E), whilst in other parts the medullary cavity is lined by an endosteal deposit of lamellar bone tissue (Fig. 3.18F). The peripheral part of the caudal region of the cross section is composed predominately of laminar

FLB and there are a number of secondary osteons present in the cortex (Fig. 3.18G, 3.18H). There are several annuli present that interrupt the bone tissue deposition in the peripheral parts of the cranial region of the cross section, (Fig. 3.18I). There also appears to be growth marks in the medial part of the cross section (Fig. 3.18J). The cortical bone tissue on the lateral side has undergone extensive bone remodeling and a large number of secondary osteons are present in the cortex (Fig. 3.18K, 3.18L). Annuli were only observed in the tibia of the female, and were located in the peripheral region of the cranial part of the cross section (Table 3.1).

3.5.4 Adult

As compared to the subadults, the midshaft cross sections of the tibia of the adults are much more elongated along the medial-lateral plane (Fig. 3.19A, 3.19B, 3.19C). The cortical bone walls average between 10-25 mm (Table A.2) and enclose a mostly vacant medullary cavity. When present cancellous bone tends to be distributed on the medial side of the medullary cavity (Fig. 3.19A). The cancellous spaces are lined with lamellar bone tissue, and are interrupted by rest lines (white arrows) (Fig. 3.19D). Lamellar bone lines the medullary cavity in areas void of cancellous bone (Fig. 3.19E), and here too there are rest interrupting (white arrows) the bone deposition (Fig. 3.19F). In several areas, the periosteal margin is smooth and is finished off by a layer of lamellar bone tissue which forms the OCL (Fig. 3.19G). Two rest lines are present in the lamellar OCL (Fig. 3.19H). The periosteal margin of the medial side of the cross section is uneven (Fig. 3.19I). According to the image, there are two rest lines visible in this region (Fig. 3.19I). In the caudal and lateral regions of the cross sections the cortical bone is extensively reconstructed and there are many secondary osteons in the cortex (Fig. 3.19J). Fig. 3.19K shows the low magnification of the cortical bone showing two different orientations of vascular canals. Fig. 3.19L, 3.19N has more longitudinal vascular canals compared to (Fig. 3.19M, 3.19O). Annuli were observed only in one of the four adult males, and were restricted to the peripheral region of the lateral part of the cross sections (Table 3.1).

3.5.5 Bone Profiler Data

The bone profiler analyses show that the foetal tibia and the adult male BT5 have similarly high compactness values (Table 3.2, Fig. 3.20). The rest of the samples have compactness values that range between 0.7-0.8, although the data for the two adult females' group closer together (Fig. 3.20).

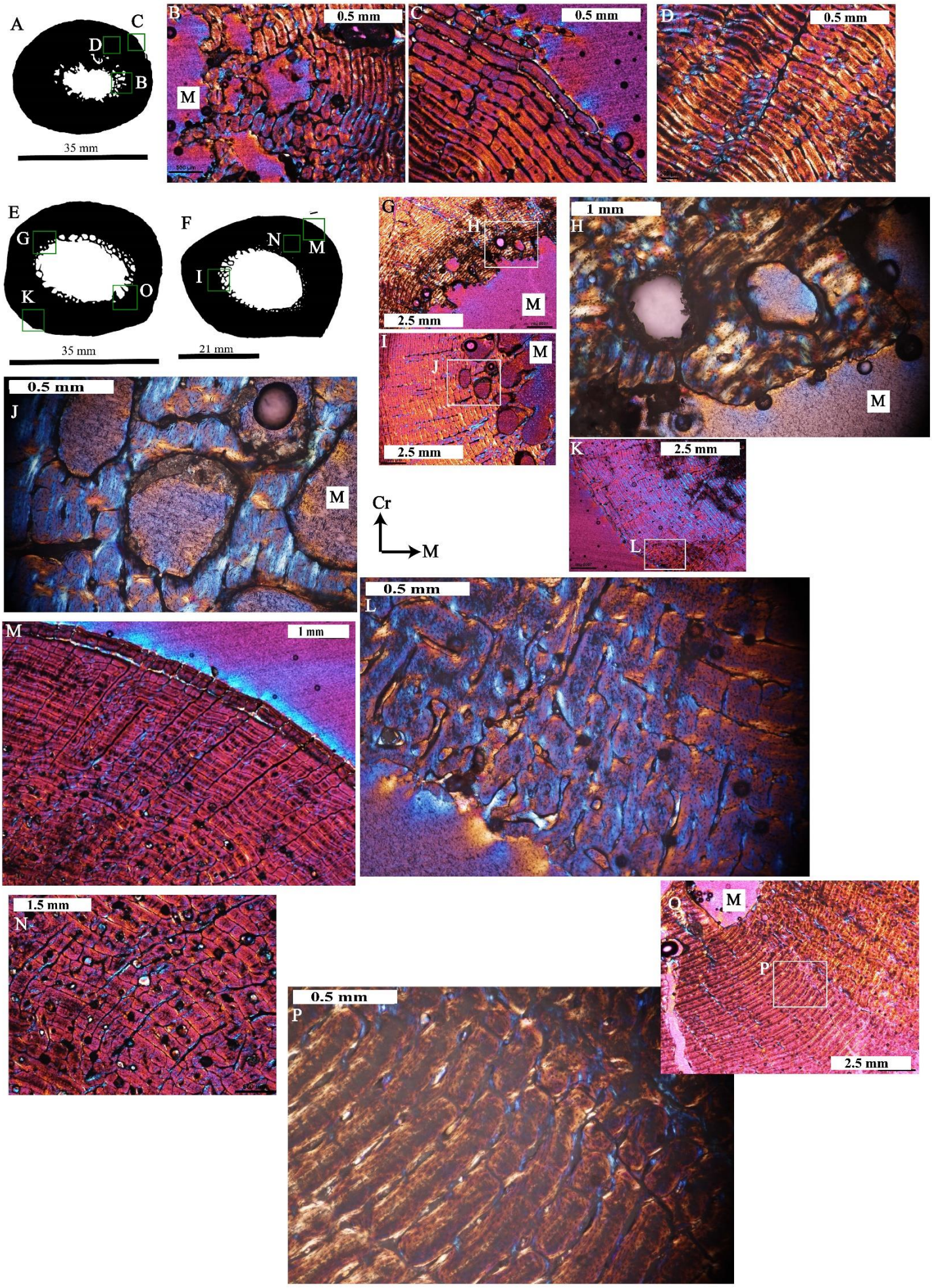
A
C
D
B
35 mm
B
0.5 mm
M
C
0.5 mm
D
0.5 mm
E
G
K
O
35 mm
F
N
M
I
21 mm
G
H
M
2.5 mm
I
J
M
2.5 mm
1 mm
H
M
0.5 mm
J
M
Cr
M
K
2.5 mm
L
0.5 mm
L
M
1 mm
1.5 mm
N
O
M
P
2.5 mm
0.5 mm
P

Figure 3.17: Tibial cortical bone tissues in the foetus and juveniles of *Giraffa camelopardalis*. Microanatomy for the cross-section of the foetal tibia, (A) BT14 ♂, showing cortical wall enclosing a central medullary cavity. Frames indicated regions for which higher magnification images are provided. (B) Higher magnification of the frame indicated in (A) showing the perimedullary region with a number of secondarily and resorption cavities. (C) Higher magnification of the frame indicated in (A) showing laminar FLB near the periphery of the bone wall. (D) Radial vascular canals extending through several laminae of laminar FLB. Microanatomy for the cross-section of the juvenile tibia. (E) BT15 ♀, and (F) BT2 ♀, showing cortical wall enclosing a medullary cavity with trabeculae extending into it. (G) Showing the perimedullary region. (H) Higher magnification of framed region in (G) showing resorption cavities (white arrows) cutting into FLB. (I) Showing the perimedullary region. (J) Higher magnification of framed region in (I) showing resorption cavities (white arrows) cutting into FLB. (K) Showing lateral periosteal region. (L) Higher magnification of framed region in (K) showing a localized patch (white brackets) of FLB in cortical laminar FLB. (M & N) Compact primary bone in the peripheral region of bone. Distinct radial vascular canals traverse the cortex. (O) Showing FLB in cortical bone in caudal region. (P) Higher magnification of framed region in (O) showing laminar FLB.

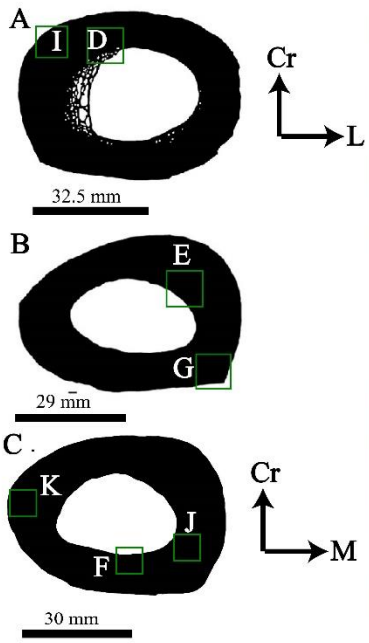
A
I
D
Cr
L
32.5 mm
B
E
G
29 mm
C
K
J
F
Cr
M
30 mm

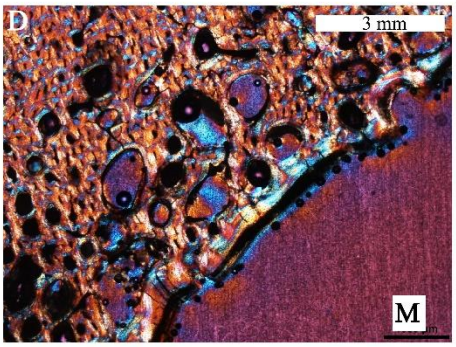
D
3 mm
M

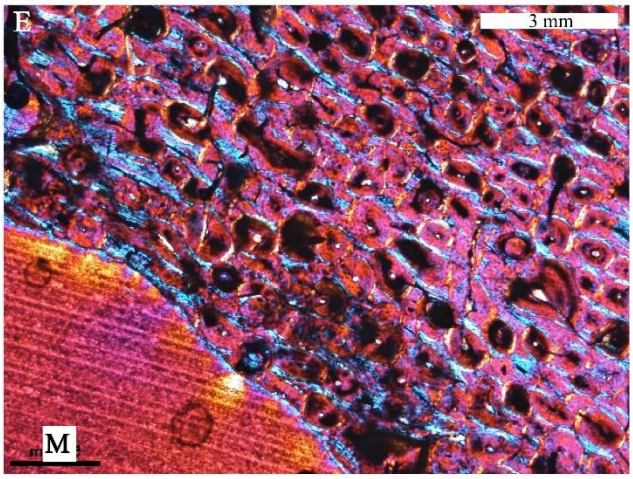
E
3 mm
M

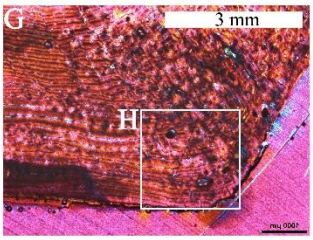
G
3 mm
H

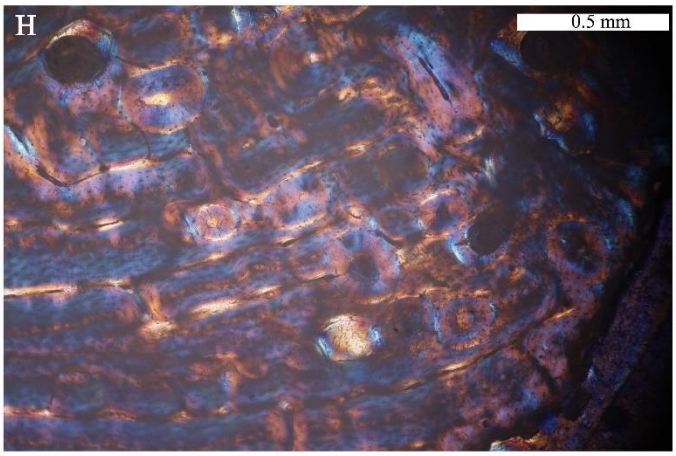
H
0.5 mm

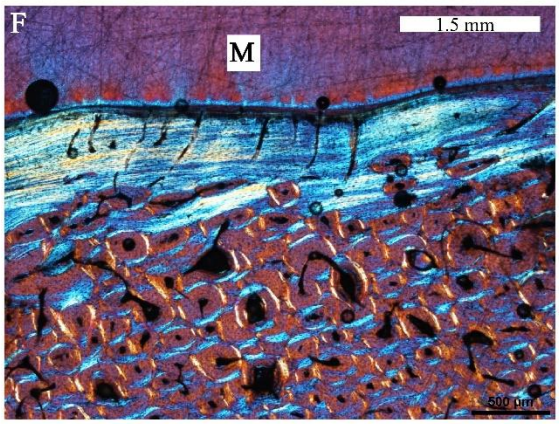
F
M
1.5 mm
500 µm

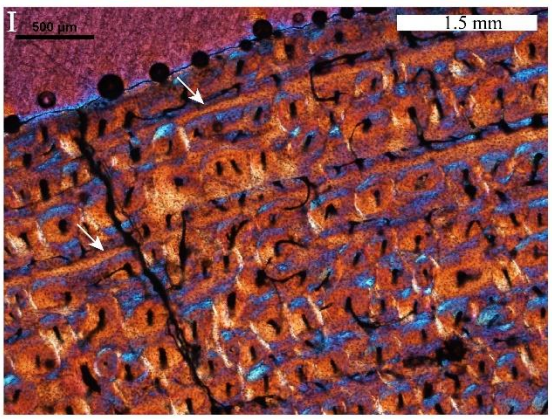
I
500 µm
1.5 mm

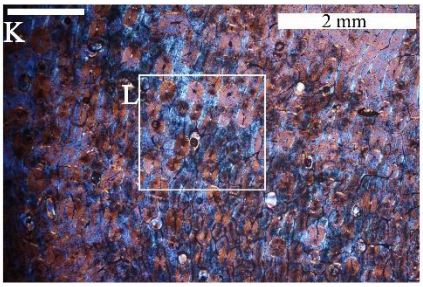
K
2 mm
L

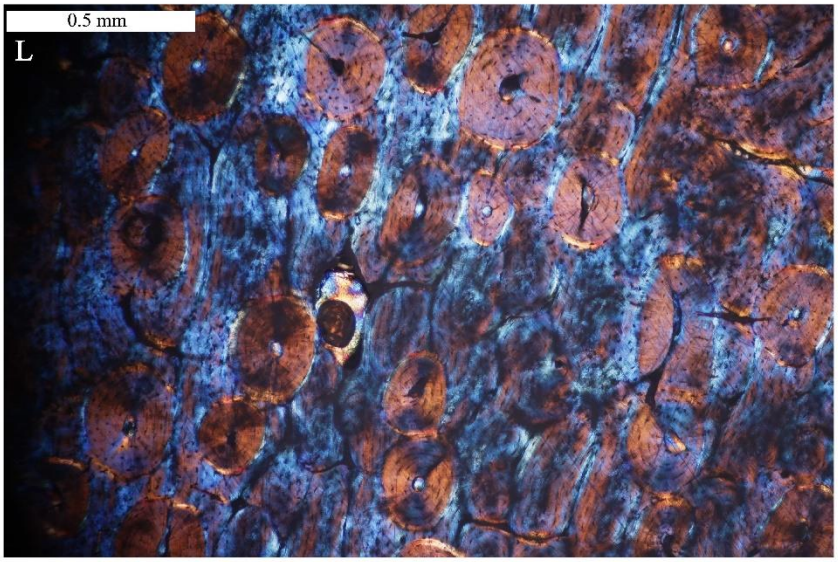
0.5 mm
L

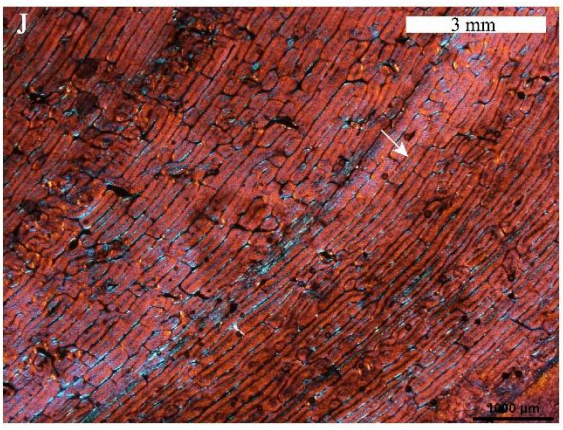
J
3 mm
1000 µm

Figure 3.18: Tibial cortical bone tissues in the subadult of *Giraffa camelopardalis*. Microanatomy for the cross-section of the subadult tibia, (A) BT10 ♂, showing cortical wall enclosing a partially vacant medullary cavity. (B) BT7 ♂, and (C) BT13, showing cortical wall enclosing a vacant medullary cavity. Frames indicated regions for which higher magnification images are provided. (D) Resorption cavities in the cranial region of the endosteal part of the compacta. Note the lamellar bone tissue lining the medullary cavity and resorption cavities (white arrows). (E) Extensive secondary remodeling in the cortical bone. (F) Lamellar bone tissue (white brackets) lining the medullary cavity, overlaying FLB with secondary osteons in the cortex. (G) Showing caudal periosteal region. (H) Higher magnification of framed region in (G) showing laminar FLB. (I) Annuli in the cranial periphery (white arrows). (J) Laminar FLB in medial cortex. (K) showing cortical bone in lateral region, and (L) showing secondary osteons in the cortex.

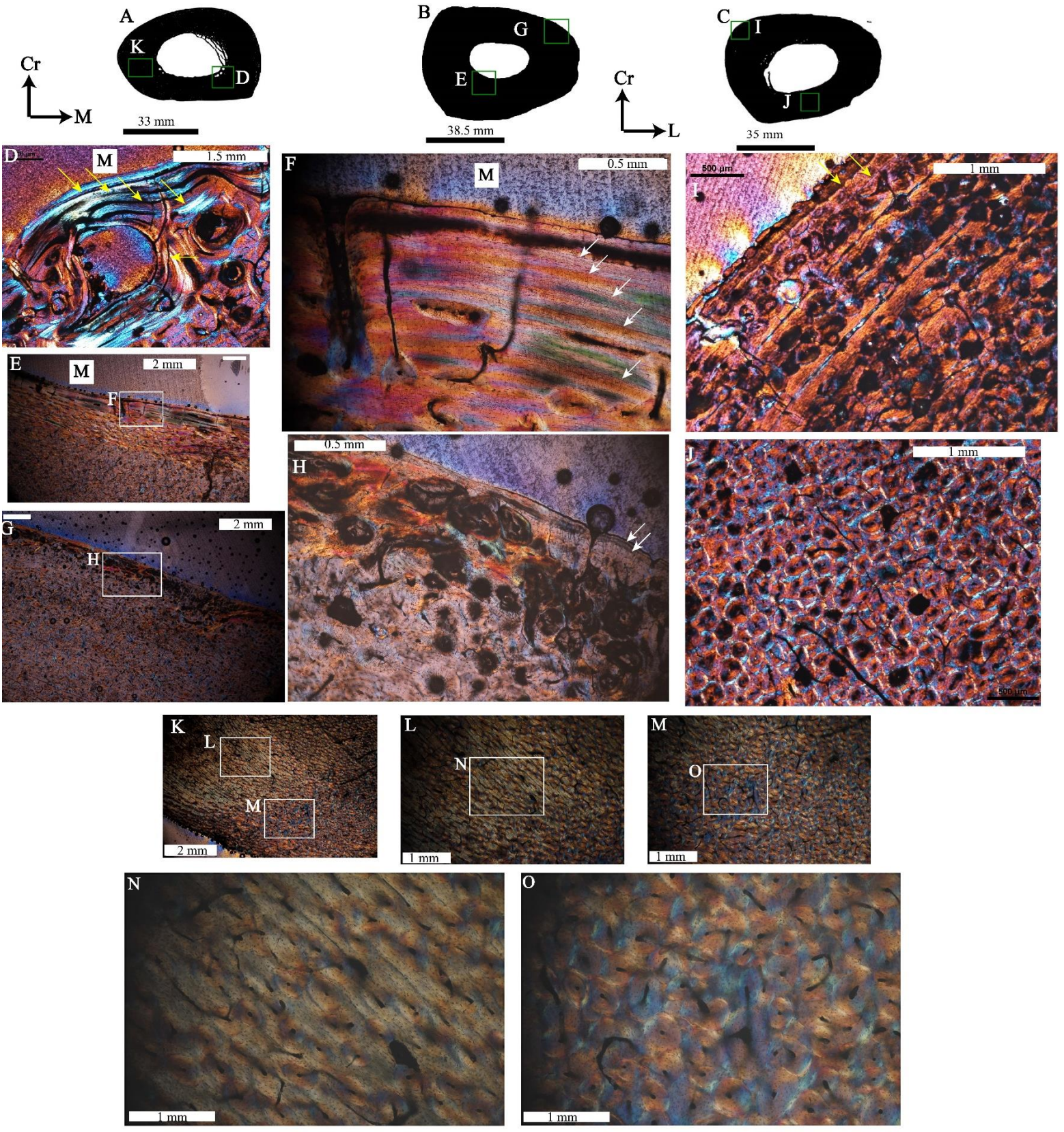
A
K
D
Cr
M
33 mm
B
G
E
38.5 mm
Cr
L
C
I
J
35 mm
D
M
1.5 mm
F
M
0.5 mm
I
500 µm
1 mm
E
M
2 mm
F
0.5 mm
H
J
1 mm
500 µm
G
2 mm
H
K
L
M
2 mm
L
N
1 mm
M
O
1 mm
N
1 mm
O
1 mm

Figure 3.19: Cortical bone tissues of the Tibiae of adult of *Giraffa camelopardalis*. Microanatomy for the cross-section of the adult tibia, (A) BT 3 ♀, showing the cortical wall enclosing a partially vacant medullary cavity. (B) BT 5 ♂, and (C) BT9 ♂, showing cortical wall enclosing a vacant medullary cavity. Frames indicated regions for which higher magnification images are provided. (D) Higher magnification of framed region in (A) shows lamellar bone tissue lining cancellous spaces and the rest lines in lamellar bone tissue (white arrows). (E) Showing caudal endosteal margin. (F) Higher magnification of framed region in (E) showing lamellar bone tissue lining the medullary cavity. (G) Showing periosteal region on the cranial side of the cross section. (H) Higher magnification of framed region in (G) indicates extensive secondary reconstruction in the peripheral region of the bone wall, and an outer circumferential layer is indicated by the white arrow. (I) Circumferential vascular canals interrupting the secondary bone tissue in the periphery of the cortex. Two annuli present in peripheral region (yellow arrows). (J) Extensively remodeled cortex in caudal region. (K) Showing cortical bone in lateral side. (L) Laminar FLB and secondary osteons in the region next to (M). (M) Secondary osteons in one region. (N) Higher magnification of framed region in (L) showing laminar FLB. (O) Higher magnification of framed region in (M) showing abundant secondary osteons.

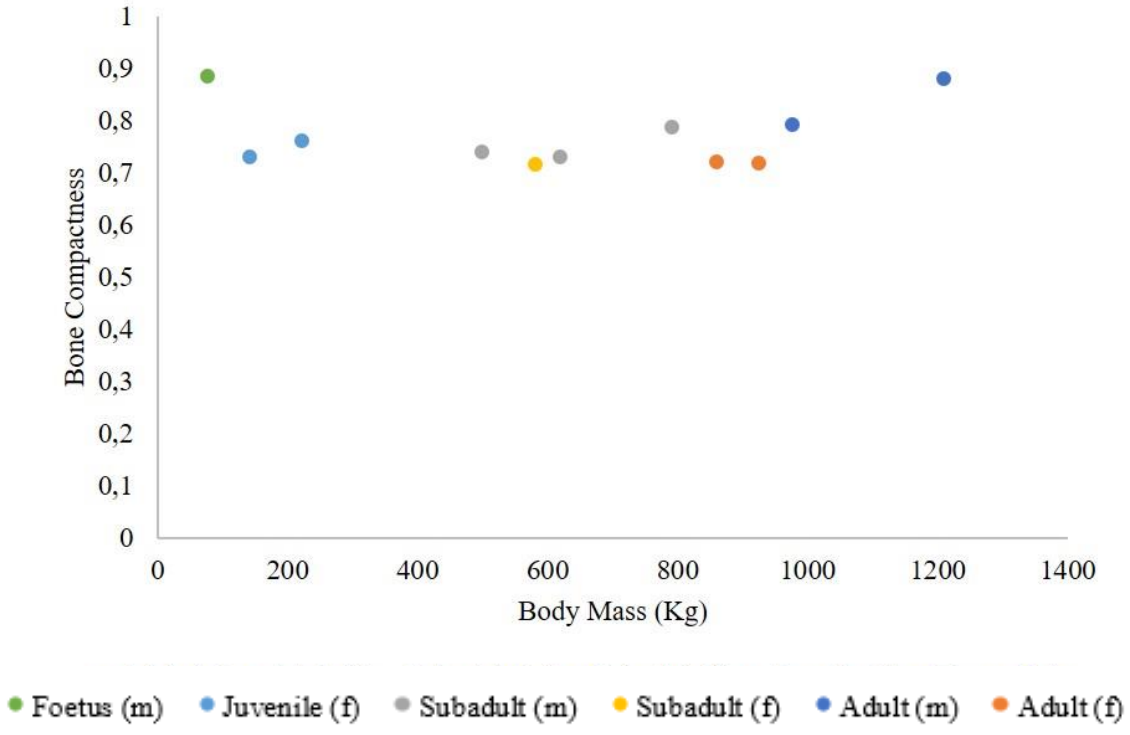

Figure 3.20: Bone profiler data (bone compactness) of the tibia plotted against the body mass (kg) of giraffe tibia (m is male, f is female). Refer to data Table 3.2, Table A.1

Table 3.1: Number of growth marks (annuli) identified in each subadult and adult cross-section of *Giraffa camelopardalis*.

Individual	Sex	Ontogenetic Stage	OCL	Humerus				Radius				Metacarpal				Femur				Tibia			
				Cr	Cd	M	L	Cr	Cd	M	L	Cr	Cd	M	L	Cr	Cd	M	L	Cr	Cd	M	L
Z24	Female	Subadult			2				2	2										3			
Z28	Male	Subadult						2								3							
Z43	Male	Subadult						2															
Z52	Male	Subadult																4					
Z51	Male	Subadult	Femur		6																		
Unknown	Male	Subadult		5																			
Z26	Female	Adult	Femur		3		3	4										4					
Z44	Male	Adult														8							
Unknown	Male	Adult														5							
Z47	Male	Adult																					5
Z29	Male	Adult	Tibia		5		7									5							

Table 3.2: Bone compactness value of each subadult and adult cross-section of *Giraffa camelopardalis*. *bone not included in current study

Individual	Sex	Ontogenetic Stage	Humerus	Radius	Metacarpal	Femur	Tibia
z27	Male	Foetus	0,914	0,786	0,782	0,726	0,886
z25	Female	Juvenile	0,645	0,7	0,768	0,604	0,763
z48	Female	Juvenile	0,693	0,771	0,75	0,626	0,731
z24	Female	Subadult	0,654	0,703	0,747	0,584	0,719
z28	Male	Subadult	0,736	0,681	*	0,616	0,732
z43	Male	Subadult	0,619	0,701	0,716	*	0,741
z51	Male	Subadult	0,538	*	0,762	0,67	0,789
z52	Male	Subadult	*	*	*	0,676	*
z07	Female	Adult	0,534	*	*	*	*
z26	Female	Adult	0,496	0,7	0,751	0,582	0,72
z30	Female	Adult	0,593	0,639	*	*	0,722
z55	Female	Adult	0,593	*	*	0,563	0,747
z29	Male	Adult	0,733	0,829	0,846	0,705	0,881
z32	Male	Adult	*	*	0,722	*	*
z44	Male	Adult	0,64	0,745	*	0,652	*
z47	Male	Adult	0,664	*	*	0,61	0,793

Chapter 4 Discussion

The histology of mammalian bone is reasonably well studied with the bones of several taxa having been examined (Table 1.1). However, only a few have looked at the histological changes through ontogeny (*Bathyergus,* Montoya-Sanhueza & Chinsamy (2017); ruminants, Kohler *et al.* (2012); Marín-Moratalla *et al.* (2013); Jordana *et al.* (2016); *Equus,* Nacarino-Meneses *et al.* (2016a); grey mouse lemur, *Microcebus murinus*, Castanet *et al.* (2004); deer, Kolb *et al.,* (2015a); and humans, Cambra-Moo *et al.,* (2012). The current study documents the pre- and postnatal microanatomy and histology of long bones of *Giraffa camelopardalis*. In addition, comparisons are made across the different growth stages, as well as within single skeletons to assess the variability in the microanatomy and histology.

4.1 Microanatomical assessment using Bone Profiler

In the current study, all the giraffe cross sections have a clear distinction between the cortical wall and the medullary cavity. All the bones have open medullary cavities, and thick cortical walls. The humeri, femora, and tibia have some trabeculae and/or cancellous bone tissue development in the perimedullary region, whereas the metacarpals and radii do not have trabeculae extending into the medullary cavity. This differs from other large terrestrial mammals like the rhinoceros (*Rhinoceros unicornis,* Houssaye *et al.* (2016b), or elephants (*Elephas* and *Loxodonta,* Houssaye *et al.* (2016b) where the medullary cavity is indistinct from the cortical wall, and is filled with many trabeculae (Houssaye *et al.*, 2016b). The African buffalo (*Syncerus caffer*) however, has a largely open medullary cavity and thick cortical wall similar to the giraffe (van Schalkwyk *et al.*, 2004; Houssaye *et al.*, 2016b). As outlined in the methods section, the proportions of compact bone and medullary cavity (and open pore spaces) is calculated by the program in Bone Profiler (Girondot & Laurin, 2003). The bone compactness values of different long bones through ontogeny obtained in the current study (humerus; subadult 0.538-0.736, and adult 0.496-0.733, and femur; subadult 0.584-0.676, and adult 0.563-0.705) is like previous compactness values obtained for a single giraffe specimen (0.576 for the femur and 0.648 for the humerus) (Houssaye *et al.*, 2016b). These Bone Profiler values are lower than the bone compactness data previously obtained for the rhinoceros, *Rhinoceros unicornis* (0.8295, humerus and 0.7275, femur); elephants, *Elephas* and *Loxodonta* (0.842 and 0.815, humerus and 0.772 and 0.855, femur); and the African buffalo, *Syncerus caffer* (0.808, humerus and 0.7295, femur).

Furthermore, the bone profiler data for the close extant relative of giraffes, the okapi, *Okapia johnstoni* is 0.555 for the humerus, and 0.632 for the femur (Houssaye *et al.*, 2016b), which is quite similar to those obtained for the giraffes in both the current study and in Houssaye *et al.* (2016b). These comparative data for bone compactness and proportions of medullary/cortical area for large terrestrial mammals seems to suggest that graviportality and semi-aquatic lifestyles influence the bone microanatomy. In graviportal animals, a large bone cross section and an increase in bone compactness is related to resisting the high compression and tension strains due to increased body size and weight, whereas increased bone compactness in aquatic tetrapods can have evolved to maintain buoyancy, and improve gravity resistance (Houssaye *et al.*, 2016a; Houssaye *et al.*, 2016b).

In the current study, the humeri, femora, and tibia bone profiler data for the juveniles are different as compared to in the bone compactness data of the foetus (Table 3.2), whereas the data for the radii and metacarpals are similar (Table 3.2). Indeed, the foetal humerus and femur bone compactness data is higher than all the subsequent age classes, but the radius, metacarpal, and tibia values remain virtually unchanged throughout ontogeny. The thicker bone walls in the foetus can probably be explained by the fact that in utero it is suspended in amniotic fluid, and does not need to support its body weight i.e. it has thick cortical bone as observed in aquatic animals (Houssaye et al. 2016b). However, after birth the bone microanatomy changes, especially in the weight bearing elements. This suggest that the changes in lifestyle is reflected in the microanatomical structure of the bones. This is not uncommon, and has been shown in various other taxa. For example, the fossorial tortoise (*Chersina angulata*) and subterranean mole rats (*Bathyergus*), shows the opposite condition to the giraffe in having much higher bone compactness values (Montoya-Sanhueza & Chinsamy, 2017; Bhat *et al.*, 2019) because of adaptations for their particular lifestyle.

The shape of the humerus, femur, and tibia cross sections changes the most during ontogeny. Generally, the cross-sectional shape of the bones morph from being more or less circular while in utero to become more elliptical in shape in the juveniles and older individuals by expansion along one plane (i.e. in the humeri and femora along the cranial-caudal plane, and tibia along the medial-lateral plane). Interestingly, the cross-sectional shape of the radii and metacarpals do not change as much as the other limb bones during further ontogenetic development. The change in shape from circular to elliptical is possibly related to the fact that

the embryo skeleton is not bearing any weight. Axial and compression load bearing studies on goats (Lieberman *et al.*, 2003) and turkey (Rubin *et al.*, 1992) found that juveniles that have undergone extra loading show a significant increase in periosteal growth as opposed to adults (that were similarly loaded) that do not show a significant increase in periosteal growth. In the femur it appears that the caudal region was loaded more, but in the tibia the cranial region was mostly affected (Lieberman *et al.*, 2003). These studies could explain the changes in cross sectional shape observed in the giraffes, particularly between the embryo and the older individuals. The embryos have restricted movement and they do not support their body weight, whereas the juveniles, subadults, and adults constantly bear their body weight and also deal with the stresses of locomotion. The change in cross-sectional shape in the two juveniles could be the result of biomechanical forces impacting on how the bone grows during locomotion (Biewener & Taylor, 1986). During ontogeny the cross section of the radius of the giraffes elongates along the medial-lateral plane. This was also observed in a study of juvenile and adult goat radii, where the bone cortex changes from circular to elliptical cross-sectional shape (Main & Biewener, 2004). The latter study found that goats experience more loading in the cranial-caudal plane, while the medial-lateral regions grows faster (Main & Biewener, 2004). Therefore, if bone is deposited faster along one plane of the bone cross section, and not the other, the cross-sectional shape of the bone will tend to be more elliptical in shape.

When comparing the bone compactness data between males and female giraffes no differences were observed in the subadult humeri, radii, and metacarpals. However, the femora and tibia of the subadult female studied has a slightly lower bone compactness. When looking at the adult bones, except for the metacarpals, the females have a lower bone compactness than the males (Table 3.2). In general, the bone compactness values are similar in all the subadult bones (0.538-0.789), while among the adults, the values are much more variable (0.496-0.881). This high variation in the data is mainly the result of the low compactness values of the female adults which show more extensive development of cancellous bone tissue (0.496). Indeed, the second lowest compactness value is of a subadult female (0.534). The adult humeri has the highest variation of bone compactness between males and females (0.496-0.664). Most of the published studies that have examined bone compactness (Canoville & Laurin, 2010; Laurin *et al.*, 2011; Houssaye *et al.*, 2016b) have not considered differences that may be sex related. However, in the case of *Bathyergus suillus* (dune mole rat) females were found to show more variation in bone

compactness, and they also exhibited more resorption cavities in their cortices (Montoya-Sanhueza 2014). There is clearly a need for further investigation into differences in cross sectional geometry and bone compactness of males and females, and especially how reproduction affects these parameters.

In a study examining the bone compactness of a number of large bodied mammals, (Houssaye *et al.*, 2016b) found that increasing body weight resulted in higher bone compactness. In the current study, this appears to also be the case: the two adult males with the largest body mass (individuals Z29, 1208 kg and Z44, 1258 kg) have the highest bone compactness values (Table 3.2).

4.2 Histological changes during ontogeny

The five *G. camelopardalis* bones studied here (humerus, radius, metacarpal, femur, and tibia) present the following general histological features (1) primary bone tissue is FLB, (2) trabeculae consists of some lamellar bone and FLB tissue in the perimedullary region of some juvenile bones, (3) Endosteally formed lamellar bone tissue lines the medullary cavity of subadults and adults, (4) secondary remodeling is limited to subadults and adults, and (5) growth marks are only found in subadults and adults, and they are restricted to the outer cortex.

All five bones have the same bone tissue in the foetal stage i.e. a cortex comprising of highly vascularised FLB and showing resorption of earlier deposited bone near the medullary cavity. The bone tissue is particularly spongy in the periosteal region where the newest bone is being formed by appositional deposition (Chinsamy-Turan, 2005). This agrees with the general bone tissue type present in young (juvenile) mammals, such as; equids (*Equus steinheimensis* and *E. osbachensis*) (Nacarino-Meneses *et al.*, 2016a; Nacarino-Meneses *et al.*, 2016b; Nacarino-Meneses & Orlandi-Oliveras, 2019), ruminants (3 species of cervids and 27 species of bovids), Jordana *et al.* (2016), a small primate, grey mouse lemur (*Microcebus murinus)* (Castanet *et al.*, 2004), red deer, *Cervus elaphus hispanicus* and *C. e. hippelaphus* (Calderón *et al.*, 2019), and a phocid seal (*Homiphoca capensis*) and a juvenile southern elephant seal (*Mirounga leonine*, Woolley *et al.* (2019). Although these mammals have varying body sizes, the overall spongy texture of the bone and the deposition of woven bone entrapping vascular spaces (incipient FLB) indicates that the bone deposition at this young stage of ontogeny is occurring at a rapid rate (de Margerie *et al.*, 2004). Of the foetal and juvenile bones, the metacarpals

qualitatively show the highest vascularization, whilst the tibia has the most organised circumferential and radial vascular canals. Giraffe (current study), Holstein calves (Mori *et al.*, 2003), and *Equus* young (foetal and juvenile) (Mori *et al.*, 2003), share similar distribution of laminar FLB in the cortex. In contrast to the giraffe foetal bones, the periosteal bone tissue is more compacted in the giraffe juveniles, subadults, and adults since endosteally formed lamellar bone infills the spaces left when the rapidly formed woven bone matrix was deposited, and results in the formation of primary osteons (Currey, 2002).

Endosteally formed lamellar bone is found lining the trabeculae of some juveniles, and lamellar bone was often seen lining the medullary cavity in almost all subadults and adults. However, the degree of lamellar bone deposited varies through ontogeny, between the sexes, and among the different skeletal elements. In some juveniles, lamellar bone tissue lines some trabeculae in the perimedullary region of the bone wall. In fossorial animals, endosteally formed lamellar bone appears more extensively developed and can often lead to infilling of the medullary cavity (Montoya-Sanhueza & Chinsamy, 2017; Legendre & Botha-Brink, 2018; Bhat *et al.*, 2019), whereas terrestrial, non-fossorial animals endosteally formed bone tends to be a narrower band of tissue that line the medullary cavity, forming the inner circumferential layer (ICL) (Canoville & Laurin, 2010; Houssaye *et al.,* 2016b). In four of the specimens (two subadults and two adults, one male and one female in each) the ICL has multiple rest lines interrupting the deposition of the lamellar bone tissue. Such pauses in the rate of endosteally formed bone tissue has been recorded in several taxa, e.g., in echidna (Chinsamy & Hurum, 2006), and cape dune mole rats (Montoya-Sanhueza & Chinsamy, 2017). The rest lines divide bands of bone tissue (Amprino, 1947; Enlow, 1963), and indicates a reduction in the rate of bone deposition (Castanet *et al.,* 2004; Chinsamy-Turan, 2005).

Secondary remodeling (as explained in Chapter 1), refers to the process of secondary reconstruction and often the end result is the formation of secondary osteons e.g., McFarlin *et al.* (2008). Secondary remodeling is most extensive in the inner cortical regions of the subadults and adults. In the periosteal regions, secondary remodeling varies in distribution: it is more extensively developed in the cranial and caudal regions of the humeri and femora, whereas it occurs in most regions of the radii (except the lateral region), and in the tibia except in the medial region. Of the adult bones, the metacarpals show the most extensive intra cortical remodeling, with very little primary bone tissue remaining in the cortex. These differences in

distribution could relate to biomechanical loading (Biewener, 1983; Francillon-Vieillot *et al.*, 1990; Rubin *et al.*, 1992; Lieberman *et al.*, 2003). The generally accepted hypothesis relating to extensive secondary remodeling in the cortical bone is related to biomechanical stresses and strains or to repair microdamage (Wolff, 1986; Frost, 1994). However, secondary remodeling can also be indicative of the animals age. To a certain extent, the number of secondary osteons increases with age (Padian *et al.*, 2016). Padian *et al.* (2016), recently presented a new hypothesis stating that the degree of secondary remodeling is rather related to the different growth trajectories of the different elements i.e. that bigger bones would have less remodeling due to faster growth as opposed to smaller bones (that do not bear weight) growing slower. This could be a part explanation for the metacarpals of the giraffe, they are thinner than the humeri, radii, femora, and tibiae. However, the metacarpals do bear weight. In the current study, juveniles show little to no secondary remodeling, unlike in deer femora (Kolb *et al.*, 2015a), where even at an early stage of ontogeny juveniles already begin to undergo secondary remodeling. The giraffe adult bones show similar levels of secondary remodeling to deer (Kolb *et al.*, 2015a). While the cortex of most giraffe bones is highly remodeled, growth marks are still visible in the cortex (see section 4.4 in discussion). Both giraffe and deer radii are highly remodeled in the caudal region, while the tibiae are remodeled in the medial and lateral sides. Habitual strain environments experienced by different limb bones in cursorial animals require regionally specific structural and material adaptations to ensure fracture resistance (Skedros *et al.*, 1994; Skedros *et al.*, 1996; Skedros *et al.*, 2003; Jasinoski & Chinsamy-Turan, 2012). Generally, secondary osteons are greatest in the more distal elements of cursorial animals as an adaptation to fatigue damage (Chan *et al.*, 2007). Stress in the radius and metacarpals general increase with increasing speed (Schellhorn & Pfretzschner, 2013), and it appears that the regions of the bones that have the highest amount of secondary remodeling/secondary osteons have the most strain/stresses. The stresses imparted on limbs depend on factors like gait, locomotion, speed, posture, bone microanatomy, and tendon and muscle attachment (Skedros *et al.*, 1994; Skedros *et al.*, 1996; Skedros *et al.*, 2003; Jasinoski & Chinsamy-Turan, 2012). While primary bone is stronger and more fatigue resistant than remodeled bone, secondary osteons are thought to prevent the further spread of microcracks (Skedros *et al.*, 1994; Skedros *et al.*, 1996; Jasinoski & Chinsamy-Turan, 2012). Therefore, based on the afore mentioned, giraffe humeri and femora experience more loading/strains along the cranial-caudal plane and the radii and tibia experience more

loading/strains along the medial-lateral plane. While the giraffe metacarpal, which presents almost full cortical secondary remodeling/extensive secondary osteons experiences the most strain in the forelimb. Further histological studies on the metatarsal need to be done before inferences can be made about the stresses and strains the hindlimb experiences.

It is worth mentioning that amongst all the study samples, specimen Z51 (Table 3.1, 3.2 & Fig. 3.2, 3.6, 3.10), a male subadult, had rather unusual histology: its humerus is highly remodeled i.e. a larger number of resorption cavities and an extensive development of cancellous bone tissue. The humerus bone wall is particularly thin, especially in the cranial region, and radius also has a much thinner bone wall as compared to the other radii. Additionally, the metacarpal, femur, and tibia have more cancellous bone tissue as compared to the other subadult bones. The rather unusual development of secondary reconstruction, without further redeposition of bone which gives a rather osteoporotic appearance to the cortices of the bones (Chinsamy-Turan, 2005) seems to point to some sort of imbalance in phospho-calcic metabolism in this subadult individual.

4.2.1 Histological variation within individuals

Of the five limb bones studied, the tibia is the only element that has long radial vascular canals that extend through large parts of the cortex and connect the circumferentially orientated vascular canals. Such long radially organised vascular canals have been previously noted in other taxa such as the femur of the elephant bird, *Aepyornis* (de Ricqlès *et al.*, 2016; Chinsamy *et al.*, 2020), and sauropterygian, *Cymatosaurus* (Klein, 2020).

The femora and humeri record the most growth marks in the outer cortex, whereas the radius and tibia record the most rest lines in the endosteal lamellar bone tissue lining the medullary cavity. Only three specimens (BF11, subadult male 791 kg, BF3, adult female 924.5 kg, and BT5, adult male 1208.5 kg) show clear evidence of an OCL, indicating that they have reached skeletal maturity (Chinsamy-Turan, 2005). BF3 and BT5 have unfused epiphyses. Therefore, the bones are still capable of growth in length although appositional growth has virtually ceased as indicated by the OCL. This situation differs from that of extant deer where the presence of an OCL and epiphyseal fusion occur concurrently in most specimens (Calderón, et al., 2019). In specimen BF11 the diaphyseal appositional growth and growth in length has ceased, which indicates that it had reached adult status and that its original designation as subadult is incorrect. It should be noted that original age-class estimation of the adult and

subadult giraffes was based on the mass of the animals (van Sitter, 2016, whereas now using the bone histology and epiphyseal fusion, a more accurate assessment of the ontogenetic status of BF11 is obtained. Digit reduction arose many times in the evolution of tetrapods (Lande, 1978). The distal limbs of artiodactyls have shifted its central axis from digit III to digit III and IV (Cooper *et al.*, 2014). Both molecular and cellular mechanisms are the reasons behind digit loss in artiodactyls (Cooper *et al.*, 2014). This study, clearly demonstrated the fusion between MC III and IV in the foetus and juvenile metacarpals sectioned.

4.3 Histological changes between sexes

Histological differences in bones between males and females is often seen in birds with females having medullary bone (Dacke *et al.*, 1993; Prondvai, 2017; Canoville *et al.*, 2019). Medullary bone is an endosteally formed bone tissue in female birds during egg laying which is used as a reserve for the production of eggshell (Bloom *et al.*, 1958; Dacke *et al.*, 1993; Prondvai, 2017; Canoville *et al.*, 2019). However, in mammals, bone histology differences in males and females are not well documented. These following studies compare these differences; white antelope (*Addax nasomaculatus*, Marín-Moratalla *et al.*, 2013), North American brown bats hibernation (*Myotis luifugus lucifugus*, Kwiecinski *et al.*, 1987), mice (Wallace *et al.*, 2007), and mole rats (*Bathyergus,* Montoya-Sanhueza & Chinsamy, 2017). In small mammals there appears to be a more noticeable difference in histology between males and females i.e. in bats, females had thin cortices after lactation although all bats had thin cortices after hibernation. However, males had the summer before hibernation to recover bone tissue lost due to resorption from the previous hibernation, whereas females that were pregnant did not have the chance to fully deposit bone tissue after hibernation (*Myotis luifugus lucifugus*, Kwiecinski *et al.*, 1987). In a study of the dune mole rat, Montoya-Sanhueza & Chinsamy (2017) found that females have more trabeculae that extend into the medullary cavity, than males, and bone resorption is also more prevalent in female humeri and femora as compared to the males. Such histological difference between the sexes is not seen so explicitly in giraffes. In the current study, males and females have similar amounts of cancellous bone tissue, secondary remodeling and resorption cavities. The study has four pregnant females, of which individual Z26 exhibits the most cancellous bone tissue of the adult humeri, but the other bones elements (from this individual) all present similar bone compactness to the rest of the adults. As stated earlier under section 4.2, the

only noticeable individual that shows a drastic difference in bone histology is the subadult male Z51. It is possible this individual could have been misidentified.

4.4 Growth mark changes during ontogeny

As outlined in Chapter 1, growth marks, in long bones and teeth, are used in the study of skeletochronology in many mammals (Klevezal, 1996; Castanet *et al.*, 2004; Chinsamy-Turan, 2005; Jordana & Köhler, 2011; Kohler *et al.*, 2012; Marín-Moratalla *et al.*, 2013; Kolb *et al.*, 2015a; Kolb *et al.*, 2015b; Jordana *et al.*, 2016; Nacarino-Meneses *et al.*, 2016b; Nacarino-Meneses *et al.*, 2017; Nacarino-Meneses & Kohler, 2018; Orlandi-Oliveras *et al.*, 2018) However, in the current study, skeletochronology was not the main objective, although the histology and occurrence and number of growths marks were noted. Of the sample studied, only the subadults and adults exhibited growth marks in the cortex i.e. out of 15 subadults and adults studied, only 11 showed growth marks in their cortices. The number of growth marks, and distribution varies between the limb bone elements from the same individual (Table 3.1). Several studies of a variety of extant vertebrates has shown that different animals will have different bones in their skeleton that best records their growth. In the current study it appears that the giraffe humerus and femur are the bones that have the highest number of growth marks recorded in both subadults and adults. Interestingly, in *Equus*, the femur is also the best bone for skeletochronology (Nacarino-Meneses *et al.*, 2016a; Nacarino-Meneses *et al.*, 2016b), whilst in deer specimens sampled by Kolb *et al.* (2015a) the humerus, femur, and tibia all kept a good track record of their growth. Kohler per. obs. (2006) suggested that using metapodials for skeletochronology does not work due to the fusion of metacarpals III and IV (Nacarino-Meneses *et al.*, 2016a). From the results of the current study the aforementioned is supported, not only due to the fusion of the metacarpals III and IV, but also due to the extensive remodeling in the metacarpal cortices. This study found that the metacarpals were too remodeled to find growth marks in either the subadults or the adults.

In the giraffe bones studied here, the femora and humeri in the adult bones show the highest amount of growth marks, whilst amongst the subadults the humeri shows the highest number of growth marks, whilst the two juvenile giraffes do not exhibit any growth marks in their cortices. Furthermore, the growth marks in the giraffe specimens studied here, tend to be present only in the peripheral regions of the cortex; and they do not extend around the circumference of the bone. Thus, unlike in the ungulates studied by Jordana et al. (2016), among

the giraffes, it is likely that bone remodeling and not medullary expansion, is the main cause for obliterating growth marks.

In the current study, the two juvenile giraffes do not exhibit any growth marks in their cortex. Interestingly, the length and circumference of each of bone compared favourably to a five months old giraffe in the vertebrate collections at Iziko South African Museum (Cape Town), suggesting therefore that these specimens were under one year old. Thus, this explains the absence of any growth marks in their cortices. Similarly, Nacarino-Meneses *et al.* (2016a); Nacarino-Meneses *et al.* (2016b) found that the foals of *Equus* did not have growth marks whilst a yearling had one growth mark.

Chapter 5 Conclusions

5.1 Outcomes of current study

This is the first study to examine (1) the cross-sectional shape changes in limb bones through ontogeny, (2) the histological changes in different limb elements through ontogeny, and (3) the histovariability in skeletons of *Giraffa camelopardalis*.

1) Cross-sectional shape changes in limb bones through ontogeny

The shape of the bone cross sections of each bone element changed through ontogeny. The humeri and femora elongate in the cranial-caudal direction, and the radii and tibia elongate in the medial-lateral direction. The change in shape is related to the bone's response to accommodate safe levels of stress across the whole bone (Bertram & Biewener 1990). The bones from the forelimbs and hindlimbs overall had similar bone wall thickness and bone compactness. This is contrary to the original expectation that the forelimb bone walls would be thicker than the hindlimbs due to the latter supporting the extra weight of the giraffe's long neck. Thus, the overall similarities in bone wall thickness and bone compactness of the forelimb and hindlimb elements leads to the rejection of the hypothesis (page 20) which postulated that there will be microanatomical differences between forelimb and hindlimb elements.

2) Histological changes in different limb elements through ontogeny

The foetal and juvenile stages have highly vascularised FLB cortical bone. The cortical bone tissue of the subadults and adults' changes to a more slowly deposited bone tissue, and growth marks tend to occur in the outer cortex. Three specimens show a narrow band of outer circumferential layer that consists of lamellar tissue and which indicates that they have reached skeletal maturity. These findings support the original hypothesis (page 20) that each ontogenetic stage of *Giraffa camelopardalis* will have distinct bone histology.

3) Histovariability in skeletons of *Giraffa camelopardalis*

The tibia is the only bone with long radial vascular canals in the cortex. This is an interesting finding because so far, such features have only been reported in the giant extinct elephant bird, *Aepyornis* and sauropterygian, *Cymatosaurus.*

The current study clearly demonstrated how the giraffe metacarpal results from the fusion of metacarpal III and IV. The histology of this bone also demonstrated that it is the most remodeled of the five bones studied. Additionally, the results showed that the bones of females

do not have more secondary remodeling or cancellous bone tissue than males, contra (Montoya-Sanhueza & Chinsamy, 2017). However, the femora of adult females tend to have a lower bone compactness as compared to the adult males, and it is also lower than the values obtained for the subadults of both sexes. All other bones of females, have similar bone compactness to the males throughout ontogeny. Thus, there is little to no difference in the bone tissues of males and females (even in the cases of pregnant females), which leads to the rejection of the hypothesis (page 20) which postulated that the attainment of sexual maturity will result in higher levels of secondary reconstruction in the bone cortices of females, and particularly pregnant females, as compared to males.

5.2 Limitations of the Current Study and Future Directions

Although the current study is novel in that it permitted insight into the histology of limb bones of several giraffes through ontogeny, it is also limited, as each ontogenetic stage is poorly represented i.e. this study examined one male foetus, two female juveniles, one female subadult and six male subadults, four female adults, and three male adults. Furthermore, the small sample size precluded the use of statistical analysis. It is proposed that future studies ensure a more robust sampling to assess the validity of the findings observed in the current study. It would also be important to examine a wider range of juveniles (especially of known ages), so that the onset of the formation of growth marks in the cortex be more rigorously assessed. The latter will have important implications as to whether the growth marks can be effectively used for skeletochronology among giraffids. It is also proposed that more females be incorporated in any future studies so that sex differences can be better addressed.

Despite the limitations mentioned above, it is evident that this study has laid the foundation for future studies concerning the growth and biology of extinct giraffids, such as the Pliocene *Sivatherium hendeyi* and *Giraffa jumae* from Langebaanweg in South Africa. Indeed, it would also be interesting to examine the bone histology of the closely related living relatives of modern giraffes, the okapi (*Okapi johnstonii*), to deduce information about their biology, which is poorly known.

References

Amprino, R. 1947. La structure du tissu osseux envisagée comme expression de différences dans la vitesse de l'accroissement. *Archives de Biologie,* 58**,** 317-330.

Badlangana, N. L., Adams, J. W. & Manger, P. R. 2011. A comparative assessment of the size of the frontal air sinus in the giraffe (*Giraffa camelopardalis*). *The Anatomical Record: Advances in Integrative Anatomy and Evolutionary Biology,* 294**,** 931-940.

Bhat, M. S., Chinsamy, A. & Parkington, J. 2019. Long bone histology of *Chersina angulat*a: Interelement variation and life history data. *Journal of Morphology,* 280**,** 1881-1899.

Biewener, A. A. 1983. Allometry of quadrupedal locomotion: the scaling of duty factor, bone curvature and limb orientation to body size. *Journal of Experimental Biology,* 105**,** 147-171.

Biewener, A. A. & Taylor, C. R. 1986. Bone strain: a determinant of gait and speed? *Journal of Experimental Biology,* 123**,** 383-400.

Bloom, M. A., Domm, L. V., Nalbandov, A. V. & Bloom, W. 1958. Medullary bone of laying chickens. *American Journal of Anatomy,* 102**,** 411-453.

Bouvier, M. & Hylander, W. L. 1996. The mechanical or metabolic function of secondary osteonal bone in the monkey *Macaca fascicularis*. *Archives of Oral Biology,* 41**,** 941-950.

Calderón, T., Demiguel, D., Arnold, W., Stalder, G. & Köhler, M. 2019. Calibration of life history traits with epiphyseal closure, dental eruption and bone histology in captive and wild red deer. *Journal of Anatomy,* 235**,** 205-216.

Cambra-Moo, O., Meneses, C.N., Barbero, M.Á.R., Gil, O.G., Pérez, J.R., Rello-Varona, S., Martín, M.C. and Martín, A.G., 2012. Mapping human long bone compartmentalisation during ontogeny: A new methodological approach. *Journal of Structural Biology*, 178(3), pp.338-349.

Canoville, A. & Laurin, M. 2010. Evolution of humeral microanatomy and lifestyle in amniotes, and some comments on palaeobiological inferences. *Biological Journal of the Linnean Society,* 100**,** 384-406.

Canoville, A., Schweitzer, M. H. & Zanno, L. E. 2019. Systemic distribution of medullary bone in the avian skeleton: ground truthing criteria for the identification of reproductive tissues in extinct Avemetatarsalia. *BMC Evolutionary Biology,* 19**,** 71.

Carroll, R. L. 1988. *Vertebrate paleontology and evolution*. WH Freeman and Company, New York.

Castanet, J. 2006. Time recording in bone microstructures of endothermic animals; functional relationships. *Comptes Rendus Palevol,* 5**,** 629-636.

Castanet, J., Croci, S., Aujard, F., Perret, M., Cubo, J. & De Margerie, E. 2004. Lines of arrested growth in bone and age estimation in a small primate: *Microcebus murinus*. *Journal of Zoology,* 263**,** 31-39.

Chan, A. H., Crowder, C. M. & Rogers, T. L. 2007. Variation in cortical bone histology within the human femur and its impact on estimating age at death. *American Journal of Physical Anthropology,* 132**,** 80-8.

Chinsamy-Turan, A. 2005. *The microstructure of dinosaur bone: deciphering biology with fine-scale techniques*, John Wiley & Sons.

Chinsamy-Turan, A. 2012. The microstructure of bones and teeth of nonmammalian therapsids. *Forerunners of mammals: radiation, histology, biology***,** 65-90.

Chinsamy, A., Angst, D., Canoville, A. and Göhlich, U.B. 2020. Bone histology yields insights into the biology of the extinct elephant birds (Aepyornithidae) from Madagascar. *Biological Journal of the Linnean Society*.

Chinsamy, A. & Dodson, P. 1995. Inside a dinosaur bone. *American Scientist,* 83**,** 174-181.

Chinsamy, A. & Hurum, J. H. 2006. Bone microstructure and growth patterns of early mammals. *Acta Palaeontologica Polonica,* 51.

Chinsamy, A. & Raath, M. A. 1992. Preparation of fossil bone for histological examination. *Palaeontologia africana,* 29**,** 39-44.

Cooper, K. L., Sears, K. E., Uygur, A., Maier, J., Baczkowski, K. S., Brosnahan, M., Antczak, D., Skidmore, J. A. & Tabin, C. J. 2014. Patterning and post-patterning modes of evolutionary digit loss in mammals. *Nature,* 511**,** 41-5.

Currey, J. 2002. Bones. *Structure and mechanics***,** 1-380.

Dacke, C., Arkle, S., Cook, D., Wormstone, I., Jones, S., Zaidi, M. & Bascal, Z. 1993. Medullary bone and avian calcium regulation. *Journal of Experimental Biology,* 184**,** 63-88.

De Margerie, E., Cubo, J. & Castanet, J. 2002. Bone typology and growth rate: testing and quantifying 'Amprino's rule'in the mallard (*Anas platyrhynchos*). *Comptes rendus biologies,* 325**,** 221-230.

De Margerie, E., Robin, J. P., Verrier, D., Cubo, J., Groscolas, R. & Castanet, J. 2004. Assessing a relationship between bone microstructure and growth rate: a fluorescent labelling study in the king penguin chick (Aptenodytes patagonicus). *Journal of Experimental Biology,* 207**,** 869-79.

De Ricqlès, A., Bourdon, E., Legendre, L. J. & Cubo, J. 2016. Preliminary assessment of bone histology in the extinct elephant bird *Aepyornis* (Aves, Palaeognathae) from Madagascar. *Comptes Rendus Palevol,* 15**,** 197-208.

Dumont, M., Borbely, A., Kaysser-Pyzalla, A. and Sander, P.M. 2014. Long bone cortices in a growth series of Apatosaurus sp.(Dinosauria: Diplodocidae): geometry, body mass, and crystallite orientation of giant animals. *Biological journal of the Linnean Society*, 112(4), pp.782-798.

Enlow, D. H. 1963. *Principles of bone remodeling*, Charles C. Thomas.

Enlow, D. H. & Brown, S. O. 1957. A comparative histological study of fossil and recent bone tissues. Part II. *The Texas Journal of Science,* 9**,** 186-204.

Enlow, D. H. & Brown, S. O. 1958. A comparative histological study of fossil and recent bone tissues. Part III. *The Texas Journal of Science,* 10**,** 187-230.

Erickson, G. M. 2005. Assessing dinosaur growth patterns: a microscopic revolution. *Trends in Ecology & Evolution,* 20**,** 677-84.

Fennessy, J., Bidon, T., Reuss, F., Kumar, V., Elkan, P., Nilsson, M. A., Vamberger, M., Fritz, U. & Janke, A. 2016. Multi-locus analyses reveal four giraffe species instead of one. *Current Biology,* 26**,** 2543-2549.

Foote, J.S., 1916. A contribution to the comparative histology of the femur (Vol. 35, No. 3). *Smithsonian institution.*

Francillon-Vieillot, H., De Buffrénil, V., Castanet, J., Géraudie, J., Meunier, F., Sire, J., Zylberberg, L. & De Ricqlès, A. 1990. Microstructure and mineralization of vertebrate skeletal tissues. *Skeletal biomineralization: patterns, processes and evolutionary trends,* 1**,** 471-530.

Frost, H. M. 1994. Wolff's Law and bone's structural adaptations to mechanical usage: an overview for clinicians. *The Angle Orthodontist,* 64**,** 175-188.

Girondot, M. & Laurin, M. 2003. Bone profiler: a tool to quantify, model, and statistically compare bone-section compactness profiles. *Journal of Vertebrate Paleontology,* 23**,** 458-461.

Harris 1976. *Pliocene Giraffoidea (Mammalia, Artiodactyla) from the Cape Province*, South African Museum.

Harris 1991. Family Giraffidae. *Koobi Fora research project,* 3**,** 93-138.

Hassanin, A. and Douzery, E.J., 2003. Molecular and morphological phylogenies of Ruminantia and the alternative position of the Moschidae. *Systematic Biology*, 52(2), pp.206-228.

Heck, C. T., Varricchio, D. J., Gaudin, T. J., Woodward, H. N. & Horner, J. R. 2019. Ontogenetic changes in the long bone microstructure in the nine-banded armadillo (*Dasypus novemcinctus*). *PloS One,* 14**,** e0215655.

Hendey, Q. B. 1982. *Langebaanweg: A record of past life*, South African Museum.

Houssaye, A., Martin Sander, P. & Klein, N. 2016a. Adaptive Patterns in Aquatic Amniote Bone Microanatomy-More Complex than Previously Thought. *Integrative and Comparative Biology,* 56**,** 1349-1369.

Houssaye, A., Waskow, K., Hayashi, S., Cornette, R., Lee, A. H. & Hutchinson, J. R. 2016b. Biomechanical evolution of solid bones in large animals: a microanatomical investigation. *Biological Journal of the Linnean Society,* 117**,** 350-371.

Janis, C.M. and Theodor, J.M., 2014. Cranial and postcranial morphological data in ruminant phylogenetics. *Zitteliana*, pp.15-31.

Jasinoski, S. & Chinsamy-Turan, A. 2012. Biological inferences of the cranial microstructure of the dicynodonts *Oudenodon* and *Lystrosaurus*. *Forerunners of Mammals. Radiation, Histology, Biology***,** 148-176.

Jordana, X. & Köhler, M. 2011. Enamel microstructure in the fossil bovid *Myotragus balearicus* (Majorca, Spain): Implications for life-history evolution of dwarf mammals in insular ecosystems. *Palaeogeography, Palaeoclimatology, Palaeoecology,* 300**,** 59-66.

Jordana, X., Marín-Moratalla, N., Moncunill-Solè, B., Nacarino-Meneses, C. & Köhler, M. 2016. Ontogenetic changes in the histological features of zonal bone tissue of ruminants: A quantitative approach. *Comptes Rendus Palevol,* 15**,** 255-266.

Kingdon, J., Happold, D., Butynski, T., Hoffmann, M., Happold, M. & Kalina, J. 2013. *Mammals of Africa*, A&C Black.

Klein, N. 2010. Long bone histology of Sauropterygia from the Lower Muschelkalk of the Germanic Basin provides unexpected implications for phylogeny. *PLoS One*, 5(7).

Klevezal, G. 1996. Recording structures of mammals: Determination of age and reconstruction of life history. Rotterdam: AA Balkema. 274 p.

Kohler, M., Marin-Moratalla, N., Jordana, X. & Aanes, R. 2012. Seasonal bone growth and physiology in endotherms shed light on dinosaur physiology. *Nature,* 487**,** 358-61.

Köhler, M. & Moyà-Solà, S. 2009. Physiological and life history strategies of a fossil large mammal in a resource-limited environment. *Proceedings of the National Academy of Sciences,* 106**,** 20354-20358.

Kolb, C., Scheyer, T. M., Lister, A. M., Azorit, C., De Vos, J., Schlingemann, M. A., Rossner, G. E., Monaghan, N. T. & Sanchez-Villagra, M. R. 2015a. Growth in fossil and extant deer and implications for body size and life history evolution. *BMC Evolutionary Biology,* 15**,** 19.

Kolb, C., Scheyer, T. M., Veitschegger, K., Forasiepi, A. M., Amson, E., Van Der Geer, A. A., Van Den Hoek Ostende, L. W., Hayashi, S. & Sanchez-Villagra, M. R. 2015b.

Mammalian bone palaeohistology: a survey and new data with emphasis on island forms. *PeerJ,* 3**,** e1358.
Kwiecinski, G. G., Krook, L. & Wimsatt, W. A. 1987. Annual skeletal changes in the little brown bat, *Myotis lucifugus lucifugus*, with particular reference to pregnancy and lactation. *American Journal of Anatomy,* 178**,** 410-420.
Kyalangalilwa, B., Boatwright, J. S., Daru, B. H., Maurin, O. & Van Der Bank, M. 2013. Phylogenetic position and revised classification of *Acacia* sl (Fabaceae: Mimosoideae) in Africa, including new combinations in *Vachellia* and *Senegalia*. *Botanical Journal of the Linnean Society,* 172**,** 500-523.
Lande, R. 1978. Evolutionary mechanisms of limb loss in tetrapods. *Evolution,* 32**,** 73-92.
Laurin, M., Canoville, A. & Germain, D. 2011. Bone microanatomy and lifestyle: A descriptive approach. *Comptes Rendus Palevol,* 10**,** 381-402.
Legendre, L. J. & Botha-Brink, J. 2018. Digging the compromise: investigating the link between limb bone histology and fossoriality in the aardvark (*Orycteropus afer*). *PeerJ,* 6**,** e5216.
Lieberman, D. E., Pearson, O. M., Polk, J. D., Demes, B. & Crompton, A. W. 2003. Optimization of bone growth and remodeling in response to loading in tapered mammalian limbs. *Journal of Experimental Biology,* 206**,** 3125-38.
Main, R. P. & Biewener, A. A. 2004. Ontogenetic patterns of limb loading, in vivo bone strains and growth in the goat radius. *Journal of Experimental Biology,* 207**,** 2577-88.
Main, R. P. & Biewener, A. A. 2006. In vivo bone strain and ontogenetic growth patterns in relation to life-history strategies and performance in two vertebrate taxa: goats and emu. *Physiological and Biochemical Zoology,* 79**,** 57-72.
Marín-Moratalla, N., Jordana, X. & Köhler, M. 2013. Bone histology as an approach to providing data on certain key life history traits in mammals: Implications for conservation biology. *Mammalian Biology,* 78**,** 422-429.
Martinez-Maza, C., Alberdi, M. T., Nieto-Diaz, M. & Prado, J. L. 2014. Life-history traits of the Miocene Hipparion concudense (Spain) inferred from bone histological structure. *PloS One,* 9**,** e103708.
McFarlin, S. C., Terranova, C. J., Zihlman, A. L., Enlow, D. H. & Bromage, T. G. 2008. Regional variability in secondary remodeling within long bone cortices of catarrhine primates: the influence of bone growth history. *Journal of Anatomy,* 213**,** 308-24.
Mitchell, G. & Skinner, J. D. 2003. On the origin, evolution and phylogeny of giraffes *Giraffa camelopardalis*. *Transactions of the Royal Society of South Africa,* 58**,** 51-73.
Montoya-Sanhueza, G. & Chinsamy, A. 2017. Long bone histology of the subterranean rodent *Bathyergus suillus* (Bathyergidae): ontogenetic pattern of cortical bone thickening. *Journal of Anatomy,* 230**,** 203-233.
Mori, R., Kodaka, T., Sano, T., Yamagishi, N., Asari, M. & Naito, Y. 2003. Comparative histology of the laminar bone between young calves and foals. *Cells Tissues Organs,* 175**,** 43-50.
Mori, R., Kodaka, T., Soeta, S., Sato, J., Kakino, J., Hamato, S., Takaki, H. & Naito, Y. 2005. Preliminary study of histological comparison on the growth patterns of long-bone cortex in young calf, pig, and sheep. *Journal of Veterinary Medical Science,* 67**,** 1223-1229.
Muller, Z., Cantor, M., Cuthill, I. C. & Harris, S. 2018. Giraffe social preferences are context dependent. *Animal Behaviour,* 146**,** 37-49.

Nacarino-Meneses, C., Jordana, X. & Kohler, M. 2016a. Histological variability in the limb bones of the Asiatic wild ass and its significance for life history inferences. *PeerJ,* 4**,** e2580.

Nacarino-Meneses, C., Jordana, X. & Köhler, M. 2016b. First approach to bone histology and skeletochronology of *Equus hemionus*. *Comptes Rendus Palevol,* 15**,** 267-277.

Nacarino-Meneses, C., Jordana, X., Orlandi-Oliveras, G. & Kohler, M. 2017. Reconstructing molar growth from enamel histology in extant and extinct *Equus*. *Scientific Reports,* 7**,** 15965.

Nacarino-Meneses, C. & Kohler, M. 2018. Limb bone histology records birth in mammals. *PloS One,* 13**,** e0198511.

Nacarino-Meneses, C. & Orlandi-Oliveras, G. 2019. The life history of European Middle Pleistocene equids: first insights from bone histology. *Historical Biology***,** 1-11.

Orlandi-Oliveras, G., Nacarino-Meneses, C., Koufos, G. D. & Kohler, M. 2018. Bone histology provides insights into the life history mechanisms underlying dwarfing in hipparionins. *Scientific Reports,* 8**,** 17203.

Padian, K., Werning, S. & Horner, J. R. 2016. A hypothesis of differential secondary bone formation in dinosaurs. *Comptes Rendus Palevol,* 15**,** 40-48.

Pickford, M. 1975. Late Miocene sediments and fossils from the northern Kenya Rift Valley. *Nature,* 256**,** 279.

Ponton, F., Elżanowski, A., Castanet, J., Chinsamy, A., De Margerie, E., De Ricqlès, A. & Cubo, J. 2004. Variation of the outer circumferential layer in the limb bones of birds. *Acta Ornithologica,* 39**,** 137-140.

Prondvai, E. 2017. Medullary bone in fossils: function, evolution and significance in growth curve reconstructions of extinct vertebrates. *Journal of Evolutionary Biology,* 30**,** 440-460.

Ramstein, G., Fluteau, F., Besse, J. & Joussaume, S. 1997. Effect of orogeny, plate motion and land–sea distribution on Eurasian climate change over the past 30 million years. *Nature,* 386**,** 788-795.

Reid, R. 1996. Bone histology of the Cleveland-Lloyd dinosaurs and of dinosaurs in general, Part I: Introduction: Introduction to bone tissues. *Brigham Young University Geology Studies,* 41**,** 25-72.

Rubin, C. T., Bain, S. D. & Mcleod, K. J. 1992. Suppression of the osteogenic response in the aging skeleton. *Calcified Tissue International,* 50**,** 306-313.

Schaffler, M. B. & Burr, D. B. 1984. Primate cortical bone microstructure: relationship to locomotion. *American Journal of Physical Anthropology,* 65**,** 191-197.

Schellhorn, R. & Pfretzschner, H.-U. 2013. Biometric study of ruminant carpal bones and implications for phylogenetic relationships. *Zoomorphology,* 133**,** 139-149.

Shorrocks, B. 2016. *The giraffe: biology, ecology, evolution and behaviour*, John Wiley & Sons.

Singh, I., Tonna, E. & Gandel, C. 1974. A comparative histological study of mammalian bone. *Journal of Morphology,* 144**,** 421-437.

Skedros, J. G., Mason, M. W. & Bloebaum, R. D. 1994. Differences in osteonal micromorphology between tensile and compressive cortices of a bending skeletal system: indications of potential strain-specific differences in bone microstructure. *The Anatomical Record,* 239**,** 405-413.

Skedros, J. G., Mason, M. W., Nelson, M. C. & Bloebaum, R. D. 1996. Evidence of structural and material adaptation to specific strain features in cortical bone. *Anatomical Record,* 246**,** 47-63.

Skedros, J. G., Sorenson, S. M. & Jenson, N. H. 2007. Are distributions of secondary osteon variants useful for interpreting load history in mammalian bones? *Cells Tissues Organs,* 185**,** 285-307.

Skedros, J. G., Su, S. C. & Bloebaum, R. D. 1997. Biomechanical implications of mineral content and microstructural variations in cortical bone of horse, elk, and sheep calcanei. *The Anatomical Record: An Official Publication of the American Association of Anatomists,* 249**,** 297-316.

Skedros, J. G., Sybrowsky, C. L., Parry, T. R. & Bloebaum, R. D. 2003. Regional differences in cortical bone organization and microdamage prevalence in Rocky Mountain mule deer. *Anatomical Record. Part A: Discoveries in Molecular, Cellular, and Evolutionary Biology,* 274**,** 837-50.

Starck, J. M. & Chinsamy, A. 2002. Bone microstructure and developmental plasticity in birds and other dinosaurs. *Journal of Morphology,* 254**,** 232-46.

Straehl, F. R., Scheyer, T. M., Forasiepi, A. M., Macphee, R. D. & Sanchez-Villagra, M. R. 2013. Evolutionary patterns of bone histology and bone compactness in xenarthran mammal long bones. *PloS One,* 8**,** e69275.

Theodor, J. M. 2001. Artiodactyla (Even-Toed Ungulates Including Sheep and Camels). *e LS*.

Van Schalkwyk, O. L., Skinner, J. D. & Mitchell, G. 2004. A comparison of the bone density and morphology of giraffe (*Giraffa camelopardalis*) and buffalo (*Syncerus caffer)* skeletons. *Journal of Zoology,* 264**,** 307-315.

Van Sittert, S. J. 2016. *Ontogenetic allometry of the postcranial skeleton of the giraffe (Giraffa camelopardalis) with application to giraffe life history evolution and palaeontology.* University of Pretoria.

Van Sittert, S. J., Skinner, J. D. & Mitchell, G. 2010. From fetus to adult--an allometric analysis of the giraffe vertebral column. *Journal of Experimental Zoology: Part B, Molecular and Developmental Evolution,* 314**,** 469-79.

Veitschegger, K., Kolb, C., Amson, E., Scheyer, T.M. and Sánchez-Villagra, M.R., 2018. Palaeohistology and life history evolution in cave bears, *Ursus spelaeus* sensu lato. PloS one, 13(11).

Wallace, J. M., Rajachar, R. M., Allen, M. R., Bloomfield, S. A., Robey, P. G., Young, M. F. & Kohn, D. H. 2007. Exercise-induced changes in the cortical bone of growing mice are bone- and gender-specific. *Bone,* 40**,** 1120-7.

Wolff, J. 1986. The Law of Bone Remodeling, translated by P. Maquet and R. Furlong. *New York, S pringer,* 1**,** 8.

Woodward, H. N., Horner, J. R. & Farlow, J. O. 2011. Osteohistological Evidence for Determinate Growth in the American Alligator. *Journal of Herpetology,* 45**,** 339-342.

Woolley, M. R., Chinsamy, A., Govender, R. & Bester, M. N. 2019. Microanatomy and histology of bone pathologies of extant and extinct phocid seals. *Historical Biology***,** 1-16.

Zedda, M., Brits, D., Giua, S. & Farina, V. 2018. Distinguishing domestic pig femora and tibiae from wild boar through microscopic analyses. *Zoomorphology,* 138**,** 159-170.

Zhisheng, A., Kutzbach, J. E., Prell, W. L. & Porter, S. C. 2001. Evolution of Asian monsoons and phased uplift of the Himalaya–Tibetan plateau since Late Miocene times. *Nature,* 411**,** 62-66.

Ziv, V., Wagner, H. & Weiner, S. 1996. Microstructure-microhardness relations in parallel-fibered and lamellar bone. *Bone,* 18**,** 417-428.

Appendix

Table A.1. General measurements of each of the bones of *Giraffa camelopardalis* analysed in this study. Giraffe individual refers to one giraffe skeleton and specimen number refers to each individual bone from each giraffe skeleton. (Abbreviations: mm-millimetres, g-grams, Cr-Cranial, Cd-Caudal, M-Medial, L-Lateral, f-female, m-male).

Giraffe individual	Specimen number	Bone Type	Age Class	Sex	Body Mass (Kg)	Bone Length (mm)	Bone Mass (g)	Cr-Cd diameter (mm)	M-L diameter (mm)	Circumference (mm)
^	BF12	Femur	^	^	^	^	^	^	^	^
^	BH11	Humerus	Subadult	m	^	^	^	^	^	^
^	BR20	Radius	^	^	^	^	3222	52,16	63,37	190
^	BT13	Tibia	^	^	^	^	^	^	^	^
z-07	BH12	Humerus	Adult	f	816,8	^	2382	65,16	61,2	204
z-24	BF1	Femur	Subadult	f	581,5	258	2681	56,93	48,57	174
z-24	BH1	Humerus	Subadult	f	581,5	450	2525	70	54,2	196
z-24	BMC1	Metacarpus	Subadult	f	581,5	670	1915	44,24	47,38	158
z-24	BR1	Radius	Subadult	f	581,5	668	2914	46,6	56,8	173
z-24	BT1	Tibia	Subadult	f	581,5	300	2297	43,9	61,5	174
z-25	BF2	Femur	Juvenile	f	222	182	1078	41,6	36,1	125
z-25	BH2	Humerus	Juvenile	f	222	163	863	41,4	40,5	132
z-25	BMC2	Metacarpus	Juvenile	f	222	228	650	31,9	33,8	112
z-25	BR2	Radius	Juvenile	f	222	230	1056	32,2	39,2	120

z-25	BT2	Tibia	Juvenile	f	222	385	905	34,8	43,1	129
z-26?	BF3	Femur	Adult	f	924,5	497	2521	69,7	54,46	186
z-26?	BH3	Humerus	Adult	f	924,5	488	2938	78,85	71,27	228
z-26?	BMC4	Metacarpus	Adult	f	924,5	668	2256	47,56	42,18	174
z-26?	BR3	Radius	Adult	f	924,5	736	3395	50,71	63,52	190
z-26?	BT3	Tibia	Adult	f	924,5	606	2585	47,2	64	185
z-27	BF14	Femur	Foetus	m	77	^	318	34,7	30,8	107
z-27	BH14	Humerus	Foetus	m	77	228	238	30,7	34	103
z-27	BMC46	Metacarpus	Foetus	m	77	^	343	27,4	29,3	98
z-27	BT14	Tibia	Foetus	m	77	251	278	28,1	34,7	103
z-27?	BR14	Radius	Foetus	m	77	^	305	27,5	29,3	98
z-28	BF4	Femur	Subadult	m	618	469	2359	57,4	46,8	171
z-28	BR4	Radius	Subadult	m	618	654	2879	48,14	57,09	169
z-28	BT4	Tibia	Subadult	m	618	569	2378	43,39	60,68	172
z-28?	BH4	Humerus	Subadult	m	618	434	2294	59,21	55,7	182
z-29	BF5	Femur	Adult	m	1208,5	556	3968	67,53	68,53	201
z-29	BH5	Humerus	Adult	m	1208,5	536	4460	81,54	73,46	247
z-29	BMC6	Metacarpus	Adult	m	1208,5	749	3659	54,61	57,76	185
z-29	BT5	Tibia	Adult	m	1208,5	664	4600	57,08	78,43	221
z-29?	BR5	Radius	Adult	m	1208,5	810	6448	61,54	75,88	226
z-30	BH6	Humerus	Adult	f	860	474	3278	72,92	66,64	219
z-30	BR6	Radius	Adult	f	860	698	3419	50,5	66,45	193
z-30	BT6	Tibia	Adult	f	860	574	2577	48,2	67	190
z-32?	BMC16	Metacarpus	Adult	m	967	788	3125	52	60,1	190

z-40	BMC23	Metacarpus	Subadult	m	500	^	1168	40,1	44,3	143
z-43	BMC28	Metacarpus	Subadult	m	498	^	1501	41,5	46,2	148
z-43?	BH7	Humerus	Subadult	m	498	^	1436	55,1	52,22	175
z-43?	BR7	Radius	Subadult	m	498	^	2008	41,7	55,7	162
z-43?	BT7	Tibia	Subadult	m	498	^	1610	41,7	58,3	165
z-44	BR8	Radius	Adult	m	1258	^	5489	57,2	73,6	22
z-44	BT8	Tibia	Adult	m	1258	^	3991	54,6	57,8	217
z-44?	BF8	Femur	Adult	m	1258	^	3419	73,4	58,6	207
z-44?	BH8	Humerus	Adult	m	1258	^	3949	80,9	74,7	254
z-47	BR9	Radius	Adult	m	975,9	^	3826	53,2	66,1	197
z-47	BT9	Tibia	Adult	m	975,9	^	3057	48,5	69,2	196
z-47?	BF9	Femur	Adult	m	975,9	^	2759	63,9	56,5	194
z-47?	BH9	Humerus	Adult	m	975,9	^	3266	73,5	66,83	224
z-48	BF15	Femur	Juvenile	f	141	324	602	35,4	30,5	110
z-48	BH15	Humerus	Juvenile	f	141	280	474	36,2	33,6	116
z-48	BMc47	Metacarpus	Juvenile	f	141	^	393	26,8	29,2	94
z-48	BR15	Radius	Juvenile	f	141	392	584	27	34,9	102
z-48	BT15	Tibia	Juvenile	f	141	344	561	29,5	36,2	108
z-51	BF11	Femur	Subadult	m	791	^	2688	61,28	53,6	184
z-51	BH10	Humerus	Subadult	m	791	^	2815	67,2	64,8	219
z-51	BMC33	Metacarpus	Subadult	m	791	^	2066	46,87	51,37	167
z-51	BT10	Tibia	Subadult	m	791	^	2700	45,4	66,7	185
z-51?	BR10	Radius	Subadult	m	791	^	3049	47,9	60,2	182
z-52	BF10	Femur	Subadult	m	706	^	^	^	^	^

z-55	BF13	Femur	Adult	f	988	^	2328	57,3	48,2	169
z-55	BT12	Tibia	Adult	f	988	^	^	^	^	^

^ No data available

Table A.2. Bone wall thickness measurements of the cross sections of *Giraffa camelopardalis* specimens analysed in this study. (Abbreviations: mm-millimetres, Cr-MC bone wall thickness measurement from cranial margin to endosteal margin of medullary cavity, Cd-MC bone wall thickness measurement from caudal margin to endosteal margin of medullary cavity, Lat to MC bone wall thickness measurement from lateral margin to endosteal margin of medullary cavity, and Med to MC bone wall thickness measurement from medial margin to endosteal margin of medullary cavity, refer to Fig 2.2).

Giraffe individual	Specimen number	Bone Type	Age Class	Sex	Cr-MC (mm)	Cd-MC (mm)	Lat to MC (mm)	Med to MC (mm)
^	BF12	Femur	^	^	11,77	11,05	9,45	10,03
^	BH11	Humerus	Subadult	m	15,95	16,48	10,25	18,38
^	BR11	Radius	^	^	11,65	7,89	14,11	12,36
^	BR12	Radius	^	^	14,5	8,25	10,93	14,88
^	BR20	Radius	^	^	12,89	10,32	13,5	14,99
^	BT11	Tibia	^	^	11,84	11,91	14,83	19,45
^	BT13	Tibia	^	^	10,52	10,84	14,94	13,9
z-07	BH12	Humerus	Adult	f	11,71	11,35	9,3	14,19
z-24	BF1	Femur	Subadult	f	10,64	15,47	22,02	13,27

z-24	BH1	Humerus	Subadult	f	20,92	9,12	41,75	17,07
z-24	BMC1	Metacarpus	Subadult	f	14,32	7,25	13,68	13,55
z-24	BR1	Radius	Subadult	f	19,27	8,59	17,58	15,53
z-24	BT1	Tibia	Subadult	f	26,5	8,63	7,75	14,91
z-25	BF2	Femur	Juvenile	f	6,29	10,06	9,59	8,73
z-25	BH2	Humerus	Juvenile	f	8,37	9,34	7,74	10,77
z-25	BMC2	Metacarpus	Juvenile	f	9,31	4,77	^	^
z-25	BR2	Radius	Juvenile	f	7,84	7,12	9,44	9,89
z-25	BT2	Tibia	Juvenile	f	9,13	7,45	11,58	11,44
z-26?	BF3	Femur	Adult	f	10,09	13,22	8,78	11,41
z-26?	BH3	Humerus	Adult	f	15,86	16,03	8,05	9,9
z-26?	BMC4	Metacarpus	Adult	f	14,55	6,99	^	^
z-26?	BR3	Radius	Adult	f	14,73	9,08	15,32	14,09
z-26?	BT3	Tibia	Adult	f	10,12	11,02	11,84	18,72
z-27	BF14	Femur	Foetus	m	5,52	7,88	6,17	10,87
z-27	BH14	Humerus	Foetus	m	10,17	11,24	12,5	12,25
z-27	BMC46	Metacarpus	Foetus	m	11,54	5,66	^	^
z-27	BT14	Tibia	Foetus	m	12,84	9,87	12,43	10,16
z-27?	BR14	Radius	Foetus	m	7,35	6,73	10,16	13,05
z-28	BF4	Femur	Subadult	m	10,03	19,68	7,68	9,81
z-28	BR4	Radius	Subadult	m	10,92	8,81	11,93	14,7
z-28	BT4	Tibia	Subadult	m	11,27	11,55	14,63	18,55
z-28?	BH4	Humerus	Subadult	m	17,7	14,93	10,61	18,52
z-29	BF5	Femur	Adult	m	19,38	14,16	13,94	14,15

z-29	BH5	Humerus	Adult	m	18,41	20,29	14,8	25,35
z-29	BMC6	Metacarpus	Adult	m	19,72	11,52	^	^
z-29	BT5	Tibia	Adult	m	18,44	18,18	22,42	25,31
z-29?	BR5	Radius	Adult	m	23,99	14,29	21,77	19,93
z-30	BH6	Humerus	Adult	f	15,98	16,61	11,68	19,12
z-30	BR6	Radius	Adult	f	12,11	7,11	14,81	11,83
z-30	BT6	Tibia	Adult	f	11,28	10,81	17,37	17,13
z-32?	BMC16	Metacarpus	Adult	m	18,04	6,75	^	^
z-40	BMC23	Metacarpus	Subadult	m	11,62	6,24	^	^
z-43	BMC28	Metacarpus	Subadult	m	11,82	5,56	^	^
z-43?	BH7	Humerus	Subadult	m	10,54	10,57	9,43	14,26
z-43?	BR7	Radius	Subadult	m	9,15	7,94	14,3	10,12
z-43?	BT7	Tibia	Subadult	m	11,37	11,02	13,95	12,37
z-44	BR8	Radius	Adult	m	14,74	12,82	14,82	17,75
z-44	BT8	Tibia	Adult	m	16,25	13,74	19,9	23,48
z-44?	BF8	Femur	Adult	m	12,55	17,22	12,18	13,19
z-44?	BH8	Humerus	Adult	m	17,09	18,1	12,23	21,24
z-47	BR9	Radius	Adult	m	11,55	11,86	13,51	15,96
z-47	BT9	Tibia	Adult	m	13,17	12,79	19,62	20,09
z-47?	BF9	Femur	Adult	m	10,39	18,39	9,61	10,48
z-47?	BH9	Humerus	Adult	m	15,55	16,97	12,64	15,21
z-48	BF15	Femur	Juvenile	f	8,47	9,79	8,86	8,32
z-48	BH15	Humerus	Juvenile	f	8,2	8,81	9,19	8,94
z-48	BMc47	Metacarpus	Juvenile	f	8,02	5,15	^	^

z-48	BR15	Radius	Juvenile	f	8,32	5,64	12,12	10,97
z-48	BT15	Tibia	Juvenile	f	8,84	7,4	9,46	8,44
z-51	BF11	Femur	Subadult	m	12,57	18,85	11,76	12,1
z-51	BH10	Humerus	Subadult	m	14,67	15,21	12,39	19,78
z-51	BMC33	Metacarpus	Subadult	m	17,09	6,43	^	^
z-51	BT10	Tibia	Subadult	m	11,97	11,28	18,26	20,86
z-51?	BR10	Radius	Subadult	m	11,02	7,27	8,62	11,47
z-52	BF10	Femur	Subadult	m	17,11	11,01	12,45	13,71
z-55	BF13	Femur	Adult	f	10,12	7,61	7,48	9,02
z-55	BT12	Tibia	Adult	f	11,38	11,07	15,74	16,49

^ No data available

Table A3. Summary of histological findings of *Giraffa camelopardalis* bones. (Abbreviations: ELB-endosteal lamellar bone, GM-growth marks, OC-outer circumferential layer, HB-Haversian bone, H-humerus, R-radius, MC-metacarpal, F-femur, T-tibia, N-not present; Y-present, ^ bone not studied)

Individual	Sex	Ontogenetic Stage	ELB					GM					OCL					HB					Rest Lines in Lamellar Bone					Radial Lines				
			H	R	MC	F	T	H	R	MC	F	T	H	R	MC	F	T	H	R	MC	F	T	H	R	MC	F	T	H	R	MC	F	T
z27	M	Foetus	N	N	N	N	N	N	N	N	N	N	N	N	N	N	N	N	N	N	N	N	N	N	N	N	N	N	N	N	N	Y
z25	F	Juvenile	N	N	N	N	N	N	N	N	N	N	N	N	N	N	N	N	N	N	N	N	N	N	N	N	N	N	N	N	N	Y
z48	F	Juvenile	N	N	N	N	N	N	N	N	N	N	N	N	N	N	N	N	N	N	N	N	N	N	N	N	N	N	N	N	N	Y
z24	F	Subadult	Y	Y	Y	Y	Y	Y	Y	N	N	Y	N	N	N	N	N	Y	Y	Y	Y	Y	N	Y	Y	N	N	N	N	N	N	Y
z28	M	Subadult	Y	Y	^	Y	Y	N	Y	^	Y	N	N	N	^	N	N	Y	Y	^	Y	Y	N	N	^	N	N	N	N	^	N	Y
z40	M	Subadult	^	^	N	^	^	^	^	N	^	^	^	^	N	^	^	^	^	Y	^	^	^	^	N	^	^	^	^	N	^	^
z43	M	Subadult	Y	Y	Y	^	Y	N	N	N	^	N	N	N	N	^	N	Y	Y	Y	^	Y	N	N	N	^	N	N	N	N	^	Y
z51	M	Subadult	Y	Y	Y	Y	Y	Y	N	N	N	N	N	N	N	N	N	Y	Y	Y	Y	Y	N	Y	N	N	Y	N	N	N	N	Y
z52	M	Subadult	^	^	^	Y	^	^	^	^	Y	^	^	^	^	N	^	^	^	^	Y	^	^	^	^	N	^	^	^	^	N	^
z07	F	Adult	Y	^	^	^	^	N	^	^	^	^	N	^	^	^	^	Y	^	^	^	^	N	^	^	^	^	N	^	^	^	^
z26	F	Adult	Y	Y	Y	Y	Y	Y	Y	N	Y	N	Y	N	N	N	N	Y	Y	Y	Y	Y	N	N	N	Y	N	N	N	N	N	Y
z30	F	Adult	Y	Y	^	^	Y	N	N	^	^	N	N	N	^	^	N	Y	Y	^	^	Y	N	N	^	^	N	N	N	^	^	Y
z55	F	Adult	^	^	^	Y	Y	^	^	^	N	N	^	^	^	N	N	^	^	^	Y	Y	^	^	^	N	N	^	^	^	N	Y
z29	M	Adult	Y	Y	Y	Y	Y	Y	N	N	Y	N	N	N	N	N	Y	Y	Y	Y	Y	Y	N	Y	N	N	Y	N	N	N	N	Y
z32	M	Adult	^	^	Y	^	^	^	^	N	^	^	^	^	N	^	^	^	^	Y	^	^	^	^	N	^	^	^	^	N	^	^
z44	M	Adult	Y	Y	^	Y	Y	N	N	^	Y	N	N	N	^	N	N	Y	Y	^	Y	Y	N	N	^	N	N	N	N	^	N	Y
z47	M	Adult	Y	Y	^	Y	Y	N	N	^	N	Y	N	N	^	N	N	Y	Y	^	Y	Y	N	N	^	N	N	N	N	^	N	Y

33